Application of a short wave infrared sensor for the perception of mobile robots in harsh weather conditions

Alexandre Riffard[1], Mathieu Labussière[1], Pierre Duthon[2], Romuald Aufrère[1]

[1] Université Clermont Auvergne, Clermont Auvergne INP, CNRS, Institut Pascal, F-63000 Clermont-Ferrand, France,

[2] Cerema, Research Team "Intelligent Transport Systems", 8-10 Rue Bernard Palissy, CEDEX 2, F-63017 Clermont-Ferrand, France.

Introduction

The use of the SWIR (Short Wave Infrared) spectrum, generally between **0.7 and 2.5 µm**, has opened up new perspectives in the field of imaging, particularly in the development of **autonomous vehicles** (AVs). While current obstacle detection solutions demonstrate appreciable effectiveness under favourable weather conditions, there is still room for improvement to increase the safety of AVs in partially **unknown road environments** subject to **difficult weather conditions** (rain, snow, fog, glare, etc.), both day and night. This is the context of this study, with the integration of a SWIR camera [1] into the sensory architecture of AVs.

Light Spectrum

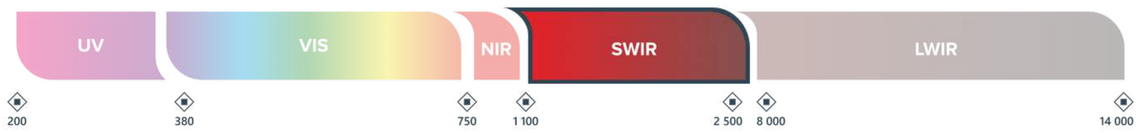

Figure 1: Light spectrum - [Fig. SWIR Spectrum from Exosens, October 5, 2023].

Context & Motivation

- This study aims to overcome the current limitations of detection systems by exploiting the particular characteristics of the SWIR spectrum, thereby offering **more reliable perception** of obstacles in **degraded weather conditions**.
- The use of a SWIR sensor reduces the spread of dust, rain and fog, among other things [2]. Such sensors would complement the conventional sensors (lidar, radar, camera...) already present on AVs.
- These advances would not only enhance the safety of AVs, but also promote their long-term autonomy, particularly in rural areas where road infrastructure is less developed.

Ongoing Work

1. Comparison between the visible spectrum and the SWIR spectrum in degraded weather conditions, with the support of Cerema's "PAVIN Brouillard & Pluie" platform [3].
2. Comparison of SWIR sensor technologies (InGaAs and CQD).

Methodology

- Comparison between the SWIR spectrum and the visible spectrum in a control environnement (PAVIN BP platform at Cerema) under different weather conditions, such as fog and rain of varying intensity, both day and night. Acquisition of images using both a regular camera for visible light and a SWIR camera.
- For the comparison between the InGaAs and CQD SWIR cameras, we used two different cameras, one of each type:
  - a SWIR Acuros® CQD® 1280 camera from SWIR Vision Systems
  - a Bobcat 320 SWIR camera from Xenics Exosens Group

SWIR & Harsh weather

- The experiments carried out at Cerema, have enabled us to obtain images such as the one shown in figure 2.

Figure 2: Artificial fog during daylight, at Cerema, visible spectrum (left) and SWIR (right).

- List of parameters tested : *(All the experiments are a variation of those.)*

Parameters	Values
Lighting	Day/Night ; LED SWIR/halogen/model car headlights
Weather	Fog (gradual dissipation) ; Rain (20 to 170mm/h)
Spectrum	Visible ; SWIR
Camera	Exposure time ; NUC

- These experiments showed an **improvement in visibility** in thick fog and heavy rain in the SWIR spectrum compared with the visible spectrum, even at night, as long as there is a light source in the scene emitting in the SWIR.

Experimental Setup

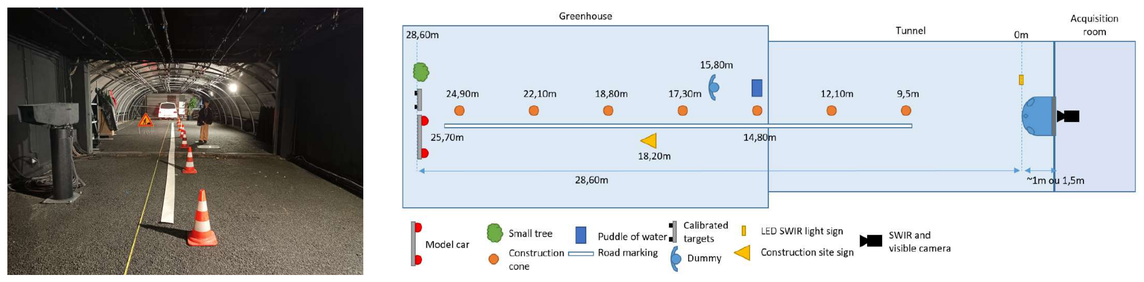

Figure 3: Diagram of the acquisition process at Cerema.

InGaAs vs CQD

- InGaAs is the most commonly used technology. CQD® sensors recently allow new technology to emerge. Some characteristics are listed below:

Sensor types	InGaAs	CQD
Resolution	640x512	1280x1024
Spectral band	0.9µm - 1.7 µm	0.4 µm - 1.7 µm
QE or D*	High	High in visible, low in SWIR
Cost	$$	$

- InGaAs SWIR cameras, despite their high production and sales costs, remain particularly reliable and high-performing sensors due to their high performance in low-light conditions, attributed to a high EQ.
- Colloidal quantum dot (CQD) cameras represent a promising breakthrough thanks to their properties, offering adjustable spectral sensitivity and higher image resolution.

Figure 4: Camera Bobcat 320 (right) and camera Acuros CQD 1280 (left).

Conclusion

- SWIR technology effectively enhances vision for autonomous vehicles in low-light and complex weather conditions.
- The SWIR camera improves visibility of road markings, signs, and obstacles, even in rain or fog, offering promising prospects for autonomous driving systems.
- The widespread adoption of SWIR technology across multiple sectors highlights its usefulness and significant potential.

Future Works

- Integrating the sensor into a multi-sensor fusion architecture for the perception of obstacles and road conditions.
- Acquisition and creation of multimodal data sets (GNSS, IMU, lidar, radar, cameras, SWIR, odometry, etc.) using the platforms available at the Institut Pascal (in particular PAVIN, EZ10 and ZOE).

Main References

[1] Nicolas Pinchon et al. "All-Weather Vision for Automotive Safety: Which Spectral Band?" In: 2019, pp. 3–15.

[2] Werner Ritter et al. "DENSE: Environment Perception in Bad Weather—First Results". In: Springer International Publishing, 2019, pp. 143–159.

[3] Sébastien Liandrat et al. *A review of Cerema PAVIN fog & rain platform: from past and back to the future*. 2022.

Acknowledgments

- This work was supported by the International Research Centre "Innovative Transport and Production Systems" of the CAP 20-25 I-SITE.

Contrôle optimal d'outils robotiques pour la réalisation de travaux agroécologiques

Stephane NGNEPIEPAYE WEMBE, Roland LENAIN[1], Alexandre PREVAULT OSMANI[2]

1 = Université Clermont Auvergne, INRAE, UR TSCF, 2 = SABI AGRI

Introduction

Les nouvelles pratiques agroécologiques requièrent de nouveaux équipements robotiques, capables d'intégrer leurs outils dans la chaine décisionnelle (gestion de l'action des outils par exemple). A cette fin cette thèse vise les développements suivants:

- **Perception des plantes d'intérêt**
- **Contrôle direct d'un point de l'outil**
- **Coordination des mobilités de l'outil et du robot**

Il s'agit de pouvoir réaliser des actions précises et répétables pour une améliorer les perforamces agro-écologiques

Methode

Perception : détection de pieds de vigne

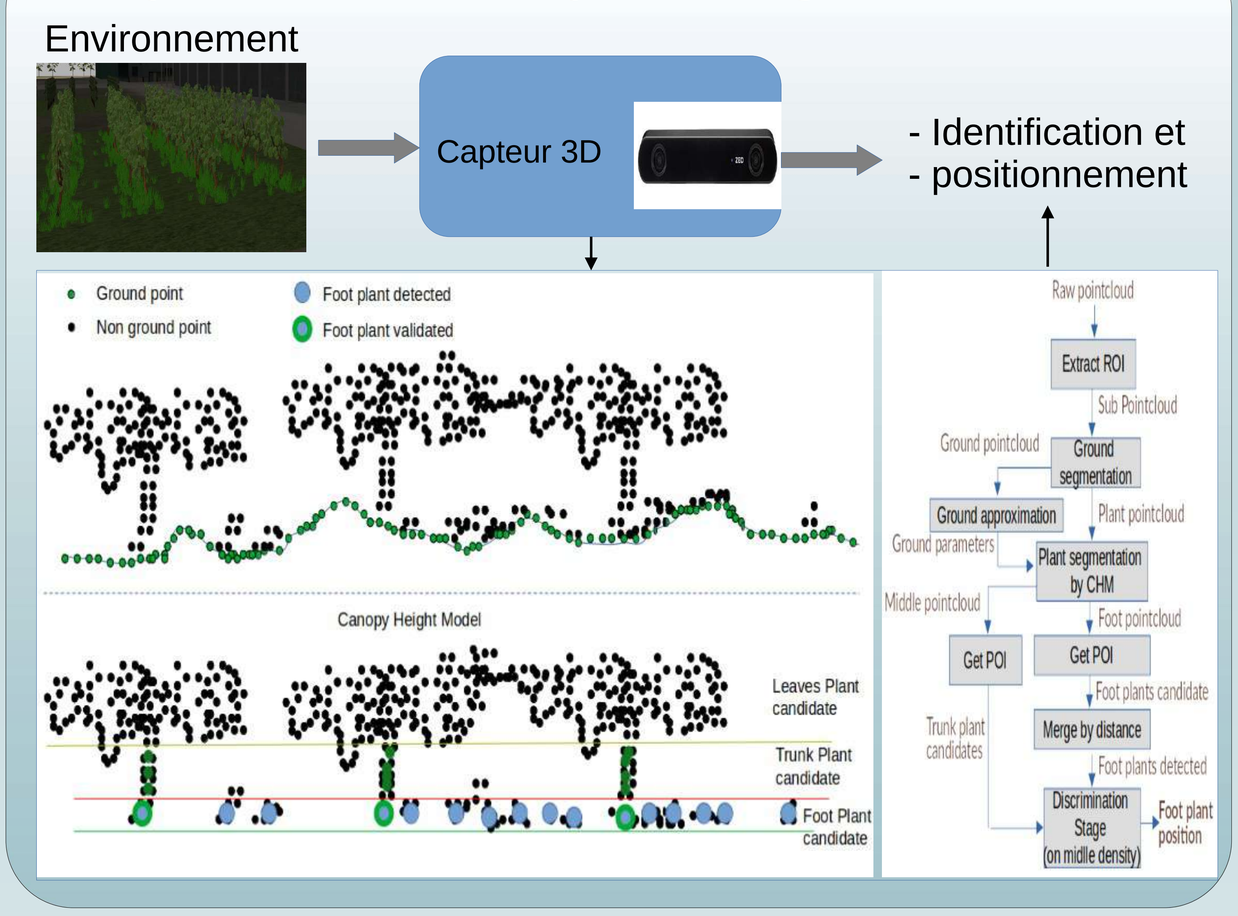

Suivie de trajectoire par un outil : cas d'un outil porté

Modèle cinématique du robot avec un outil porté

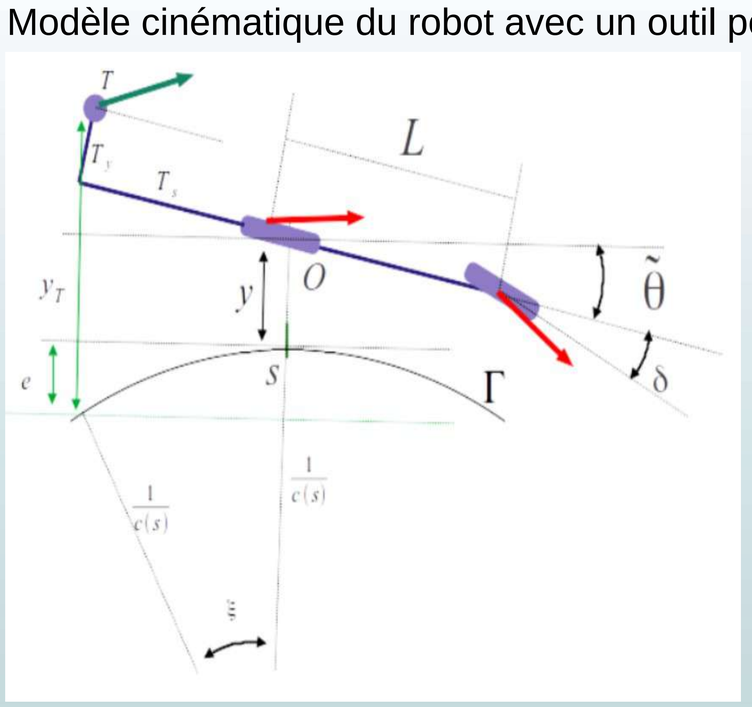

Etapes :

- Calcul de l'orientation pour ralier la trajectoire
- Calcul de l'angle de braquage pour orienter le robot

Necessité d'anticiper les variations de courbures :

- Commande optimale prédictive

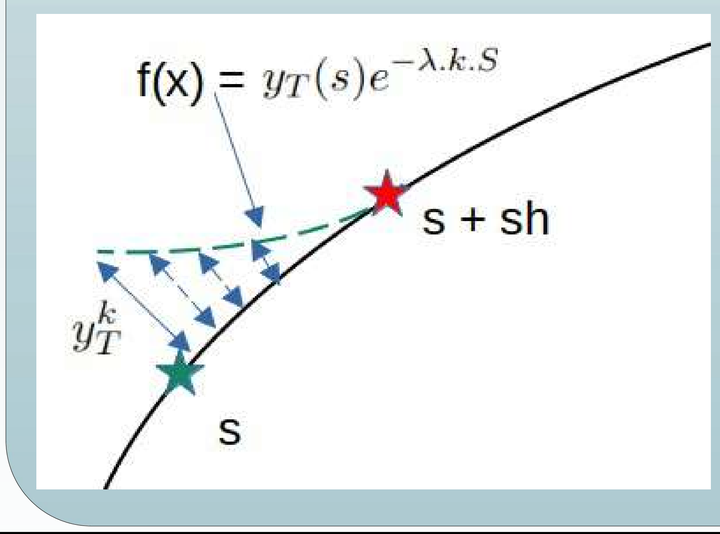

Critère d'optimisation :

minimiser les écats latéraux sur un horizon de prédiction donné

Premiers résultats

Perception de l'environnement

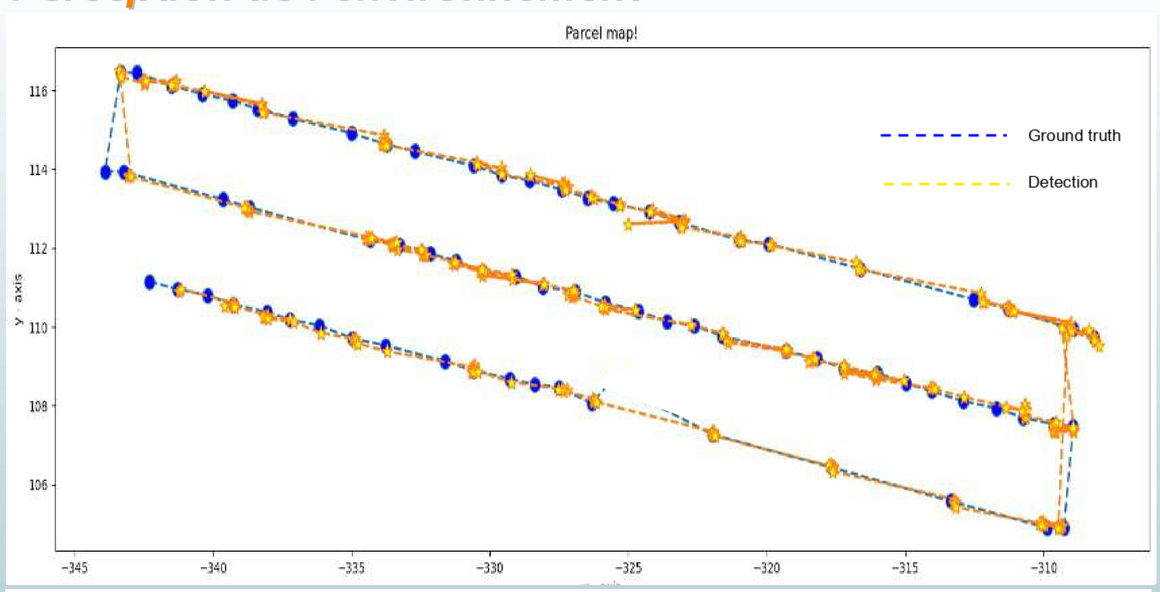

$$P = \frac{TP}{TP + FP} \qquad R = \frac{TP}{TP + FN} \qquad MPE = \frac{\sum(P_{G.T} - P_i)}{n}$$

	Nombre de souche (n)	P (%)	R (%)	MPE (cm)
Deep Learning (YOLO) [1]	74	96.8	84	18
Ombre portée [2]	74	83,4	80.3	25
Notre méthode	74	98.3	84.5	19

TP = True Positive FN = False Negative $P_{G.T}$ = Position Ground Truth

FP = False Positive MPE = Mean Position Error P_i = Position detected

Contrôle d'un point de l'outil

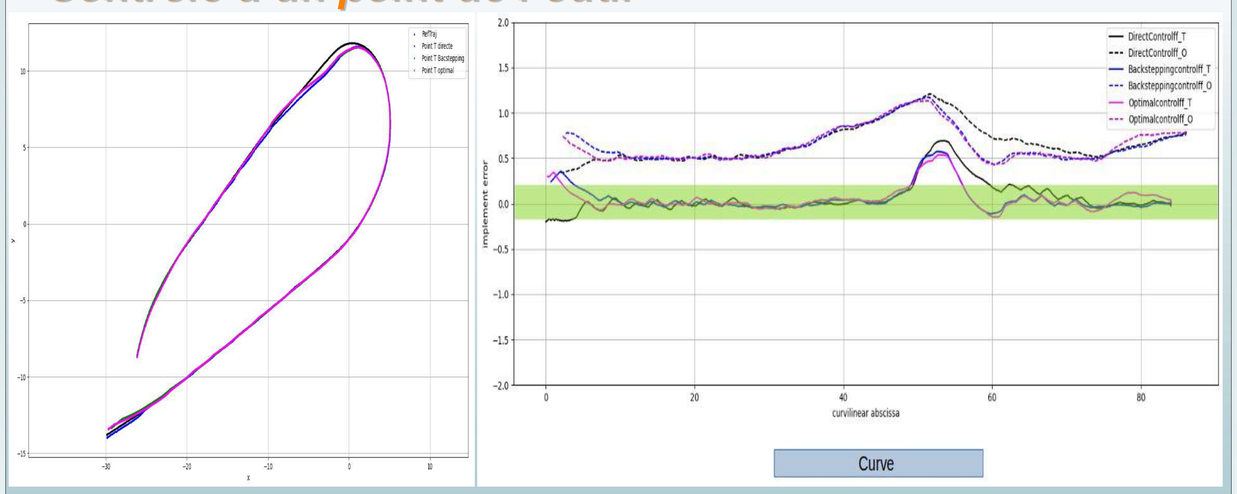

- Erreur lattérale de suivie inférieure à 20cm dans les régimes permanents
- Déport inévitable de l'outil dans les virages
- Méthode optimale aussi performante que les autres méthodes [3], [4]

Perspectives

Perception

- Utilisation des inforamations liées à l'image RGB dans l'algorithme
- Cartographie en temps réel à partie des résultats de détection

Contrôle

- Utilisation d'outils actifs pour éléminer les déports dans les virages

Bibliographie

[1] http://arxiv.org/abs/1506.02640
[2] https://doi.org/10.5753/sbiagro.2023.26580
[3] https://doi.org/10.5220 /0007915501040113
[4] https://doi.org /10.1007/s10514-006-7806-4

Contacts :
stephane.ngnepiepaye-wembe@inrae.fr
stephane.ngnepiepaye-wembe@sabi-agri.com

Amélioration de la performance thermique des briques d'argile cuites produites en RD Congo

LEWO NKONDI Blanca[1,2], AZAMA Nilas[2], BLAYSAT Benoit[1], MOUTOU PITTI Rostand[1,3]

[1]Université Clermont Auvergne, Clermont Auvergne INP, CNRS, Institut Pascal, Clermont Ferrand, France

[2]Institut National du Bâtiment et des Travaux Publics, RD Congo,

[3]CENAREST, IRT, BP14070, Libreville, Gabon

1 Contexte

Situation actuelle	Solution envisagée
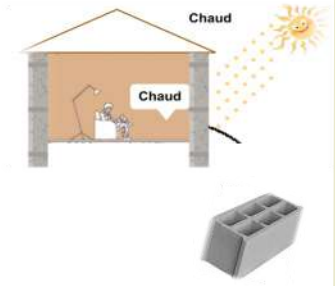	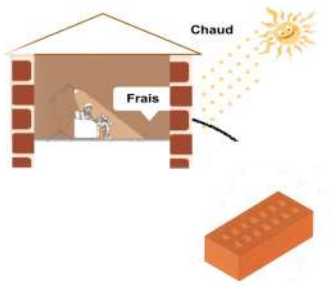
× Matériaux de construction énergivores × Bâtiments non éco-durables × Bilan carbone cycle complet élevé	✓ Matériaux de construction économes en énergie (1), (2) ✓ Bâtiments éco-durables (3) ✓ Bilan carbone cycle complet bas

2 Méthodes

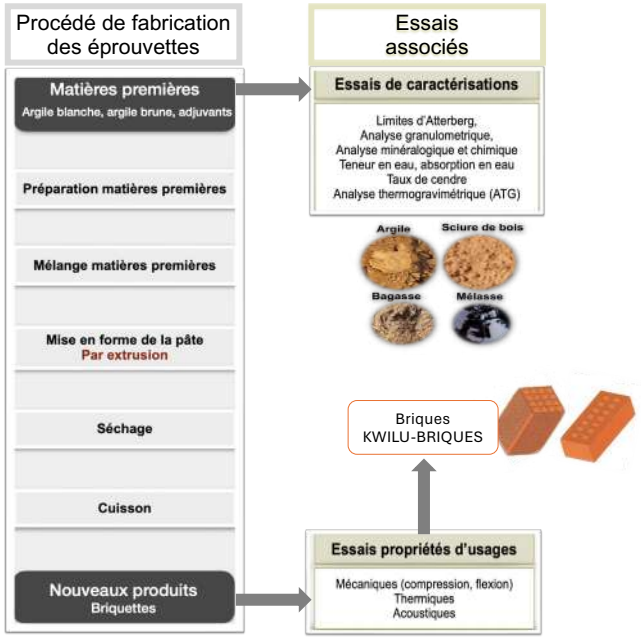

3 Premiers tests

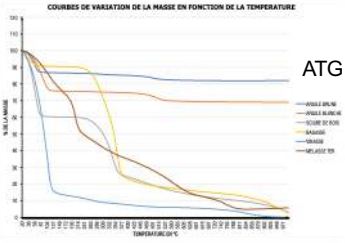

ATG

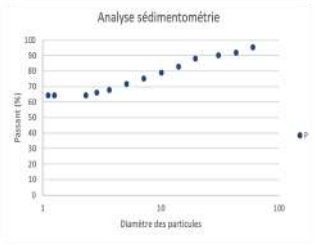

	Argile brune	Argile blanche	Bagasse	Sciure de bois
Teneur en humidité	16,30 %	25,17 %	21,51 %	42,47 %
Teneur en cendre	_	_	2,42 %	0,77 %

❑ Essai de compression sur brique cuite entière dans le sens de la pose, à la 32ème sec. la brique se rompt avec une force de 83, 81kN

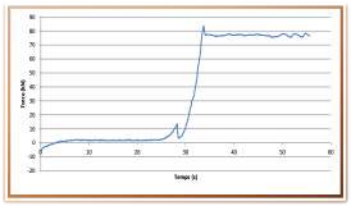

❑ Essai de compression sur la moitié d'une brique cuite dans le sens de la pose , elle se rompt avec une force de 67,65 kN à la 60ème sec.

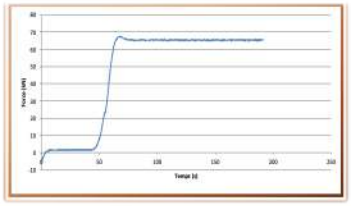

4 Perspectives

❑ Conception des briques d'argiles à base des matériaux locaux

❑ Réalisation des essais mécaniques et analyses des résultats

❑ Identification des paramètres mécaniques par LSA

❑ Proposition d'un modèle numérique de briques et adjuvants

Remerciements

RÉPUBLIQUE FRANÇAISE
CAMPUS FRANCE
KWILU BRIQUES
anr agence nationale de la recherche

5 Références

1.Azama N., Mutonkole P. (décembre 2019), Réduction de la consommation énergétique des bâtiments en zones chaudes par le choix des matériaux de construction; Modern Science : Materials of the 1st All-Russian Scientific and Practical Conference, Tambov, November 2019

2.Moutou Pitti R., Ekomy Ango S., Soumbou S., Feldman Pambou Nziengui C. (février 2023) Conception et fabrication d'une brique adobe à partir des sciures de bois d'origine du bassin du Congo; Materials of the 1st All-Russian Scientific and Practical Conference, Tambov, November 2019

3.ECOMAT (juin 2022). 2ème Conférence des Eco-Matériaux en Afrique -CEMA'2022, SALY https://cema2021.sciencesconf.org/

Plan d'expérience optimal sous incertitudes de campagnes d'essais de ténacité

A. Quintin[1,4] (anthony.quintin@cea.fr) R. Chocat[1] T. Petit[2] C. Mattrand[3] J-M. Bourinet[4]

[1]Université Paris-Saclay, CEA, Service de Génie Logiciel pour la Simulation, Gif-sur-Yvette, France
[2]CEA-DAM, Centre de Gramat, Gramat, Gif-sur-Yvette, France
[3]UCA, Clermont Auvergne INP, CNRS, Institut Pascal, 63000 Clermont-Ferrand, France
[4]UCA, Clermont Auvergne INP, CNRS, LIMOS, 63000 Clermont-Ferrand, France, France

1) Contexte

Intégrité structurelle d'une cuve de REP assurée par la **surveillance du domaine fragile** de l'acier de cuve

Estimation de la **température de transition ductile-fragile T_0** d'acier de cuve par **méthodologie Master Curve [1]** : assure la surveillance du domaine fragile

Campagne d'essais de ténacité éprouvettes CT préfissurées

Essai n° 1: Température d'essai T_{test}^1 → Ténacité $K_{J_c}^1$

Essai n° 2: Température d'essai T_{test}^2 → Ténacité $K_{J_c}^2$

Essai n° N_e: Température d'essai $T_{test}^{N_e}$ → Ténacité $K_{J_c}^{N_e}$

N_e: Nombre d'éprouvettes

Mini-CT (4mm d'épaisseur)

Méthodologie Master Curve: Estimation de T_0

Estimation de T_0 par maximum de vraisemblance: K_{J_c} décrite par une loi de **Weibull** $f(\cdot)$ paramétrée par T_0

$$\ln \mathcal{L}\left(T_0 | T_{test}^{1:N_e}, K_{J_c}^{1:N_e}\right) = \prod_i f\left(K_{J_c}^i | T_{test}^i, T_0\right)$$

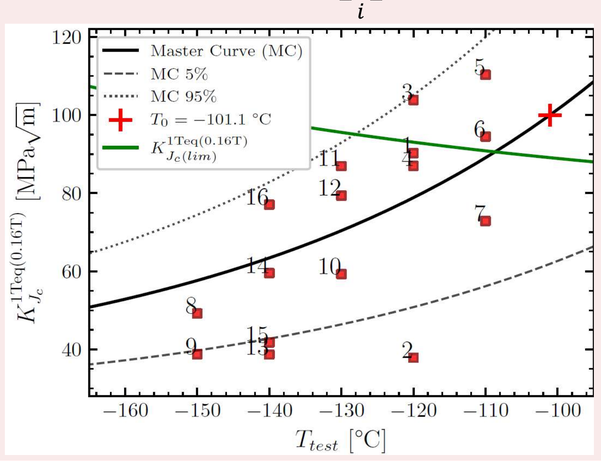

Verrous techniques & scientifiques de la Master Curve:

Incertitudes significatives sur l'estimation de T_0:

- Variabilité intrinsèque à la rupture fragile
- **Matrice d'essai** (dimension d'éprouvette CT, nombre d'essais et températures associées)
- Incertitudes d'essais (défauts de fabrications, précision des instruments de mesure, conditions de chargement…)

➢ Comment planifier optimalement les essais pour **réduire l'incertitude de T_0?**

2) Objectif

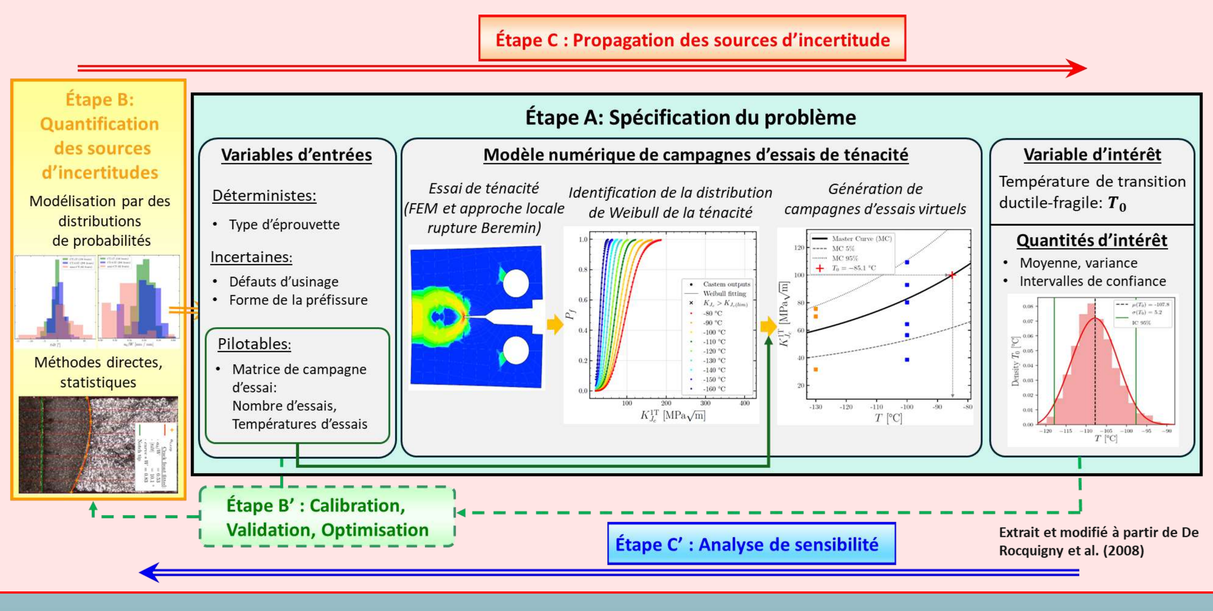

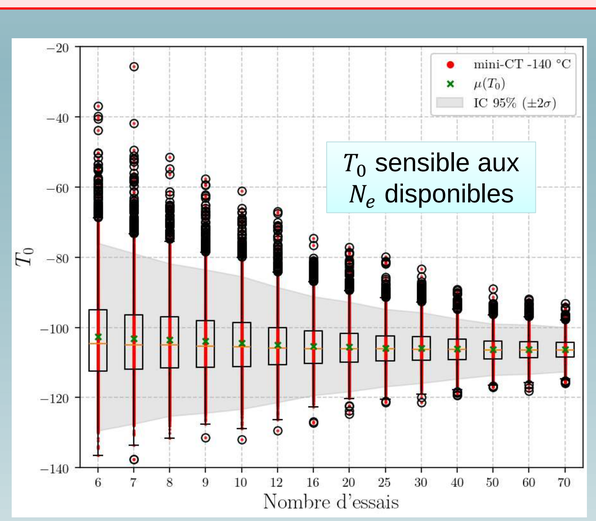

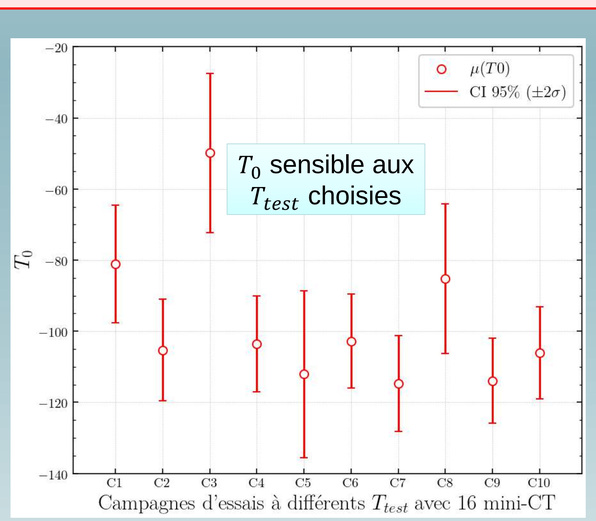

➢ **Objectif:** Trouver la séquence de températures d'essais optimale qui minimise la variance d'estimation T_0, sous budget fixé ⇔ $\boldsymbol{S_{T_{test}}^* = \arg\min \mathrm{Var}_{T_0}(S_{T_{test}})}$

$$\mathbf{Var}_{\mathbf{T_0}}\left(S_{T_{test}}\right) = Var\left[\pi\left(T_0 \middle| T_{test}^{1:N_e}, K_{J_c}^{1:N_e}\right)\right]$$

$\pi(T_0|\cdot)$: la distribution a posteriori d'une campagne d'essai $\left\{T_{test}^{1:N_e}, K_{J_c}^{1:N_e}\right\}$ générée par le modèle numérique

3) Méthodes

***Plan d'expérience par méthode d'entropie-croisée* [2][3]**

Deux étapes principales répétées itérativement jusqu'à un critère d'arrêt spécifique :

1. Générer N_s séquences de températures d'essais $S_{T_{test}}$ à partir d'une matrice de transition $P_{\mathcal{T}\times\mathcal{T}}$
   Evaluer $\mathrm{Var}_{T_0}\left(S_{T_{test}}^{(k)}\right)$, pour tout $k \in \{1, N_s\}$, puis choisir γ comme le $\rho^{ième}$- fractile

2. Mettre à jour les paramètres des distributions de la matrice de transition $P_{\mathcal{T}\times\mathcal{T}}$ par:

$$P_{i,j} = \frac{\sum_{k=1}^{N_{sim}} \left[\mathbb{I}_{\left\{Var_{T_0}\left(S_{T_{test}}^{(k)}\right)\leq\gamma\right\}}\left(S_{T_{test}}^{(k)}\right) n_{i,j}\left(S_{T_{test}}^{(k)}, N_e\right)\right]}{\sum_{k=1}^{N_{sim}} \left[\mathbb{I}_{\left\{Var_{T_0}\left(S_{T_{test}}^{(k)}\right)\leq\gamma\right\}}\left(S_{T_{test}}^{(k)}\right) n_i\left(S_{T_{test}}^{(k)}, N_e\right)\right]}$$

$n_{i,j}$: nombre de transitions de T_{test}^i à T_{test}^j

n_i : nombre de transitions partant de T_{test}^i

***Plan d'expérience par fonctions d'utilité* [4]**

$$T_{test}^{*i+1} = \arg\max \mathbb{E}\left[U\left(T_{test}^{1:i+1}, K_{J_c}^{1:i+1}, T_0\right)\right] \quad , i \in \{1, \cdots, N_e\}$$

$$= \arg\max \iint U\left(T_{test}^{i+1}, K_{J_c}^{i+1}, T_0\right) f\left(K_{J_c}^{1:i+1} | T_{test}^{1:i+1}, T_0\right) \pi(T_0) dK_{J_c} dT_0$$

$U(\cdot)$ fonction d'utilité qui quantifie l'utilité apportée par T_{test}^{i+1}

Critère de « D-optimalité » populaire pour minimiser la variance d'estimation de T_0:

$$U\left(T_{test}^{1:i+1}, K_{J_c}^{1:i+1}, T_0\right) = \det\left(\Sigma_{1:i+1}^{-1}\right) = -\mathbb{E}\left[\frac{\partial^2}{\partial T_0^2}\left\{\ln\left(\mathcal{L}\left(T_0 \middle| T_{test}^{1:i+1}, K_{J_c}^{1:i+1}\right)\pi(T_0)\right)\right\}\right]^{-1}_{|T_0 = T_{0,MAP}}$$

4) Résultats

➢ Estimation de $S_{T_{test}}^*$ avec 16 essais sur mini-CT d'acier 16MND5 non-irradié

Entropie-croisée

$S_{T_{test}}^* = [-140, -140, \cdots, -140]$ °C

✓ Méthode robuste et flexible
○ Cout important

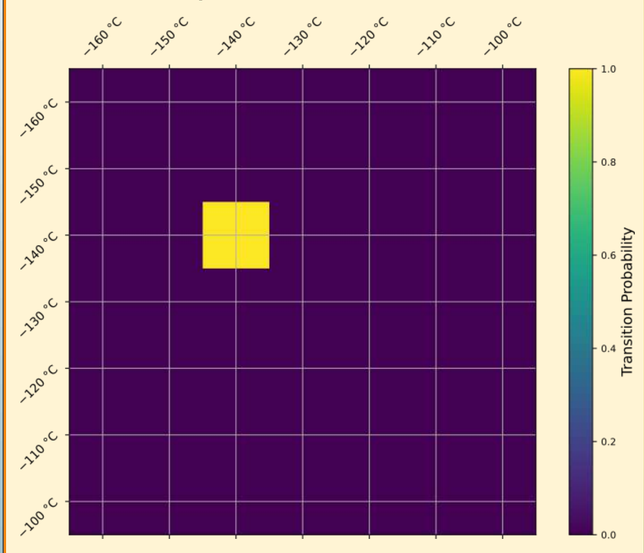

Bayésien D-optimalité

$S_{T_{test}}^* = [-140, -140, \cdots, -140]$ °C

✓ Cout rapide
○ Hypothèse forte (approximation de Laplace)

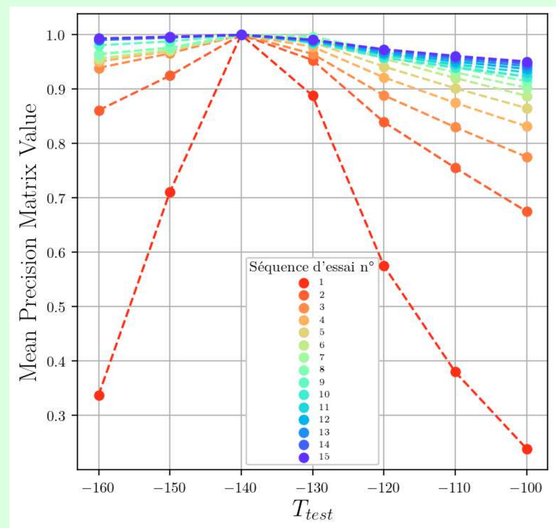

5) Conclusions/Perspectives

✓ Quantification de T_0 par modèle numérique générant des campagnes virtuelles d'essais de ténacité représentatives d'acier 16MND5 non irradié

✓ Identification d'une température d'essai optimale $T_{test}^* = -140$ °C pour réduire l'incertitude sur l'estimation de T_0 (mini-CT d'acier 16MND5 non irradié)

➢ **Améliorer la fonction « objectif » et ajouter des fonctions d'utilité**

➢ Généraliser les plans d'expériences **pour acier inconnu et irradié (actualiser séquentiellement le modèle de rupture de Beremin)**

Bibliographie

1. **ASTM E1921-21, Standard Test Method for Determination of Reference Temperature T0 for Ferritic Steels in the Transition Range (2021)**
2. **R. Rubinstein, The cross-entropy method for combinatorial and continuous optimization, Methodology and computing in applied probability (1999)**
3. **P.-T. De Boer, D. P. Kroese, S. Mannor, R. Y. Rubinstein, A tutorial on the cross-entropy method, Annals of operations research 134 (2005)**
4. **K. Chaloner, I. Verdinelli, Bayesian experimental design: A review, Statistical science (1995)**

Study of the mechanical behavior of steel-CLT composite floors and their connections

ZAAFOURI Saleh[1], JAAFARI Chaima[1], DURIF Sebastien[1], BOUCHAIR Hamid[1]

[1]Université Clermont Auvergne, INP Clermont Auvergne, CNRS, Institut Pascal, F-63000 Clermont-Ferrand, France.

Introduction

Context

- Reducing the carbon footprint by replacing concrete with wood (CLT).

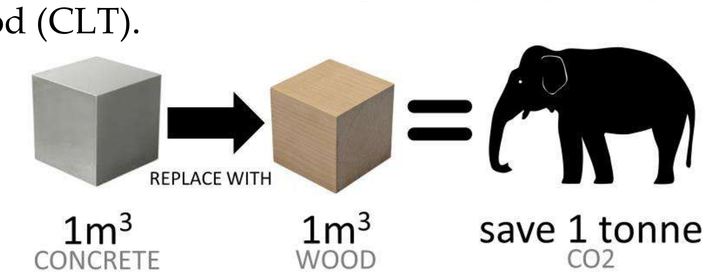

Environmental impact of replacing concrete with wood [1]

- A demountable structure allows for reuse.

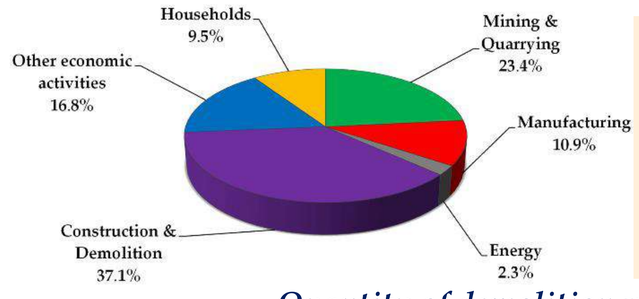

Quantity of demolition waste worldwide [2],[3]

Objectives

- Determine the mechanical behaviors of steel-CLT composite floors.
- Study of the spacing between CLT blocks.
- Study of steel-CLT connection systems via bolting.

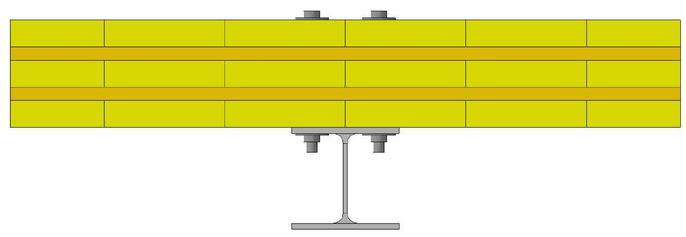

Cross-sectional view of steel-CLT composite floors

Experimental Study

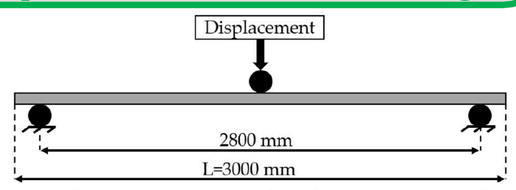

Mechanical diagram of the 3-point bending test

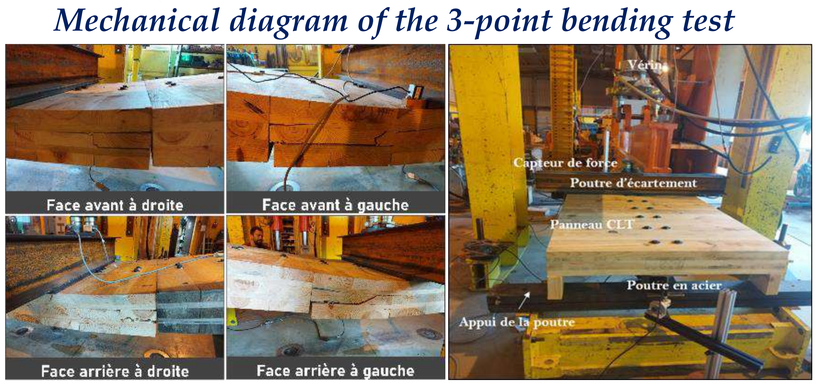

Three-point bending test of the composite floor

- The failure mode of this floor was associated with wood crushing, which occurred in a direction perpendicular to the fibers. Brittle rolling shear and cracks occurred in a direction perpendicular to the fibers.

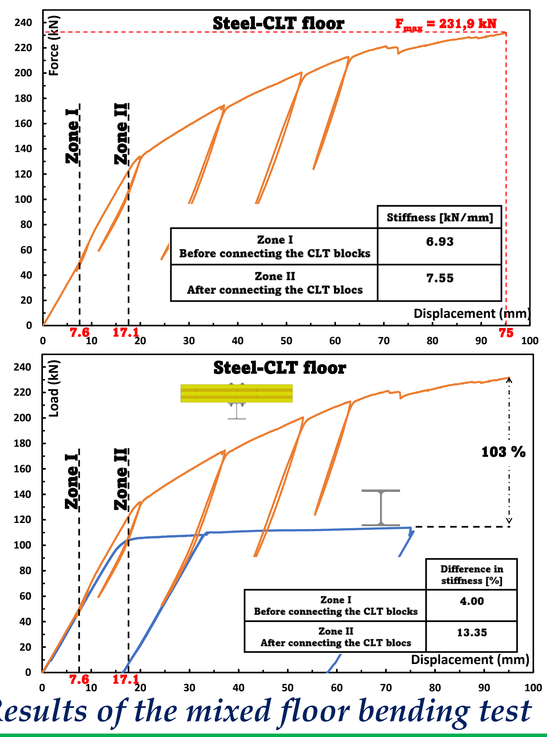

Results of the mixed floor bending test

Numerical Study

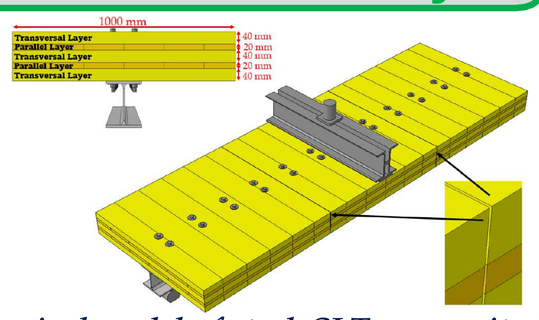

Numerical model of steel-CLT composite floor.

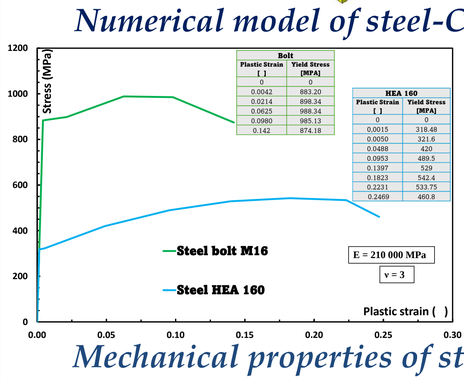

Bolt	
Plastic Strain [ ]	Yield Stress [MPA]
0	0
0.0042	883.20
0.0214	898.34
0.0625	988.34
0.0980	985.13
0.142	874.18

HEA 160	
Plastic Strain [ ]	Yield Stress [MPA]
0	0
0.0015	318.48
0.0050	321.6
0.0488	420
0.0953	489.5
0.1397	529
0.1823	542.4
0.2231	533.75
0.2469	460.8

Lamelle. Long (C18)	
Module	MPa
$E_L = E_1$	9000
$E_R = E_2$	300
$E_T = E_3$	300
$G_{LR} = G_{12}$	560
$G_{LT} = G_{13}$	560
$G_{RT} = G_{23}$	50

Lamelle. Trans (C24)	
Module	MPa
$E_L = E_1$	11 000
$E_R = E_2$	370
$E_T = E_3$	370
$G_{LR} = G_{12}$	690
$G_{LT} = G_{13}$	690
$G_{RT} = G_{23}$	50

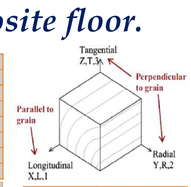

C.Poisson (C18 et C24) [4]	
$\vartheta_{LR} = \vartheta_{12}$	0,48
$\vartheta_{LT} = \vartheta_{13}$	0,48
$\vartheta_{RT} = \vartheta_{23}$	0,24

Mechanical properties of steel and CLT wood

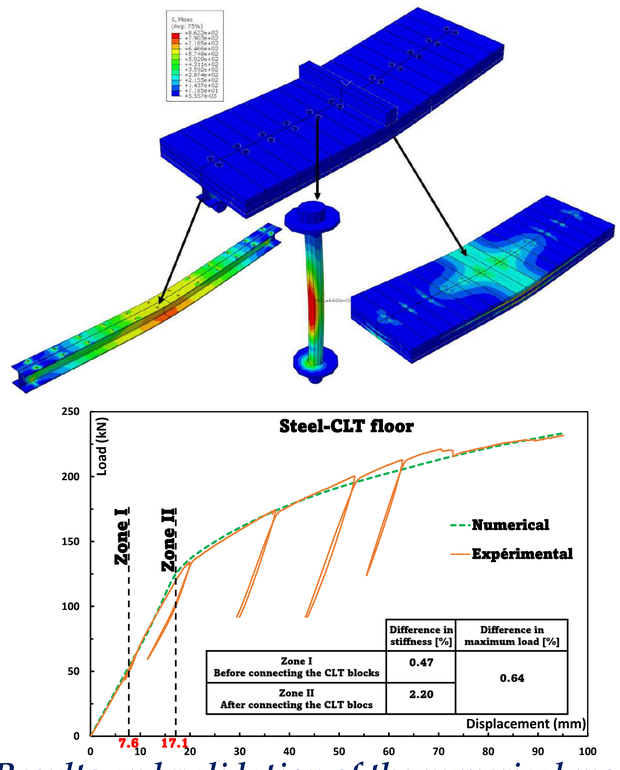

Results and validation of the numerical model

Parametric Study

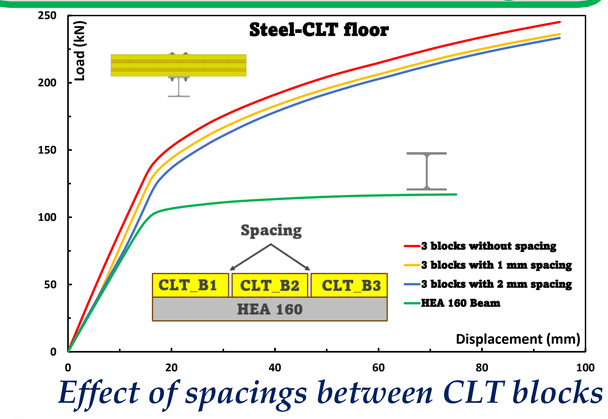

Effect of spacings between CLT blocks

Improvements in the steel-CLT connection

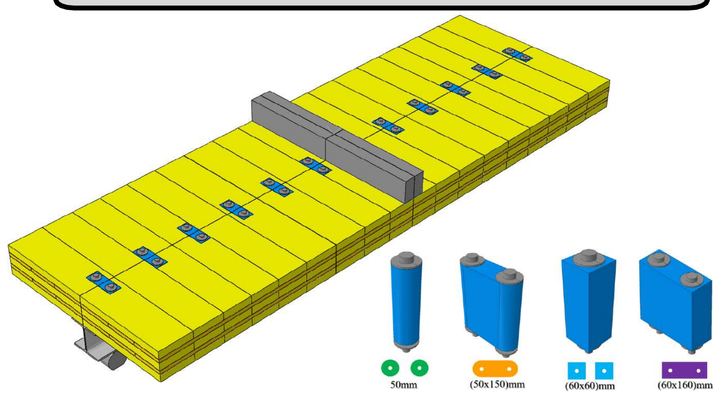

Geometry of the epoxy

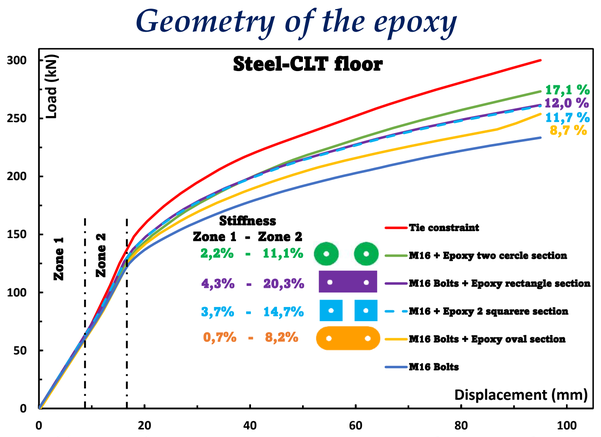

The effect of epoxy presence on the mechanical behaviors of composite floors

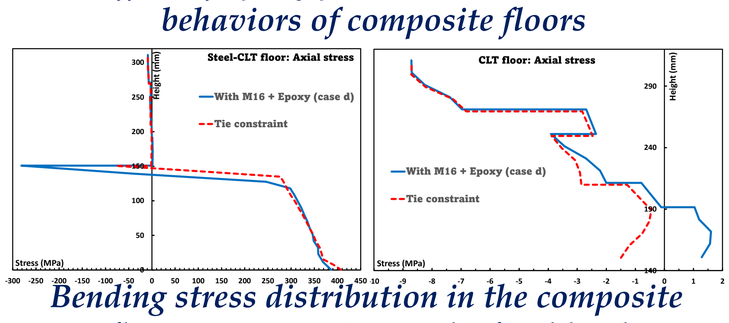

Bending stress distribution in the composite floors cross-section at the final load

Conclusions

- A steel-CLT composite floor can support a maximum load of 232 kN, with an initial stiffness of 6.93 kN/mm before contact between the CLT blocks, which increases to 7.55 kN/mm after this contact.
- The combination of CLT with a HEA160 profile results in a slight increase in the stiffness of the composite floor, but it doubles the maximum strength compared to using only a HEA160 beam.
- Increasing the spacing between CLT blocks reduces the mechanical behavior of the composite floor.
- The use of epoxy around the bolts at the CLT level improves the connection between steel and CLT. Additionally, increasing the contact surface between the CLT and epoxy enhances the degree of connection, although it does not achieve perfect contact.

Bibliography

[1] The Impact of Cement Sustainability Initiative on the South African Cement Industry's Performance - ProQuest.

[2] P. M. Pereira and C. S. Vieira, "A Literature Review on the Use of Recycled Construction and Demolition Materials in Unbound Pavement Applications.

[3] BigRentz, "24 Construction Waste Statistics | BigRentz,"

Study of the mechanical behavior of bio-based concrete by digital image correlation (DIC)

Bardouh Rafik[1], Toussaint Evelyne[1], Amziane Sofiane[1]

1 Université Clermont Auvergne, Clermont Auvergne INP, CNRS, Institut Pascal, F-63000 Clermont-Ferrand, France

Introduction

❑ Context :

Bio-based concrete is a composite material comprising bio aggregates (hemp, rapeseed, miscanthus, bamboo, …) mixed with a mineral binder (prompt natural cement, lime-based binder…) and water. The formulation of these constituents directly influences the mechanical properties obtained for this type of material.

❑ Problematic

The main problem is the heterogeneous response of this type of material based on the constituents and the orientation of aggregates. The variability of the mechanical properties according to the type of aggregate or mineral binder used in the composition of bio-based concrete is very crucial which gives a general approach to what extent the type of constituents used can affect the mechanical properties of bio-based concrete. Another major factor that needs to be considered is the interfacial transition zone (ITZ) which corresponds to a non-hydrated zone around the aggregates that imparts significantly the mechanical properties of bio-based concrete.

❑ Objectives

Generally, the objective is to evaluate the effect of the constituents (aggregates and mineral binder), and the orientation of bio-aggregates on the mechanical properties of bio-based concrete. In order to scientifically investigate this influence, the mechanical properties of bio-based concrete are determined under two scales: macroscopic and local. The local mechanical properties are determined by means of digital image correlation which enables quantifying the floating modulus from the displacement and deformation maps of the bio-based specimen.

Experimental methodology

❑ Bio-based concrete:

- 1 type of mineral binder (the most optimized mineral binder with highest mechanical properties).
- 4 types of bio-aggregates (Hemp, rapeseed, bamboo, reed).
- Formulation: Aggregate:Binder:Water ratio of 1:2:2

Except for Bamboo-based specimens (same rheology): Aggregate:Binder:Water ratio of 1.2:2:2

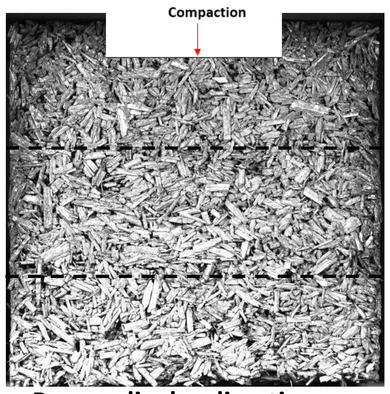

Perpendicular direction

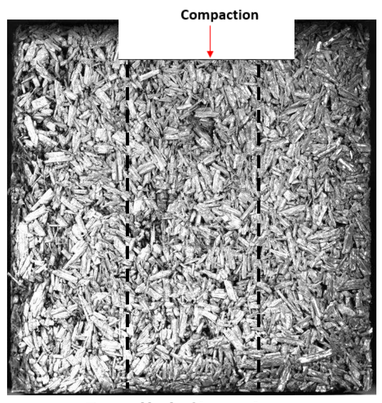

Parallel direction

❑ Tests setup:

- Cyclic compression tests with a global deformation between 1% and 10% with an increment of 0.5 % after each cycle.
- Loading speed: 3 mm/min.
- Unloading speed: 10 mm/ min.
- Floating modulus calculated at an interval of 0.1% in deformation.

❑ Method of measurement

- Non-contact field measurement
- Digital image correlation
- PCO camera of 2048 × 2048 pixels.
- Acquisition frequency of 1Hz (1 image / second).

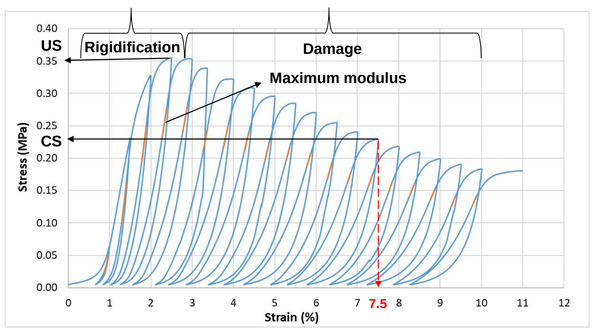

(a)

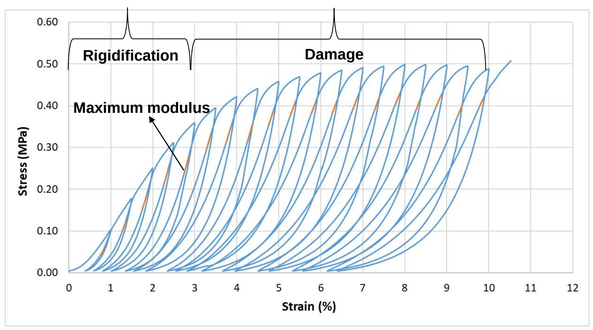

(b)

Example of cyclic compression stress-strain curves for a particular bio-based specimen (CEMIV-Hemp) with 19 cycles of loading-unloading, and the exploitation methodology of the floating modulus (orange lines) for the two aggregates' orientation, (a): parallel orientation ; (b): perpendicular orientation.

Results

❑ Mechanical macroscopic properties of CEMIV-based specimens with the different types of aggregates

➢ Compressive strength (CS) and Useful strength (US)

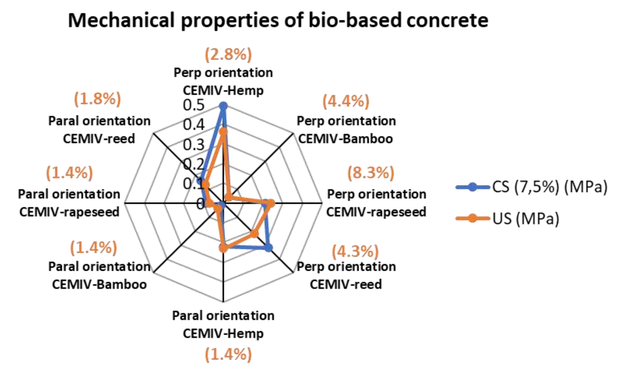

➢ Modulus of elasticity (E)

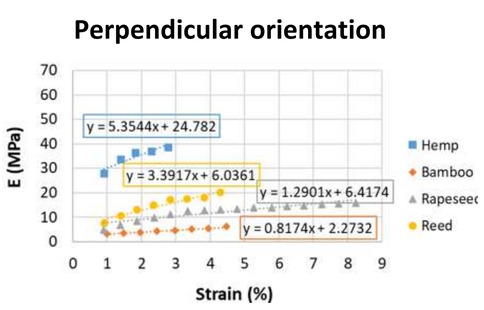

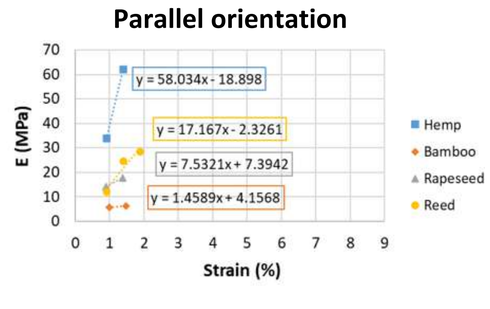

❑ Damage behavior of bio-based specimens

$E_{end} = E_0 (1-D)$

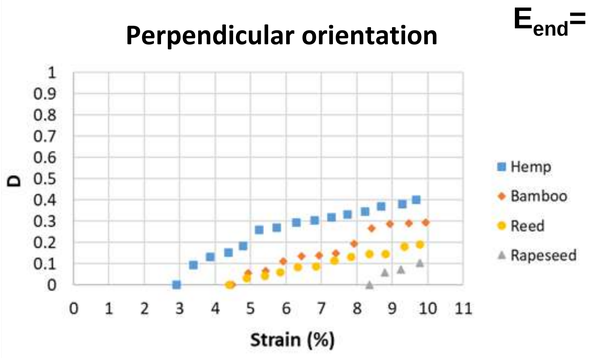

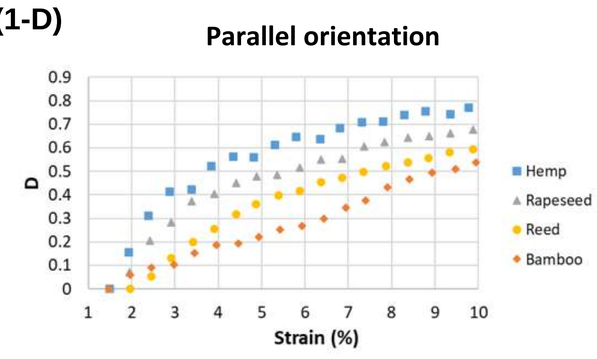

❑ Vertical displacement maps through DIC during damage

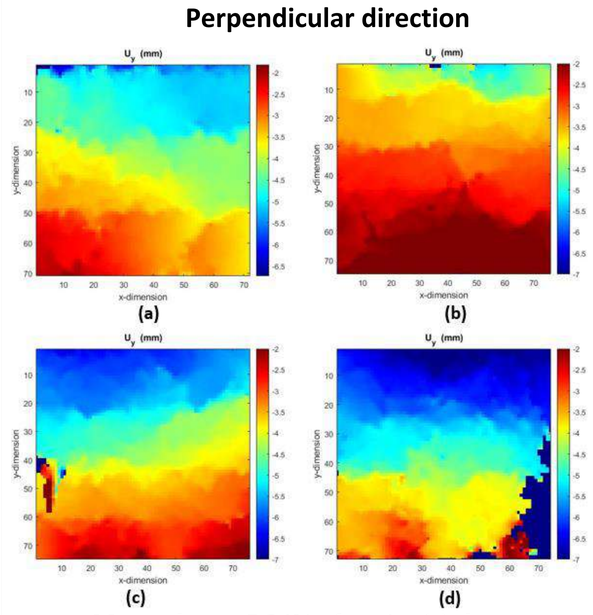

Maps taken at 5.24% of strain, (a): hemp concrete, (b): rapeseed concrete, (c): reed concrete, (d): bamboo concrete

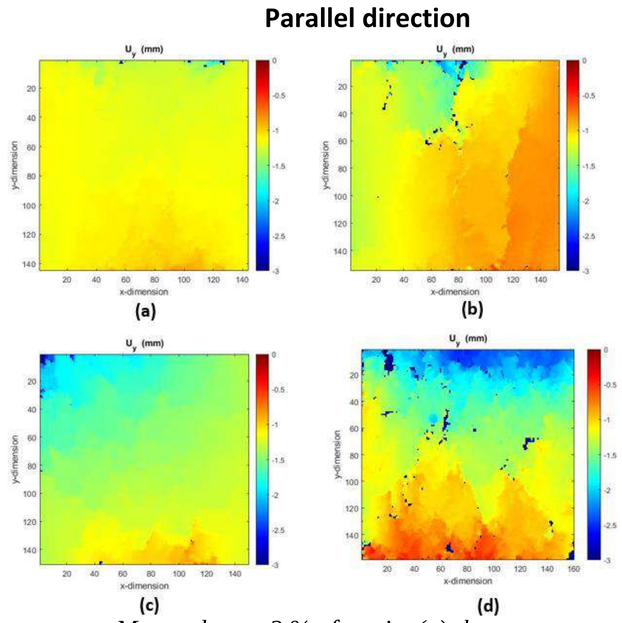

Maps taken at 2 % of strain, (a): hemp concrete, (b): rapeseed concrete, (c): reed concrete, (d): bamboo concrete

Conclusions and perspectives

- The specimens tested in parallel orientation are more rigid at low strain than those tested perpendicularly except the bamboo-based specimens.
- Useful strength in the parallel orientation determines the coating strength between mineral binder and aggregate rather than the actual strength of the material.
- The most damaged specimen (Hemp concrete) is the least displaced and vice-versa.
- Future perspectives are about determining the local mechanical properties around the aggregate in a zone commonly called interfacial transition zone (ITZ) as seen below.

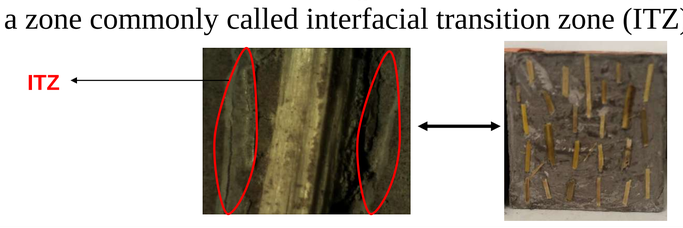

Bibliography

- Niyigena, César, et al. "Variability of the mechanical properties of hemp concrete." *Materials Today Communications* 7 (2016): 122-133.
- Delhomme, Fabien, et al. "Effect of hemp on cement hydration: experimental characterization of the Interfacial Transition Zone." Results in Chemistry 4 (2022): 100440.
- Amziane, Sofiane, and Florence Collet, eds. *Bio-aggregates based building materials: State-of-the-art report of the RILEM technical committee 236-BBM*. Vol. 23. Springer, 2017.
- Bardouh, Rafik, et al. "Towards Biobased Concretes with Tailored Mechanical Properties." *International Conference on Bio-Based Building Materials*. Cham: Springer Nature Switzerland, 2023.

Molecular Modeling and Prediction of the Physicochemical Properties of Polyols in Aqueous Solution

Maria Fontenele [♠◇] Claude-Gilles Dussap [♠] Vincent Dumouilla [◇] Baptiste Boit [◇]
[♠]Institut Pascal, Université Clermont Auvergne, CNRS, Clermont Auvergne INP, Clermont-Ferrand, France
[◇]Roquette Frères, Biotechnology and Process Development, Lestrem, France

1 Introduction

Roquette uses advanced modeling and simulation techniques to optimize their industrial processes, focusing on aqueous mixtures of polyols, specifically sorbitol and mannitol. These compounds have similar structures, but different solubilities in water. We employ the COSMO-UCA model, developed by Institut Pascal's GePEB team, which integrates quantum mechanics tools and molecular dynamics simulations to predict phase equilibrium properties based on the molecules' structures. This allows accurate predictions of physicochemical properties like activities and solubilities in aqueous solutions.

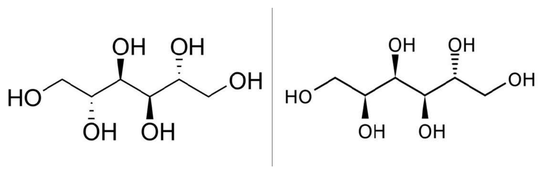

Figure 1: Mannitol (right) and sorbitol (left) structures.

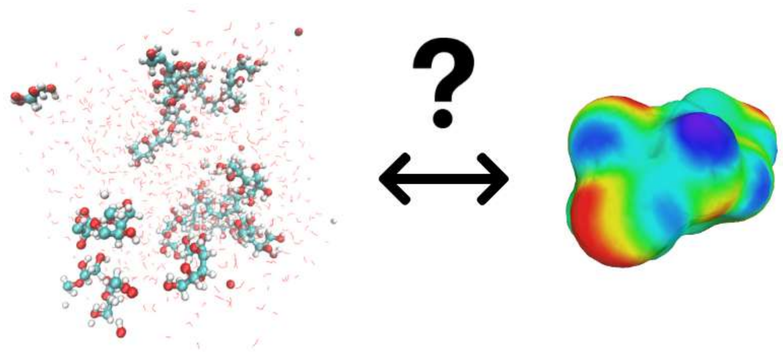

Figure 2: Simulation box containing 10 molecules of sorbitol (left) and COSMO surface of the sorbitol molecule (right).

2 Methods

2.1 Molecular Dynamics Simulations

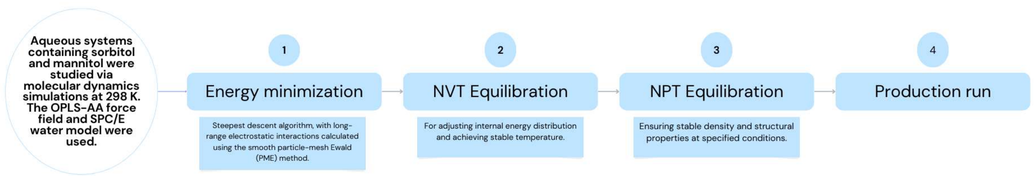

Figure 3: Flowchart of the calculation method on molecular dynamics.

A time autocorrelation function is used to measure hydrogen bonds and to compute lifetimes.

2.2 COSMO Models

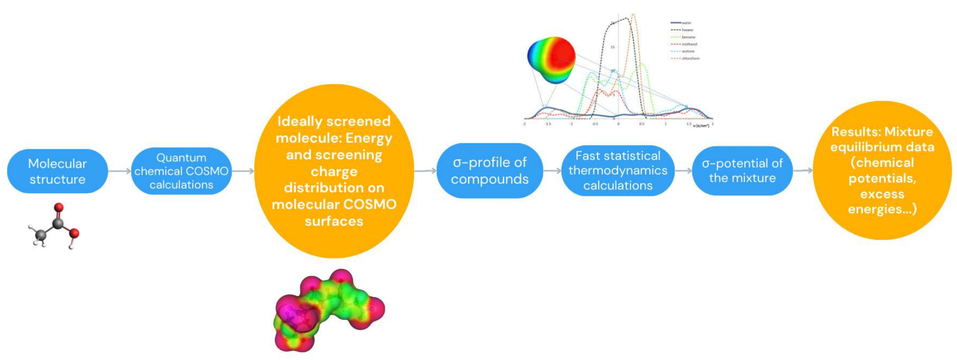

Figure 4: Flowchart of a COSMO calculation.

Activity values were calculated using the COSMO-UCA approach. The solubility of sorbitol and mannitol in water was modeled using the following equation:

$$-ln(x_i\gamma_i^L) = \frac{\Delta H^0_{i,fus}(T_m)}{RT_m}\left(\frac{T_m}{T}-1\right) + \frac{\Delta Cp_{i,fus}}{R}\left(ln\frac{T_m}{T}+1-\frac{T_m}{T}\right) \quad (1)$$

3 Results

3.1 Hydrogen Bond Lifetime

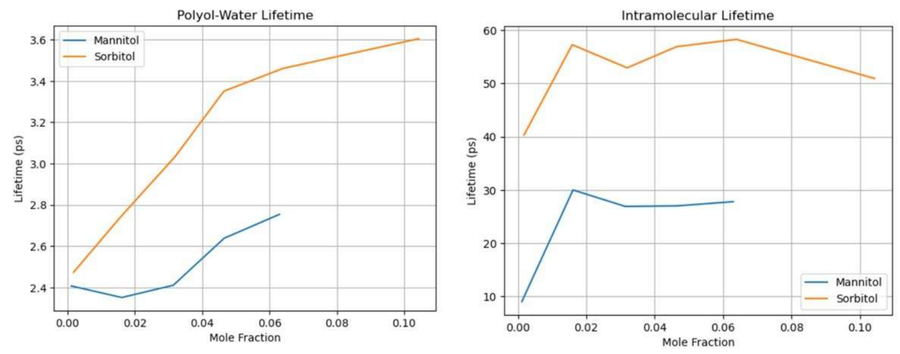

Figure 5: Lifetimes of the hydrogen bond between polyol and water for different concentrations (left); Lifetimes of the polyol intramolecular hydrogen bonds for different concentrations (right).

3.2 Solubilities

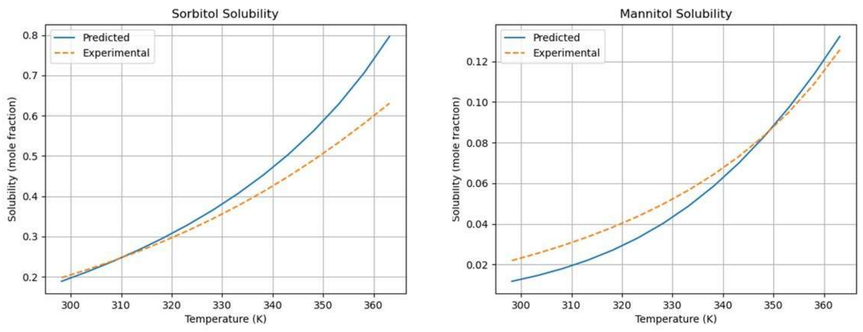

Figure 6: Solubilities of sorbitol (left) and mannitol (right) as predicted by COSMO-UCA.

4 Conclusions

Through molecular dynamics simulations, we determined the lifetimes of hydrogen bonds between water and polyols, as well as intramolecular hydrogen bonds. Interestingly, sorbitol exhibits significantly longer average hydrogen bond lifetimes with water compared to mannitol, potentially elucidating its greater solubility. Conversely, mannitol displays longer lifetimes of intramolecular hydrogen bonds.
When computing the solubilities of sorbitol and mannitol in water using COSMO models, the COSMO-UCA model demonstrates favorable agreement with experimental data, boasting standard deviation values of 0.041 for sorbitol and 0.008 for mannitol in mole fraction.

References

[1] C-G. Dussap O. Toure, A. Lebert. Extension of the cosmo-rs-pdhs model to the prediction of activity coefficients in concentrated water-electrolyte and water-polyol solutions. *Fluid Phase Equilibria*, 2016.

[2] J. Barnoud T. J. E. Reddy M. N. Melo S. L. Seyler D. L. Dotson J. Domanski S. Buchoux I. M. Kenney R. J. Gowers, M. Linke and O. Beckstein. Mdanalysis: A python package for the rapid analysis of molecular dynamics simulations. *S. Benthall and S. Rostrup, editors, Proceedings of the 15th Python in Science Conference*, pages 98–105, 2016.

Methods to assess and improve the QoIS(1) of an agricultural/environmental CT(2)

Samy Benhoussa Gil De Sousa Jean-Pierre Chanet

INRAE + clermont auvergne métropole

CLERMONT AUVERGNE INP ÉCOLE DOCTORALE DES SCIENCES POUR L'INGÉNIEUR

UCA UNIVERSITÉ Clermont Auvergne

(1) : Quality Of Information Service
(2) : Connected Thing

Introduction

The advent of connected devices, often referred to as the Internet of Things (IoT), has revolutionized numerous sectors, with environmental and agriculture being among the most profoundly impacted. These devices, embedded with sensors, software, and other technologies, are capable of exchanging data with other devices and systems over the internet. This interconnected network enables real-time data collection, analysis, and decision-making, paving the way for smarter, more efficient practices.

In the following thesis subject, we focus on a metric that we define as «The Quality of Information Service». This metric defines how much is a connected device providing useful data to the user, but also, how much the decision making process is correct, and all of that must be achieved while respecting the energy, memory and computational contraints of connected devices.

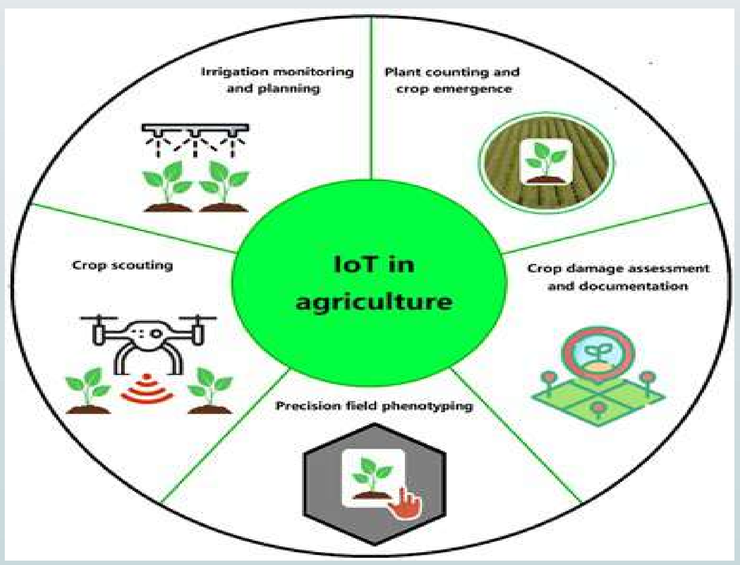

© Paola G. Vinueza-Naranjo

Methods

Layers of data

We define 3 levels of data : Raw data, Information and Knowledge. Example : for a classification/object detection task done by a smart camera, data exist as one of the following layers :

Pixels (Raw data)

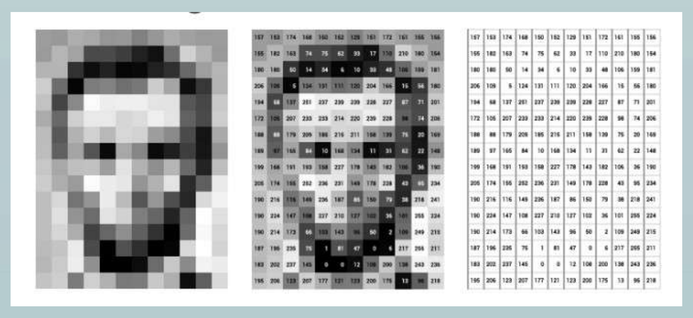

© Thomas Smits

Features (Information)

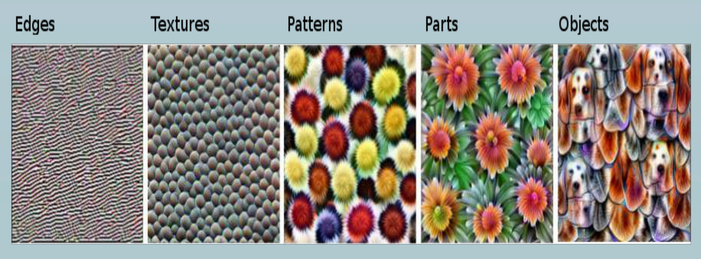

© Christoph Molnar

Predicted labels (Knowledge)

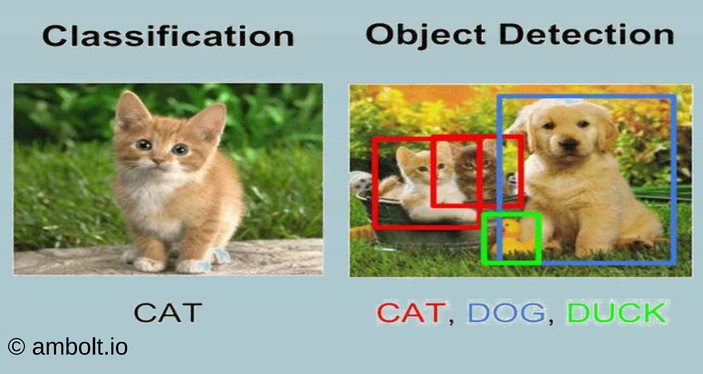

© ambolt.io

The Quality of Information Service

In the litterature, we found that Quality of Information was already studied in some papers. The QoI is usually related to one of the previously evoqued data layers.
In our study we define QoIS relatively to the process of transforming data from its first layer (raw data) to the final one (knowledge). We aim to find a method that deduces knowledge from raw data with the less energy cost in connected devices.
Deducing knowledge from raw data susually takes a decision making process that relies on machine learning. The training phase is much more costing in energy and computational concerns. An innovative method to have the best QoIS of a connected device accordingly to our definition is Federated Learning.

Federated Learning

In federated learning, the model is trained in each device locally, then the weights are aggregated to develop a global knowledge. It is more energy efficient since big amounts of data are not transmitted between devices but only the model weights.

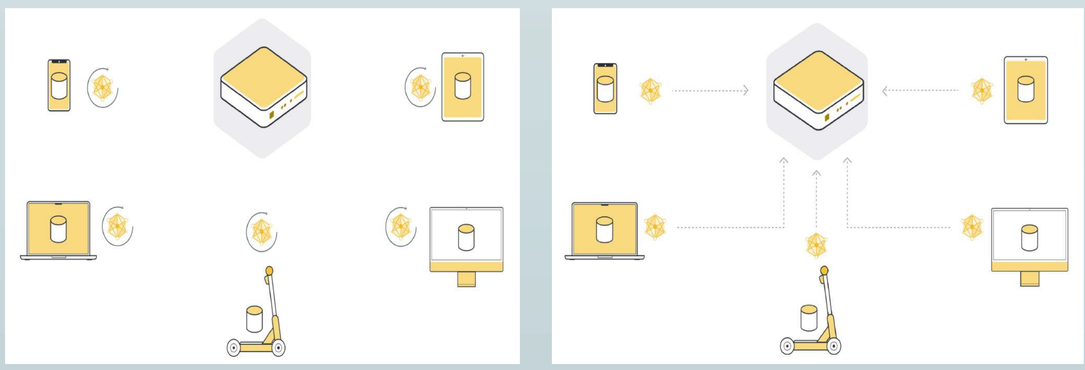

© Github/flower

Results

We can get the same performance with Federated Learning compared to the classical centralized Machine Learning scheme but with less energy loss.

Conclusions

The use of IoT and connected devices in environmental and agricultural use cases showed great benefits. But the use of big amounts of data and its transmission can be problematic. In our study we proposed a method to achieve a good decision making process by limiting the energetic waste : Federated Learning. The metric we used to evaluate our novel method is the Quality of Information Service as we define it. An implementation of the system using RaspBerry Pis connected to cameras showed a good performance of Federated Learning compared to a classical centralized Machine Learning scheme.

Bibliography

1. **Atzori, L.; Iera, A.; Morabito, G. The internet of things: A survey. Computer networks 2010, 54, 2787–2805**
2. **Sachidananda, V.; Khelil, A.; Suri, N. Quality of Information in Wireless Sensor Networks: A Survey. Dependable, Embedded Systems and Software Group 2010, 10.**
3. **Bharati, Subrato and Mondal, M. Rubaiyat Hossain. Federated learning: Applications, challenges and future directions**

Skeleton-Based Action Recognition with Spatial-Structural Graph Convolution

Jingyao WANG
LIMOS, CNRS UMR 6158
LPC, CNRS UMR 6533
Université Clermont Auvergne
Jingyao.wang@uca.fr

Emmanuel BERGERET
LPC, CNRS UMR 6533
Université Clermont Auvergne
emmanuel.bergeret@uca.fr

Issam FALIH
LIMOS, CNRS UMR 6158
Université Clermont Auvergne
issam.falih@uca.fr

1) Introduction

Human activity recognition

Smartwatch: Fall detection, sports recognition
Security camera: Abnormal activity recognition
Smarthome: Gesture control

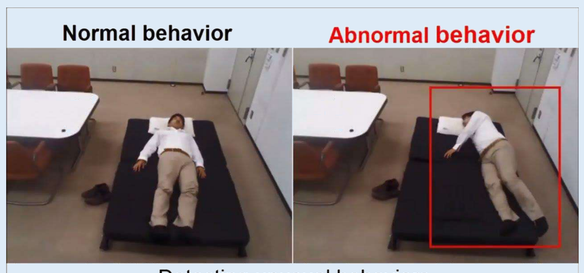

Detecting unusual behaviors
(lying on the stomach or falling, for instance)

Skeleton data

Source: RGB data, depth data

Characteristic: Spatial-temporal data, Limited computing cost, Privacy protection, Preservation of topology

Representation: Matrix, Graph

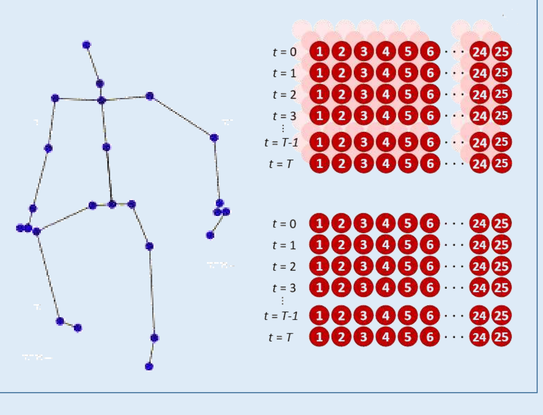

2) Graph Neural Network (GCN)

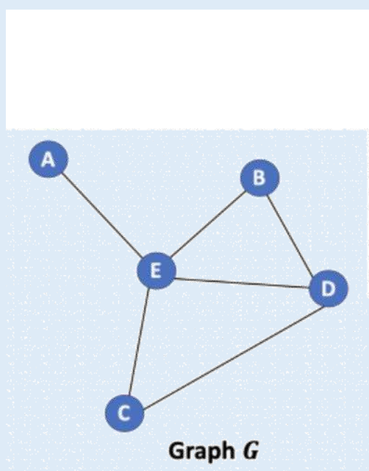

Graph *G*

	A	B	C	D	E
A	0	0	0	0	1
B	0	0	0	1	1
C	0	0	0	1	1
D	0	1	1	0	1
E	1	1	1	1	0

Adjacency matrix *A*

	A	B	C	D	E
A	1	0	0	0	0
B	0	2	0	0	0
C	0	0	2	0	0
D	0	0	0	3	0
E	0	0	0	0	4

Degree matrix *D*

$$X' = D^{-\frac{1}{2}}(A+I)D^{-\frac{1}{2}}XW$$

A	-1.1	3.2	4.2
B	0.4	5.1	-1.2
C	1.2	1.3	2.1
D	1.4	-1.2	2.5
E	1.4	2.5	4.5

Feature vector *X*

Physical topology →
Does the skeleton topology well represent the skeleton data ?

GCN over-smoothing problem →
How to overcome GCN over-smoothing problem ?

3) Spatial-Structural Graph Convolution (SpSt-GCN)

Conventional Spatial connection:
Fixed, maintains topology of skeleton data
Structural connection:
Dynamic, depends on the type of movement the human body is performing

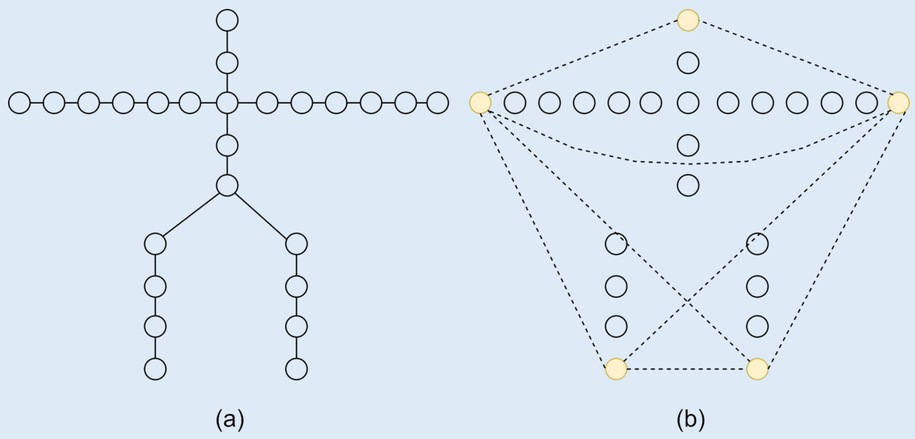
(a) (b)

Conventional spatial graph convolution $f_{outSpatial} = \sum_j W_j f_{in} \Lambda_j^{-\frac{1}{2}} A_j \Lambda_j^{-\frac{1}{2}}$

To increase the flexibility $f_{outSpatial} = \sum_j W_j f_{in} (\Lambda_j^{-\frac{1}{2}} A_j \Lambda_j^{-\frac{1}{2}} + B_j)$

Structural graph convolution $f_{outStructural} = \sum_j M_j f_{in} A s_j$

Final output of SpSt-GCN block $f_{out} = f_{outSpatial} + f_{outStructural}$

4) Spatial-Structural Graph Convolution (SpSt-GCN)

Algorithm 1: Structural Adjacency Matrix Calculation

Input: input sequence $i[C_{in}, T_{in}, V_{in}]$
Output: structural adjacency matrix As with size $[V_{in}, V_{in}]$

D: an all-zero array with size $[V_{in}, V_{in}]$;
I: an identity array with size $[V_{in}, V_{in}]$;
edge: edge nodes set;
foreach *i* **do**
  for *a in edge* **do**
    for *b in edge* **do**
      if $a \neq b \wedge D[a][b] == 0$ **then**
        D[a][b] = FastDTW(i[:,:,a], i[:,:,b]);
        D[b][a] = D[a][b];
      end
    end
    $As = -D^{-1} + I$;
  end
end

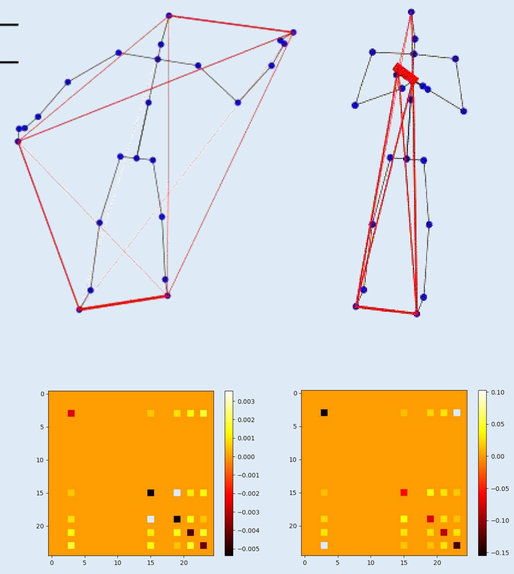

5) Model

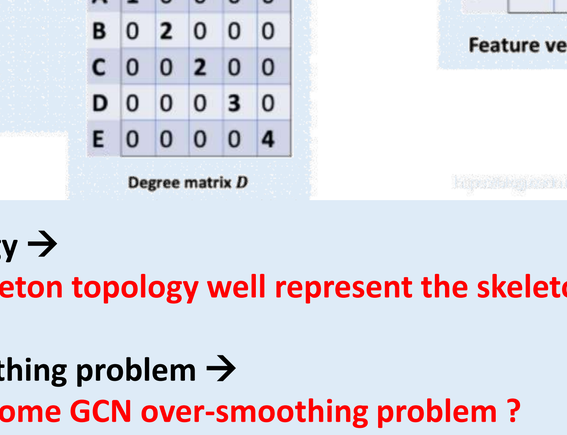

(a) Initial block (b) GCN layer (C) GCN block

6) Evaluation

Inputs	Spatial GCN	Spatial-Structural GCN
Joint	86.89	**87.88**
Velocity	87.17	**87.29**
Bone	87.82	**88.20**
Joint+Velocity	90.19	**90.69**
Joint+Bone	89.53	**90.02**
Velocity+Bone	90.66	**91.03**
Joint+Velocity+Bone	91.10	**91.62**

TABLE I: Comparisons of different inputs on NTU60 X-sub benchmark in accuracy (%)

Inputs	Spatial GCN	Spatial-Structural GCN
Joint	91.82	**92.35**
Velocity	93.27	**93.53**
Bone	92.27	**92.94**
Joint+Velocity	95.08	**95.23**
Joint+Bone	94.10	**94.47**
Velocity+Bone	95.28	**95.51**
Joint+Velocity+Bone	95.61	**95.79**

TABLE II: Comparisons of different inputs on NTU60 X-view benchmark in accuracy (%)

Model	Acc	FLOPs	Param
ST-GCN* [28]	81.5	16.32*	3.10*
SR-TSL* [23]	84.8	4.20*	19.07*
AS-GCN* [10]	86.8	26.76*	9.50*
2s-AGCN* [21]	88.5	37.32*	6.94*
SGN [33]	89.0	-	0.69
AGC-LSTM [22]	89.2	-	22.89
PL-GCN [7]	89.2	-	20.70
NAS-GCN [15]	89.4	-	6.57
DGNN [20]	89.9	-	26.24
EfficientGCN-B0 [25]	90.2	2.73	0.29
4s-Shift-GCN [6]	90.7	10.0	2.76*
DC-GCN+ADG* [5]	90.8	25.72*	4.96*
MS-G3D* [14]	91.5	48.88*	6.40
Dynamic-GCN [30]	91.5	-	14.40
MST-GCN [4]	91.5	-	12.00
CTR-GCN [3]	92.4	1.97	1.46
Sp-GCN(ours)	91.1	4.25	0.44
SpSt-GCN(ours)	91.6	4.90	0.48

*: These results are implemented by [25]

TABLE V: Comparisons with SOTA methods on NTU RGB+D X-sub benchmark on accuracy(%), FLOPs($\times 10^9$) and parameter number ($\times 10^6$), Sp-GCN has only spatial branch in GCN layer, SpSt-GCN has both spatial and structural branch in GCN layer.

7) Conclusion

1. We propose a spatial-structural graph convolution method which can better represent symmetrical human structures and edge nodes.
2. We adopt a differential approach to initialize the structural connections of various samples.
3. We utilize the inverse adjacency matrix to discern information pertaining to edge nodes to address the over-smoothing problem in GCN.

Artificial Intelligence: The Driver of Autonomous Cars Facing the Weather Challenge

[1]Hamed Ouattara

Directed by [1]Frédéric Bernadin and [2]Omar AIT-AIDER, and supervised by [1]Pierre Duthon

[1] CEREMA - 8 Rue Bernard Palissy, 63100 Clermont-Ferrand [2]Institut Pascal – Campus Universitaire des Cézeaux, 4 Av. Blaise Pascal, 63178 Aubière

Introduction

Autonomous cars aim to drive without a human driver. But what happens when clear skies turn into a storm? Rain, fog, or heavy snow can disrupt sensors, making object detection tricky. This is the challenge tackled by the ROADVIEW project (Robust Automated Driving in Extreme Weather). In partnership with Cerema, my thesis is part of this project : Simulation and Measurement of Degraded Weather Conditions Using Artificial Intelligence and Computer Vision. It is split into two parts:

1- Weather Simulation: Transforming an image or video of one weather condition into another (e.g., sunny to rainy).

2- Weather Detection: Identifying the weather (rain, snow, fog) and its intensity from images or videos.

Weather Simulation: How To Do It?

Data

We have created a dataset with 1,500,000 images containing pictures of the four weather conditions: rain, snow, fog, sunny. These images will need to go through an algorithm to change the weather

How to Organize This Data for Better Learning?

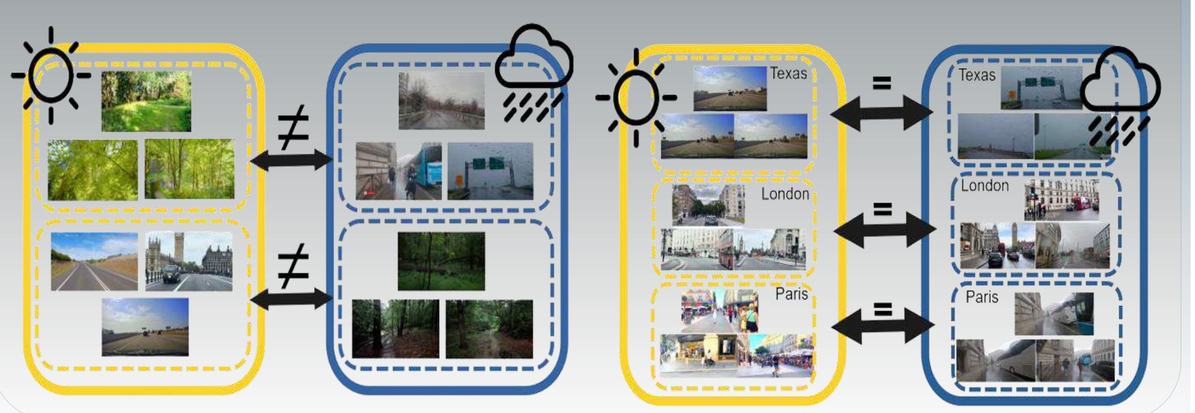

Algorithms

We have chosen the CycleGAN[1] algorithm, which enables style transfer between unpaired images (showing different scenes), meaning it can learn to transition from sunny weather to rainy weather using images of sunny Paris and rainy Rome.

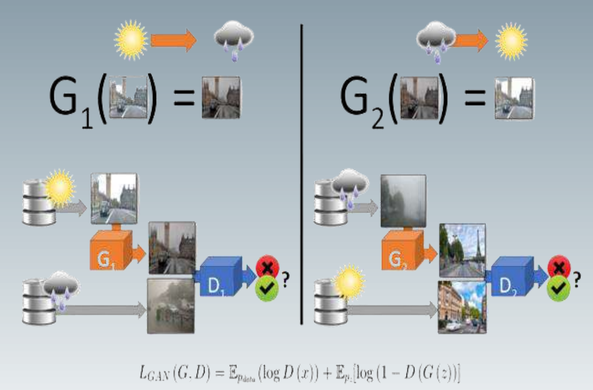

$$L_{GAN}(G, D) = \mathbb{E}_{p_{data}}(\log D(x)) + \mathbb{E}_{p_z}[\log(1 - D(G(z))]$$

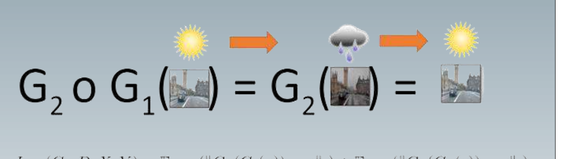

$$L_{cycle}(G_2, D, X, Y) = \mathbb{E}_{x \sim P_r}(\|G_2(G_1(x)) - x\|_1) + \mathbb{E}_{y \sim p_y}(\|G_1(G_2(y)) - y\|_2).$$

1. Jun-Yan Zhu, Taesung Park, Phillip Isola, Alexei A. Efros, Unpaired Image-to-Image Translation using Cycle-Consistent Adversarial Networks, Zhu2017

New Methods and Resuts

We propose a new method called Group2Group, which involves parallelizing sets of images differing only in weather conditions

Usual Methods

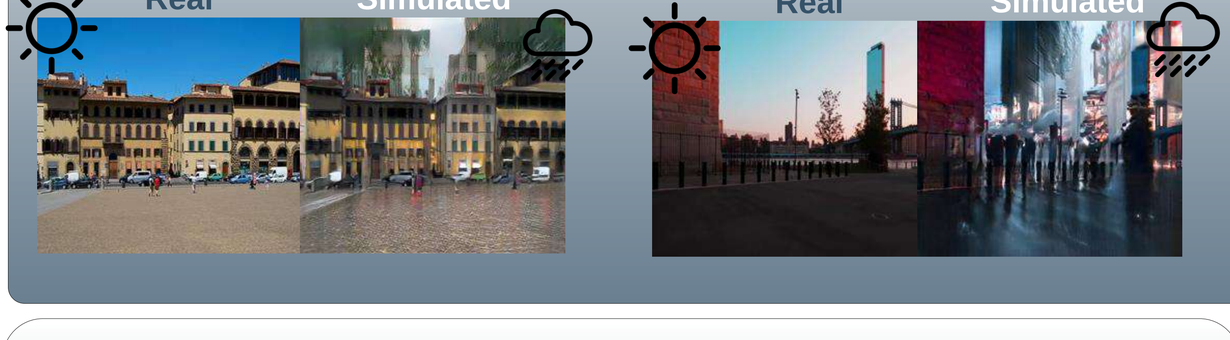

Methods Group2Group

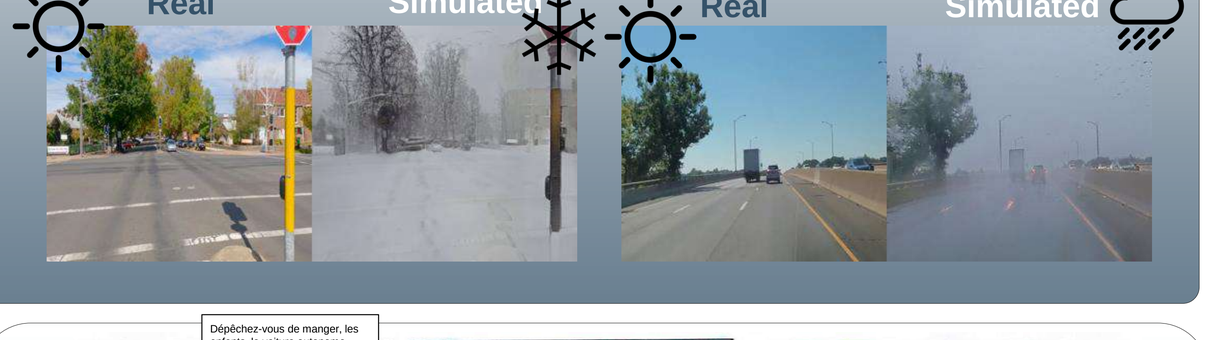

More results with Methods Group2Group

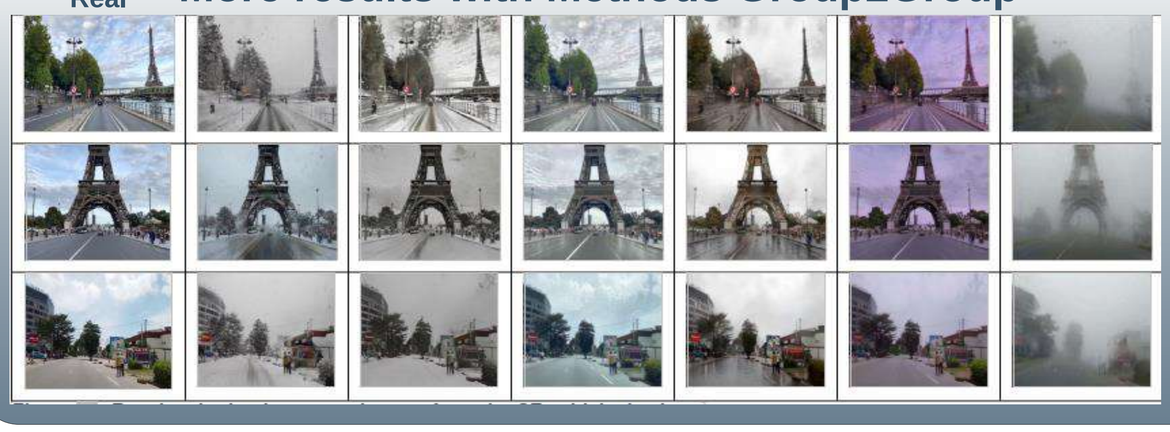

Remaining Tasks:

- Develop an initial prototype model for weather detection (measurement.)
- Reduce data costs by exploring other methods to minimize artifacts.
- Implement objective evaluation methods to weather generation.

Funded by the European Union(grant no. 101069576). Views and opinions expressed are however those of the author(s) only and do not necessarily reflect those of the European Union or European Climate, Infrastructure and Environment Executive Agency(CINEA) . Neither the European Union nor the granting authority can be held responsible for them. UK and Swiss participants in this project are supported by Innovate UK(contrat no. 10045139) and the Swiss State Secretariat for Education, Research and Innovation (contract no. 22.00123) respectively.

We want to contribute to a better world, contact us!

Kinematic Measurment by Digital Image Stereo-Correlation on a Finite Element Basis

Houssein MATAR[1], Benoît BLAYSAT[1], Thomas JAILIN[1], Omar AIT-AIDER[1], Michel GRÉDIAC[1], Hélène CHANAL[1]

[1]CNRS, Institut Pascal, Université Clermont Auvergne, Clermont-Ferrand

Contact: houssein.matar@uca.fr

Introduction

- Stereo Digital Image Correlation (**S-DIC**) is a powerful technique used in experimental mechanics to measure the 3D displacement of a sample surface during mechanical testing. **S-DIC** requires at least two cameras.
- Two avenues exist for **S-DIC** formulation: **Local** or **Global approaches**. The **global** framework is chosen in this work, especially because it enables measurements expressed in the physical coordinate system based on a **finite element** model.

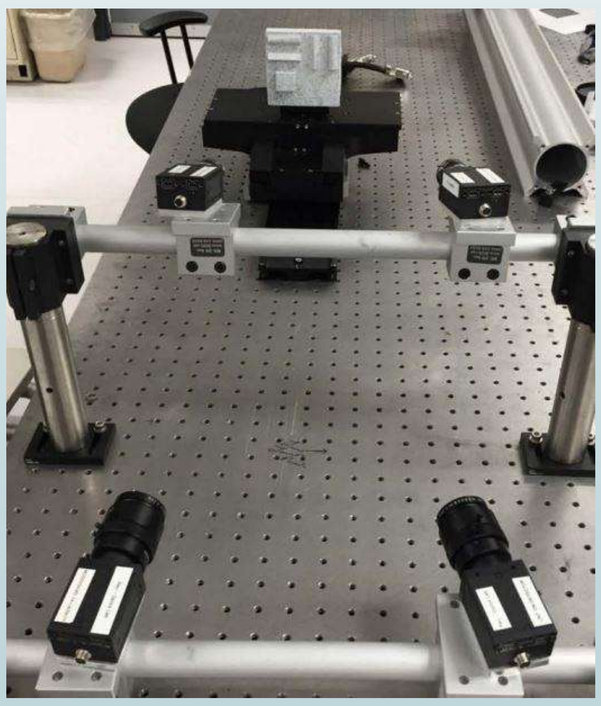

Figure 1. Aerotech stage setup with two usual stereo-based camera systems. The front system relies on two 16-mm lenses, and the back system on two 35-mm lenses. (Stereo-DIC Challenge data set [1]).

Goals

- To propose a **unified framework** for multi-camera system calibration, shape fine-tuning, and kinematic measurements.
- To freely provide a robust **FE-based S-DIC Python library**. Well-known and optimized open-source libraries will be extensively used for computational cost reduction.

Methods

Introducing the unified framework:

The usual **S-DIC** problem is formulated in the object reference system. The formulation uses a mesh representation of the object of interest. With N cameras, the **S-DIC** criterion writes:

$$\underline{\theta}^*, \underline{F}^* = \underset{(\underline{\theta},\underline{S})\in\mathbb{R}^{6N}\times\mathbb{L}^2}{\operatorname{argmin}} \frac{1}{2} \sum_{i_{\mathrm{cam}}=0}^{N-1} \sum_{j_{cam}=i_{cam}+1}^{N} \left(r_{i_{cam},j_{cam}}\right)^2, \text{where:}$$

$$r_{i_{cam},j_{cam}} = I_{i_{cam}} \circ P\left(\underline{X}+\underline{F},\underline{\theta}_{i_{cam}}\right) - I_{j_{cam}} \circ P\left(\underline{X}+\underline{F},\underline{\theta}_{j_{cam}}\right)$$

- $I_{i_{cam}}$: Image taken by the i_{cam}^{th} camera.
- P: World to sensor plane projection operator; where collects the camera extrinsic parameters.
- $\underline{X}$: 3D integration points, defined within the mesh of the object surface.
- $\underline{\theta}$: Vector collecting the extrinsic parameters of N cameras.
- $\underline{F}$: Field of interest, defined through a FE-model.
- $\boldsymbol{r_{i_{cam},j_{cam}}}$: Residual corresponding to the perception difference of the object surface between i_{cam} and j_{cam} cameras.

Experimental scene fine tuning:

Two steps must be performed before **3D displacement measurement**. They aim at adjust the **calibration of the camera systems** and to update the **CAD shape** of the object to make it corresponding to the real one.

Kinematic measurments:

$$\underline{F}^* = \underset{(\underline{\theta},\underline{F})\in\mathbb{R}^{6N}\times\mathbb{L}^2}{\operatorname{argmin}} \frac{1}{2} \sum_{t=0}^{N-1} \sum_{i_{\mathrm{cam}}=0}^{N-1} \sum_{j_{cam}=i_{cam}+1}^{N} \left(r^t_{i_{cam},j_{cam}}\right)^2$$

$$r^t_{i_{cam},j_{cam}} = I^t_{i_{cam}} \circ P\left(\underline{X}+\underline{F},\underline{\theta}_{i_{cam}}\right) - I^t_{j_{cam}} \circ P\left(\underline{X}+\underline{F},\underline{\theta}_{j_{cam}}\right)$$

- $I^t_{i_{cam}}$: Image taken by the t camera at i_{cam} instant.

Results

- 3D finite element mesh projected into the reference image of the Stereo-DIC Challenge data set [1].

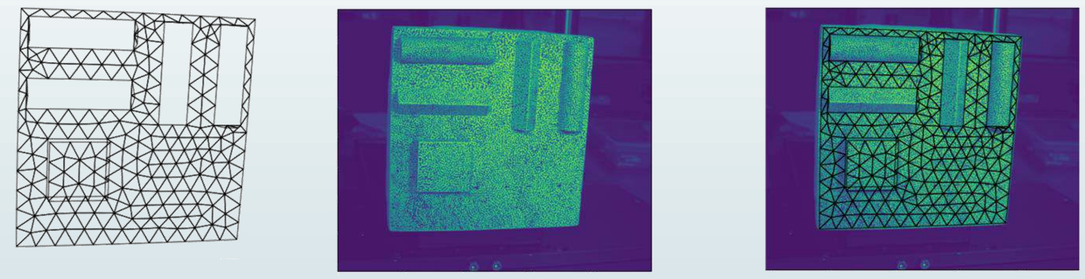

- Maps of initial difference residual $\boldsymbol{r_{i_{cam},j_{cam}}}$ and convergence of the residual map after S-DIC iterations.

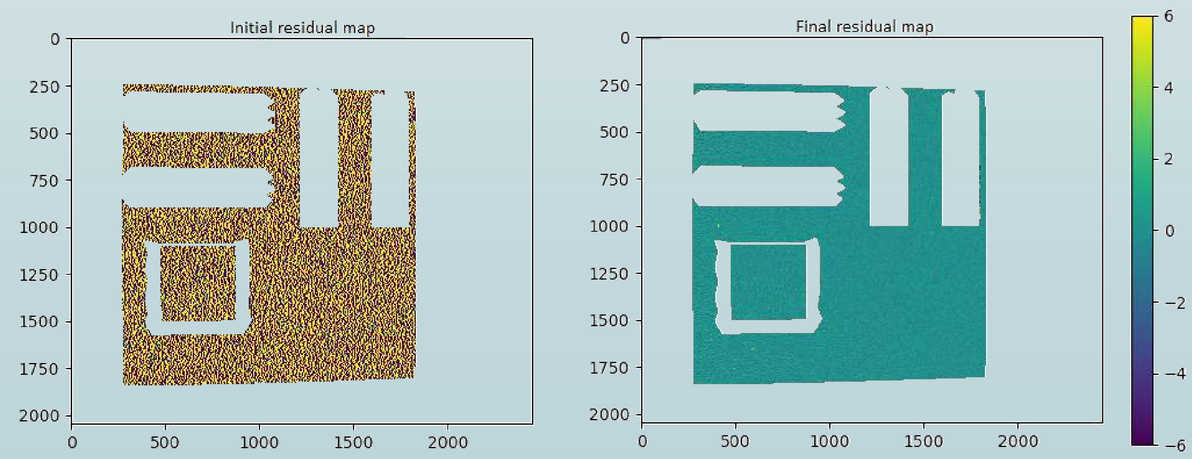

- Comparison between proposed method solution and DIC-Challenge [1] solution, for the multi-camera system calibration. (Right camera of 35-mm system **figure 1**.)

Rotation (radians):			
	r_x	r_y	r_z
Proposed method solution	-0.0105	0.184	-0.0053
DIC-Challenge [1] solution	-0.0103	0.185	-0.0051

Translation (mm):			
	t_x	t_y	t_z
Proposed method solution	-17.5133	-3.6308	-301.371
DIC-Challenge [1] solution	-17.692	-3.581	-301.74

Conclusions

- ✓ The algorithm converge very quickly towards an acceptable solution.
- ✓ The displacement expressed in the finite element space is calculated in the 3 directions between a reference state and the deformed state on the basis of a 3D geometry and this one is expressed in the same discretization space as that used for the simulations.
- ✓ 4 cameras were employed.
- ✓ Python library designed to perform (S-DIC) with (FE) analysis, directly in the reference system of interest.
- ✓ Results are in agreement with the exact solution of Stereo DIC Challenge set [1].

Bibliography

1. **Balcaen, R., Wittevrongel, L., Reu, P.L. et al. Stereo-DIC Calibration and Speckle Image Generator Based on FE Formulations.**
2. **COLANTONIO, Guillaume, MARENIC, Eduard, et PASSIEUX, Jean-Charles. Stéréo-DIC globale appliquée à l'identification des paramètres d'une loi de comportement. In : 24e Congres Français de Mécanique (CFM). 2019.**

Investigation of the crack pattern of an FRCM eco-composite using the digital image correlation method (DIC): effects of mineral pre-impregnation and short flax fibres

Gatien O. AGOSSOU[1], Omayma HOMORO[1], Sofiane AMZIANE[1]

[1]Université Clermont Auvergne, Clermont Auvergne INP, CNRS, Institut Pascal, F-63000 Clermont-Ferrand, France

Introduction

Context:

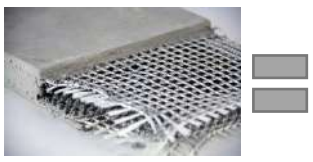

Mineral matrix + **Continuous yarns**

Mineral matrix	Continuous yarns
Portland cement, calcium aluminate cement, phosphate cements...	▪ **Nature of fibres:** glass, aramid, basalt, carbon... ▪ **textile technology:** weaving, knitting, braiding...

Fabric Reinforced Cementetious Matrix (FRCM)

- ✓ high tensile strength
- ✓ Compatibility with substrates
- ✓ Easy to apply …

⚠ Synthetic fibres + Cement ⇨ Non-negligible environmental impact

Problematic:

The cracking mechanism of FRCM composites is an important aspect that highlights the capacity of the composite action, which is essential for the effectiveness of reinforcement systems. It is therefore important to focus on the crack pattern and its evolution during loading. Commonly used measurement methods such as LVDT and strain gauges have limitations when it comes to characterising mechanical behaviour at the local scale, especially regarding the propagation, number and opening of cracks in FRCM composites. Moreover, they often tend to confuse out-of-plane movements with deformations, leading to an overestimation of the actual deformation of the material.

Objective:

- Evaluate the influence of textile pre-impregnation in the mineral matrix on the mechanical behaviour of the FRCM.
- Evaluate the influence of short fibres in the matrix on the mechanical behaviour of the FRCM
- Quantify the number and propagation of cracks in the FRCM

Experimental mode

- Flax texile

- Short Flax fibres (6 mm): volume fraction substitution (0.5%)

- Flax-FRCM

- Prompt Natural Cement (CNP) W/C= 0,5

Experimental configurations

- FRCM.2L.FL: Flax-FRCM composite with two layers (2L) of non-pre-impregnated linen fabric (FL);
- FRCM.2L.FL.I: Flax-FRCM composite with two layers (2L) of pre-impregnated (I) flax fibre (FL);
- FRCM.2L.FL.F: Flax-FRCM with two layers (2L) of non-pre-impregnated flax textile (FL) and addition of short flax fibres (F) in the matrix;
- FRCM.2L.FL.F.I: Flax-FRCM composite with two layers (2L) of pre-impregnated (I) flax textile (FL) and the addition of short flax fibres (F) in the matrix.

Experimental method

- Tensile test with a load rate of 0.3 mm/min
- Use of stereo digital image correlation
- Data processing software: MatchID stereo

Figure 1. Test setup

Results

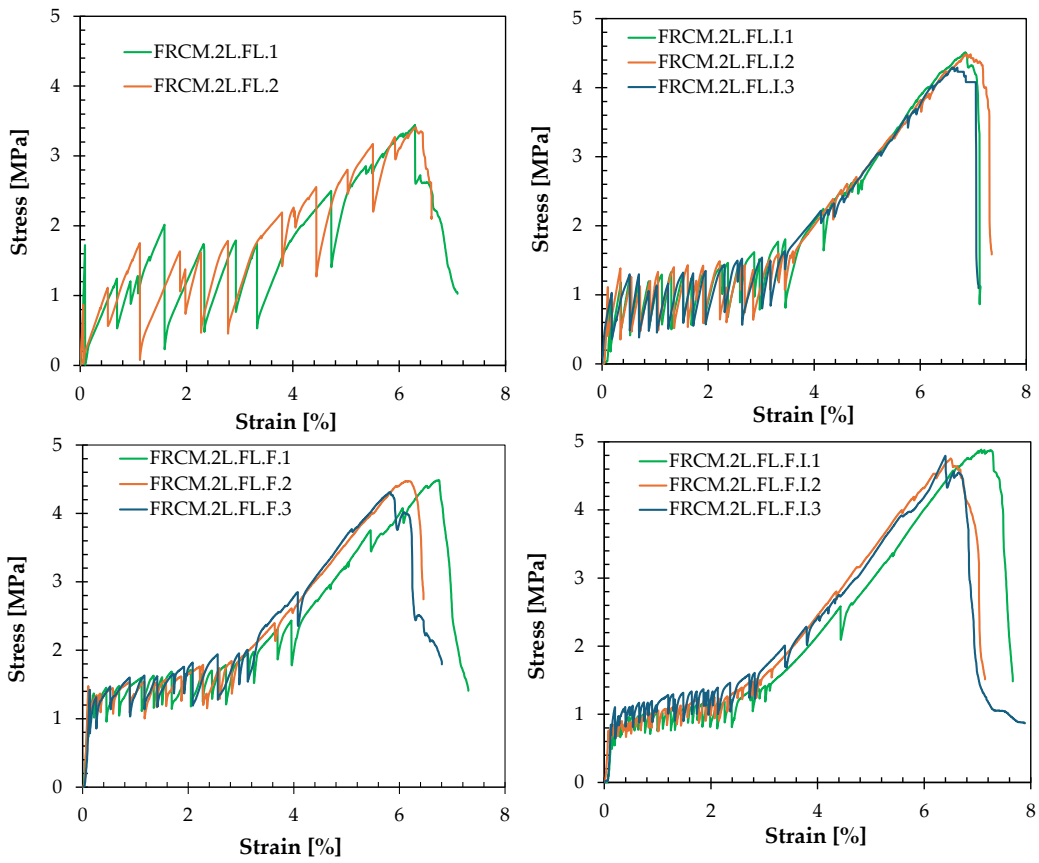

Figure 2. Mechanical behaviour of Flax- FRCM

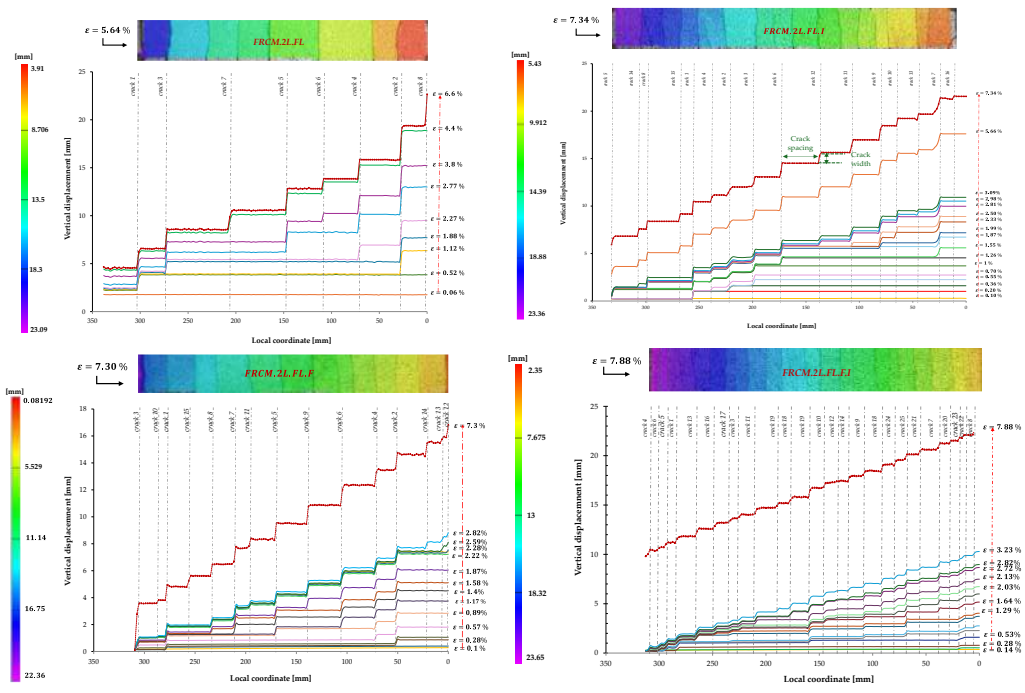

Figure 3. Cracking mechanism of Flax-FRCM: Each jump in displacement is representative of the appearance of a crack, and the difference between the displacement values at the ends of each jump measures the crack width; the distance between two jumps in displacement represents the spacing between the cracks.

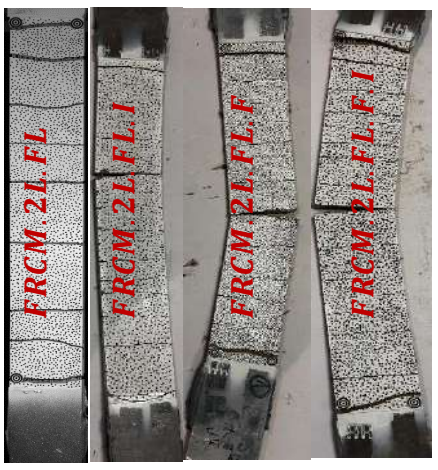

Figure 5. Failure mode of Flax-FRCM

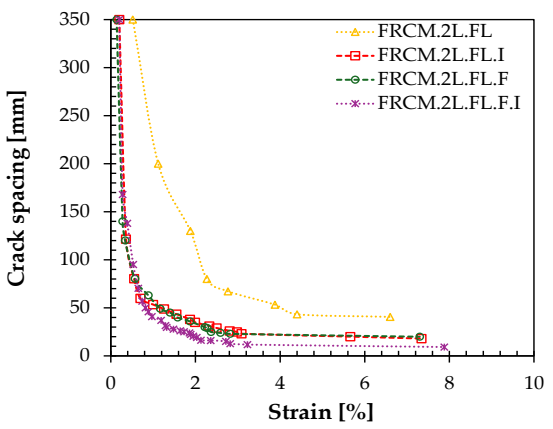

Figure 4. Crack spacing evolution of Flax- FRCM

Bibliography

O. A. Cevallos and R. S. Olivito, 'Effects of fabric parameters on the tensile behaviour of sustainable cementitious composites', *Composites Part B: Engineering*, vol. 69, pp. 256–266, Feb. 2015, doi: 10.1016/j.compositesb.2014.10.004

N. Trochoutsou, M. Di Benedetti, K. Pilakoutas, and M. Guadagnini, 'Mechanical Characterisation of Flax and Jute Fabric-Reinforced Mortars', *Construction and Building Materials*, vol. 271, p. 121564, Feb. 2021, doi: 10.1016/j.conbuildmat.2020.121564.

G. Ferrara, M. Pepe, R. D. Toledo Filho, and E. Martinelli, 'Mechanical Response and Analysis of Cracking Process in Hybrid TRM Composites with Flax Textile and Curauá Fibres', *Polymers*, vol. 13, no. 5, Art. no. 5, Jan. 2021, doi: 10.3390/polym13050715.

Conclusions and future works

- Digital image correlation was used to quantify the number and width of cracks and the distance between cracks
- Pre-impregnation and short flax fibres had a beneficial effect on crack propagation, particularly the number and width of cracks.
- The best response of the FRCM composite is used to reinforce planted concrete: bending reinforcement, diagonal compression of planted concrete walls.

Query Answering in Incomplete Databases under Causal Specifications of Missingness Mechanisms

M.I.DAOUADI, F. TOUMANI, M. BURON, LIMOS, Clermont-FD, FRANCE
L. BERTOSI, SKEMA, CANADA

1 Research question

Missing values (MVs) in databases are often noted as '***na***' or '***null***' and can arise from various reasons (data entry errors, technical glitches, non-response in surveys ...).

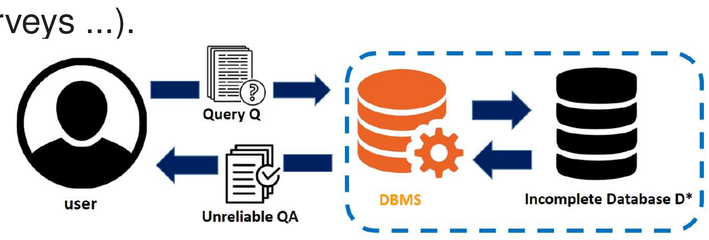

✓ How can we query a DB D^* containing MVs and ensure high-quality QA?
✓ How do we address the issue of an incomplete discrete data utilizing missingness mechanisms, with a focus on aggregate queries?

2 Missingness mechanism (MM)

The Missingness graph (MG) is a DAG (V,E) where V = $V^o \cup V^* \cup V^m \cup I$.

- V^o: the fully observed variables (i.e attributes with no MVs in D^*).
- V^*: the missing features in the D^*.
- V^m: the complete version of V^* (unobserved).
- I: the indicator variables (taking values 0 or 1).

✓ Each $v^* \in V^*$ is associated with a $v^m \in V^m$ and a $I^v \in I$.

$$v^* = \begin{cases} v^m & \text{if } I^v = 0 \\ na & \text{if } I^v = 1 \end{cases}$$

MM	***MCAR***	***MAR***	***MNAR***
	if $V^m \cup V^o \perp\!\!\!\perp I$	if $V^m \perp\!\!\!\perp I \mid V^o$	otherwise (e.g. self-censorship)
MG	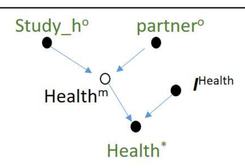	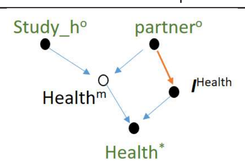	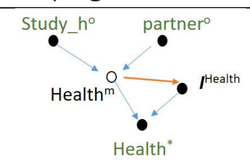

Missingness mechanism in graphical representation

3 Global strategy (imputation)

An ***incomplete database*** D^* is a finite set of database instances W = $\{W_1, \ldots, W_n\}$.

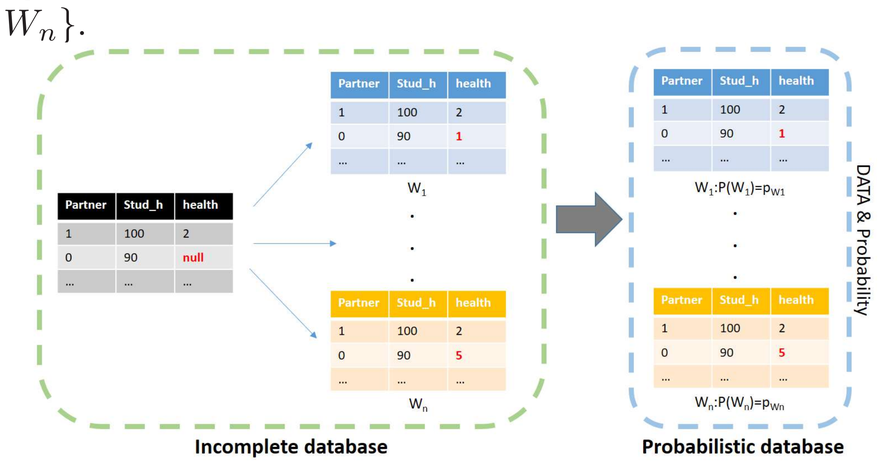

- The possible instances can be seen as multiple imputation.
- ✔ We aim to choose the optimal instance → evaluate the query.

4 Recovering distributions using MG [1]

The attributes of the DB that can be queried are $V^o \cup V^*$.

- MCAR:

$$\begin{aligned} P(Study\_h^o, partner^o, health^m) &= P(Study\_h^o, partner^o, health^m \mid I^{health} = 0) \\ &= P(Study\_h^o, partner^o, health^* \mid I^{health} = 0) \end{aligned}$$

- MAR:

$$\begin{aligned} P(Study\_h^o, partner^o, health^m) &= P(Study\_h^o, health^m \mid partner^o) * P(partner^o) \\ &= P(Study\_h^o, health^m \mid partner^o, I^{health} = 0) \\ &\quad * P(partner^o) \\ &= P(Study\_h^o, health^* \mid partner^o, I^{health} = 0) \\ &\quad * P(partner^o) \end{aligned}$$

5 Block independent probabilistic database (BID)

- ***Probabilistic database (PDB)***: data coupled with probabilities.
- ***BID***: PDB with independent blocks and disjoint tuples within each block.

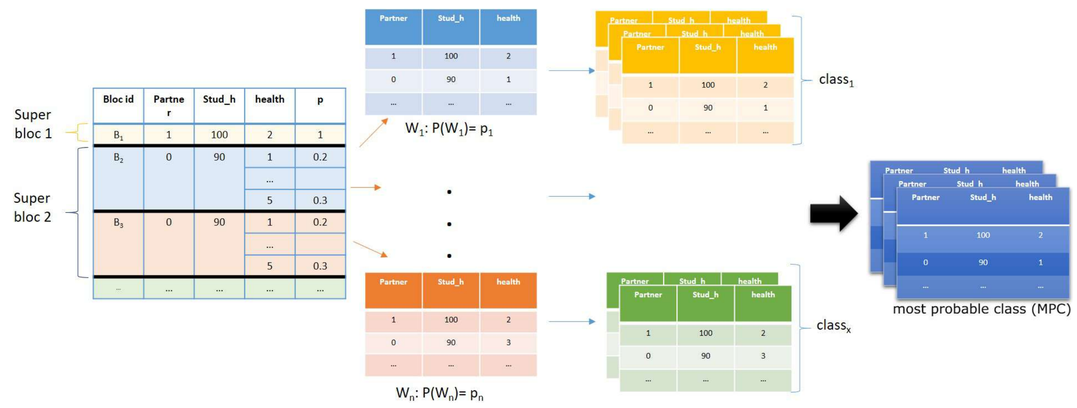

- A ***class*** in BID: the set of possible worlds that share the same empirical joint distribution.
- The probability of a class C: $P(C) = \sum_{w \in C} P(w)$.

6 Finding the MPC (optimization problem)

⋆ **input:** database with missing values D^*, MG

1. Recover the joint distribution of D^* using MG.
2. Transform D^* into BID.
   - Each tuple $\hat{t}$ in D* is a block $B_{\hat{t}}$ in BID.

$$\forall t \in B_{\hat{t}} : p(t) = P(health^m = v \mid partner^o = \hat{t}[partner^o], stud\_h^o = \hat{t}[stud\_h^o])$$

3. Organize the BID with respect to the notion of super blocks.
   - Within the superblock, the blocks share the same domain $B = \{t_1, \ldots, t_m\}$.
   - The set of superblocks in BID is $\{S_1, \ldots, S_l\}$.
   - $P_i(t_j)$ is the probability of tuple t_j in superblock S_i.
4. Solve an optimization problem to find the MPCs:

$$\prod_{1 \le i \le l} \binom{|S_i|}{k_{i,1}} (P_i(t_1))^{k_{i,1}} \binom{|S_i| - k_{i,1}}{k_{i,2}} (P_i(t_2))^{k_{i,2}} \ldots \binom{|S_i| - k_{i,1} \cdots - k_{i,m-1}}{k_{i,m}} (P_i(t_m))^{k_{i,m}}$$

$$\text{s.t. } \forall S_i \in BID, \sum_{1 \le j \le m} k_{i,j} = |S_i|$$

- $k_{i,j}$ is $\#t_j$ coming from superblock S_i.

7 Experiment results

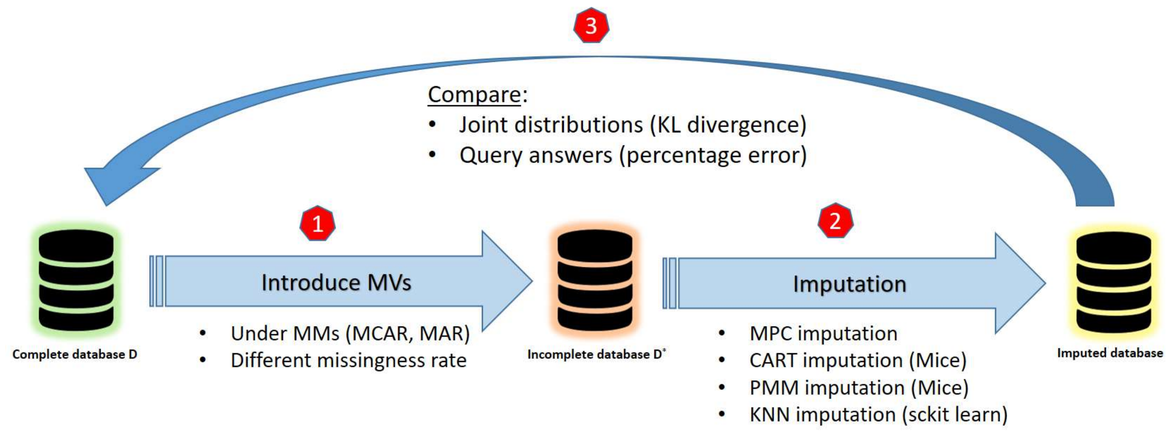

$D_{\mathrm{KL}}(P \parallel Q)$	Percentage error
$\sum_{x \in \mathcal{X}} P(x) \log \frac{P(x)}{Q(x)}$	$ABS(\frac{QA_{complete} - QA_{imputed}}{QA_{complete}}) \times 100$

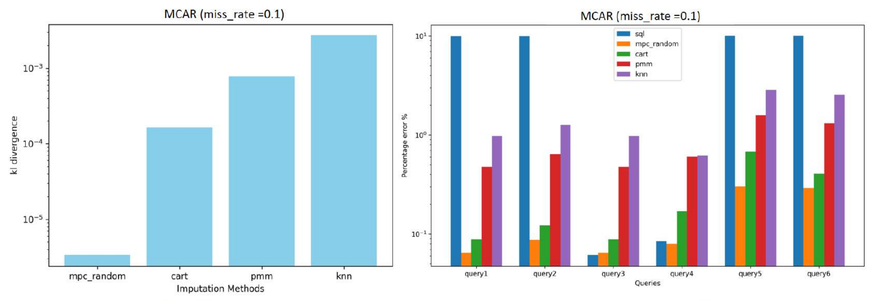

KL-divergence — Query evaluation

8 Conclusion

- MPC imputation exhibits better effectiveness across MCAR, MAR, and varying missingness rates.
- **Future work:** It is necessary to explore the MNAR cases.

KEY REFERENCES

[1] Mohan, K. *Graphical Models for Inference with Missing Data.* PhD Thesis, UCLA, 2017. https://escholarship.org/uc/item/6mk2b174
[2] Suciu, D., Olteanu, D., Ré, C., & Koch, C. *Probabilistic Databases.* Journal Article, 2011. https://doi.org/10.1007/978-3-031-01879-4
[3] *Multivariate Imputation by Chained Equations* https://github.com/amices/mice

ACKNOWLEDGEMENT AND PARTNERS

LIMOS · Université Clermont Auvergne · Clermont Auvergne INP – École doctorale des sciences pour l'ingénieur · clermont auvergne métropole

MORE INFORMATION

Moulay Idris DAOUADI
PhD candidate
LIMOS lab
Clermont Auvergne University

Stent deployment simulation from custom data extracted from intraoperative images

A. Boldron, L. Sarry, B. Blaysat, T. Jailin

Université Clermont Auvergne, CHU Clermont-Ferrand,
Clermont Auvergne INP, CNRS, Institut Pascal, F-63000 Clermont-Ferrand, France

Introduction

Stent: cylindrical endoprosthesis widely used for The treatment of coronary artery disease, formation of lipid plaques hindering blood circulation in the coronary arteries.

Stent placement: Percutaneous Coronary Intervention (PCI) 1 in 5 deaths in Europe in 2014 (~1.8 million),1 in 4 in 2019, leading cause of death among cardiovascular diseases.

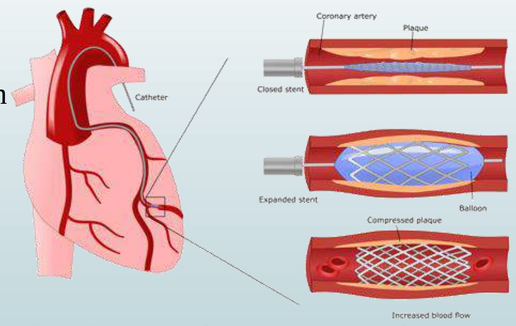

Figure: Percutaneous Coronary Intervention with a stent
INCCI, Institut National de Chirurgie Cardiaque et de Cardiologie Interventionnelle https://www.incci.lu/fr/les_maladies/maladie-coronarienne/

Advantage: interventional installation less invasive than surgery
Problem: Long-term effectiveness could be further improved, particularly for more complex clinical cases, risks of complications (restenosis, etc.)

Current models efficient for theoretical artery representation yet need to be adapted for patient custom data

Aim: Allow the deployment of stents to be simulated precisely and with limited calculation times in in vivo conditions using images collected during the PCI

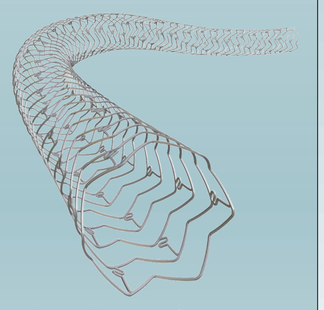

Figure: Drawing of a stent
Cardiac Interventions Today, https://citoday.com/news/ivascular-launches-long-lengths-of-angiolite-des

Stent in the form of a long wire with a thin section

→ more precise modeling on the axis of the wire than along the section → beam model

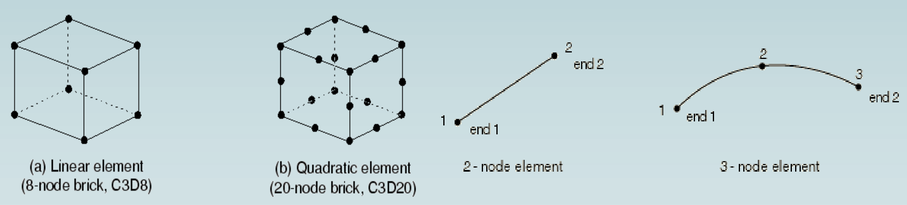

Figure: Continuum solid elements vs beam elements in ABAQUS software
ABAQUS, Inc, https://classes.engineering.wustl.edu/2009/spring/mase5513/abaqus/docs/v6.6/

Fewer nodes with beams → less computation time

→ Modeling of stents using beam elements → proof of concept + reduction of calculation times compared to other models for free deployment (without contact with an artery model) [C. Krewcun, 2020]

Can this method be used for personalized patient stent and artery data?

Methods

Stent model design: master student project

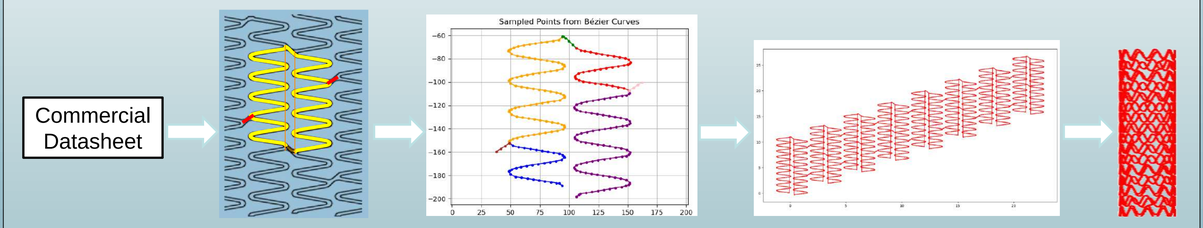

1. Simulation of stent inflation with commercial finite element software ABAQUS with solid and beam elements [Dassault Systèmes, 2006]

2. Implementation on SOFA, open-source framework for interactive mechanical simulation, with emphasis on biomechanics
→ implementation of personal patient data

→ Beam model theory used in ABAQUS consistent for elastoplastic beams?

$$\sigma_v = \sqrt{\frac{1}{2}\sum_{i=1}^{3}\sum_{j=1,j\neq i}^{3}(\sigma_i - \sigma_j)^2 + 3\sum_{k=1}^{3}\sigma_k^2}$$

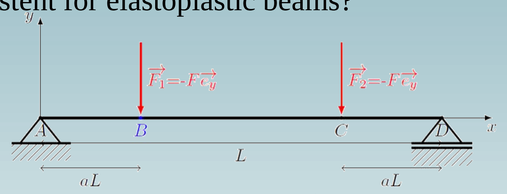

If $\sigma_v > \sigma_{threshold}$ → plastic strain i.e. irreversible deformations (i.e. stent inflation at the end of the PCI)
→ Reference test with analytical case: 4 point bending of elastic beam

→ Stent data: segments (1D) → how to assign consistent section orientation ?

Results

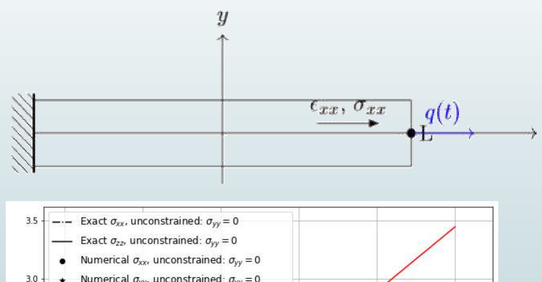

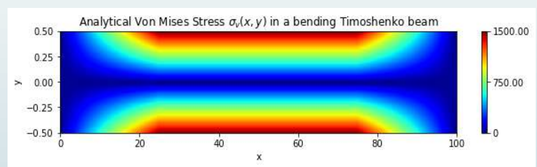

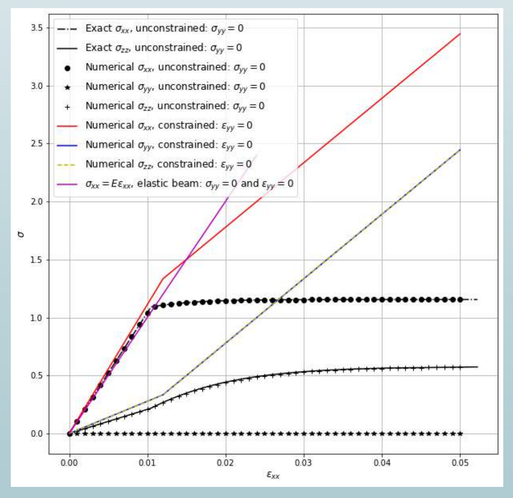

Figure: Stress-strain curves for a 2D elastoplastic traction test [M.Bonnet, 2005], with different modeling assumptions

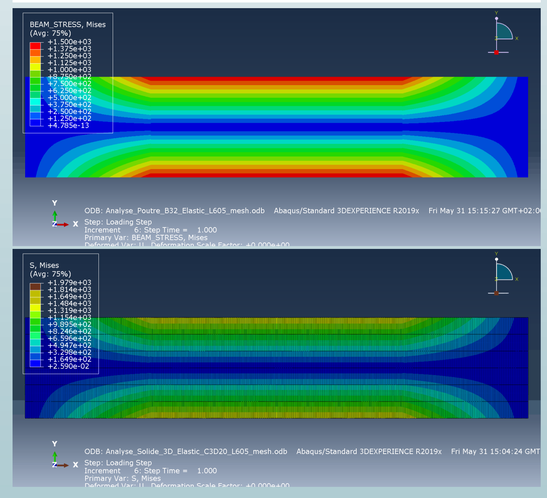

Figure: 4 point bending of a beam: von Mises stress σ_v for 3 models: Analytical Timoshenko beam, Numerical Timoshenko beam elements, Numerical solid brick elements (from top to bottom)

Beam model assumptions (here $\varepsilon_{yy} = 0$ and $\sigma_{yy} = 0$) incompatible with the constitutive laws like Hooke's law for linear elasticity

- ***Beam model assumptions → different stresses → different plastic strains***

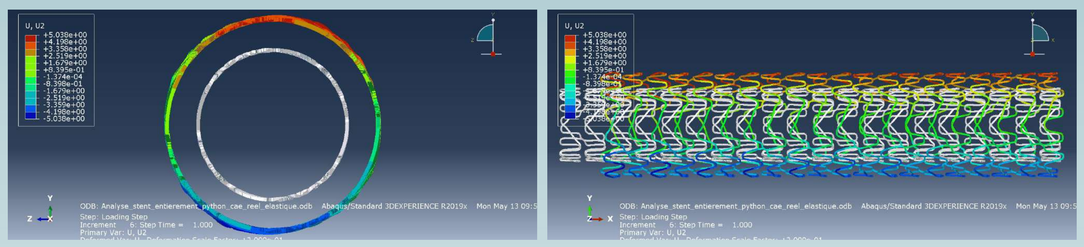

Figure: Stent (Ultimaster Nagomi by Terumo) modeling and inflation in ABAQUS

- ***Stent sampling data usable in ABAQUS for imposed inflation (radial displacement)***

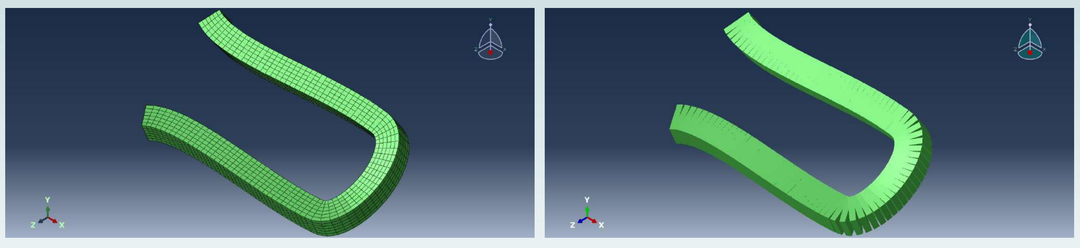

Figure: Part extracted from the stent: modeling using brick elements (left) and beam elements (right)

- ***Consistent solid/beam section assignment***

Conclusions

- Possible to implement a custom stent on ABAQUS and apply free deployment
- Computation time greatly reduced with beam elements

→ Need further investigations to quantify consequences on plastic strains induced by beam model

→ Implementation of the stent deployment in real artery geometries

Bibliography

1. **C. Krewcun (2020). Simulation numérique de déploiement de stent coronaire en vue d'un traitement personnalisé – validation sur fantôme acquis en imagerie microdensitométrique. Bio-informatique [q-bio.QM]. Université Clermont Auvergne [2017-2020], 2020. Français. NT : 2020CLFAC086. tel-03518646**
2. **Dassault Systèmes (2006). ABAQUS Analysis User's Manual, Section 23.3 Beam elements. Retrieved from https://classes.engineering.wustl.edu/2009/spring/mase5513/abaqus/docs/v6.6/index.html**
3. **M. Bonnet (2005). Analyse des structures mécaniques par la méthode des éléments finis. École Polytechnique, Département de Mécanique, Majeure 2 SeISM.**

Contributing to reproducible software measurements of energy consumption for machine learning and artificial intelligence

Anthony Bertrand, David Hill, Engelbert Mephu Nguifo

ABSTRACT

High-performance computing and large-scale computing require a careful management of the power and energy. Much of the work to achieve these energy consumption limitation goals is and will have to be done with hardware improvements. On the other hand, the work of using the hardware tools made available falls to the software but also to the applications. If hardware consumption “measurements” exist, software measurements must also be available to evaluate the consumption of applications and particularly those of high-performance computing in the context of artificial intelligence applications. Several deep learning applications will be considered and evaluated on recent hardware.

REPRODUCIBLE RESEARCH

Definitions [1]

Reproducibility

Different team, same experience
Measures have to be done with the declared precision by another team using the same measure procedure, the same system of measurement, in the same conditions.

Replicability

Different team, different experience
Measures have to be done with the declared precision by another team using a different system of measurement.

Repeatability

Same team, same experience
Measures have to be done with the declared precision by the same team using the same measure procedure, the same system of measurement, in the same conditions.

MACHINE LEARNING

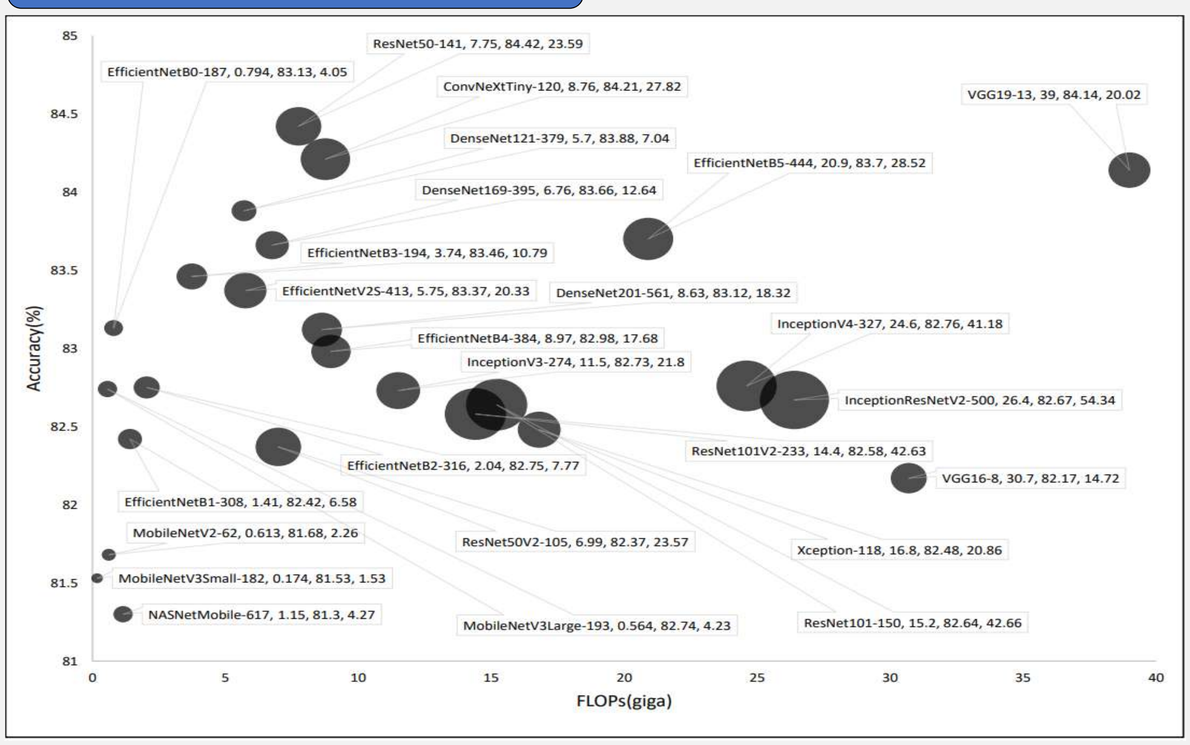

Model accuracy vs floating point operations. Bubble size represents the number of parameters.

An example : Multiple ML architectures have been tested to diagnosis Lyme disease from images [4]. Are these results reproducible ? What is the energy cost of each architecture ?

ENERGY MEASUREMENT

Measurement

Different units :
CO_2eq (Carbon dioxide equivalent), gCO_2e (Grams of carbon dioxyde equivalent), J (Joules), W (Watt), kWh (Kilowatt hour).

Can we standardize it ?

Different methods :

- Hardware-based : Meters, Embedded captors, Sensors.
- Software-based : Build power models to estimate the power dissipation [2].

How to make precise measurements ?

Energy measurement tools [3]

Date	Tool name	Tool type	AI only
2009	pTop	Command line	NO
2013	PyJoules	Python library	NO
2019	Energy Usage	Python library	NO
2019	ML CO_2 impact	Web	NO
2020	Experiment impact tracker	Python library	NO
2020	Carbon Tracker	Python library	**YES**
2020	Cumulator	Python library	**YES**
2021	Green algorithms	Web	NO
2021	CodeCarbon	Python library + Command line	NO
2022	PowerJoular	Command line	NO

WORK

Experiment on language benchmark reliability

We are comparing the time and energy consumption of a program written in different languages. We use different existing benchmarks to check result consistency.
The objective is to check if using different benchmarks can lead to different scientific conclusions, questioning the implementation of solid benchmarks.

REFERENCES

[1] Benjamin A. Antunes, David R.C. Hill. Reproducibility, Replicability, and Repeatability: A survey of reproducible research with a focus on high performance computing. 2024. ⟨hal-04450487v2⟩

[2] Hui Chen and Weisong Shi. 2012. Power measuring and profiling: the state of art. Handbook of Energy-Aware and Green Computing (2012), 649–674.

[3] Bannour, Nesrine, Ghannay, Sahar, Névéol, Aurélie, et al. Evaluating the carbon footprint of NLP methods: a survey and analysis of existing tools. In : Proceedings of the Second Workshop on Simple and Efficient Natural Language Processing. 2021. p. 11-21.

[4] Sk Imran Hossain et al., Exploring convolutional neural networks with transfer learning for diagnosing Lyme disease from skin lesion images, Computer Methods and Programs in Biomedicine, Volume 215, 2022, 106624, ISSN 0169-2607, https://doi.org/10.1016/j.cmpb.2022.106624.

FUTURE DIRECTIONS

1. Make experiments to compare the different energy consumption measurement tools.
2. Check the reproducibility of the work of ML architectures to classify Lyme disease images.

ACKNOWLEDGEMENT

I would like to thank the CPER IDEAL and Clermont Auvergne Métropole (CAM) for funding this work.

CONTACT

anthony.bertrand@doctorant.uca.fr
(+33) 07 82 24 89 89
anthony-bertrand-256989206/
DragSoul

Le calcul parallèle au service de la robotique

Louis Guigon, Andrés Kecskeméthy, Chedli Bouzgarrou, Benjamin Boudon, Youcef Mezouar

Contexte

Les algorithmes de contrôle modernes requièrent plus de ressources pour respecter les contraintes de temps réel.

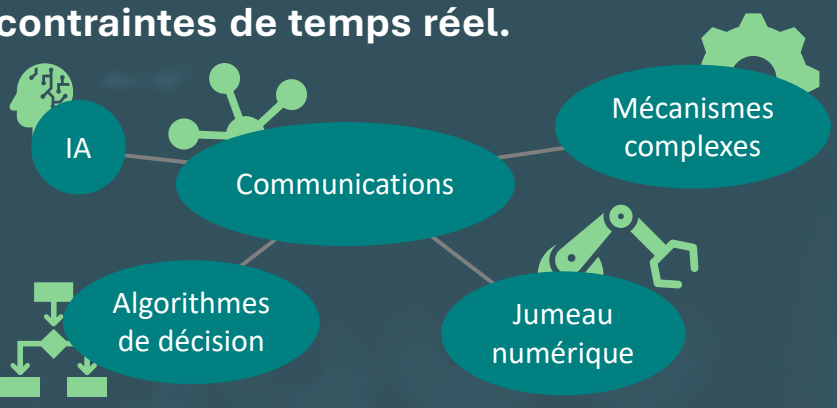

De la détection d'objets, à la coordination de plusieurs robots dans un même espace, les demandes d'automatisation requièrent toujours plus de puissance de calcul.

Exemple avec le Kuka Robocoaster :

Simulation en réalité virtuelle de l'environnement de roller-coaster

Synchronisation du robot avec la simulation pour imiter les accélérations du roller-coaster

source: Duisburg Kuka Robocoaster

Source: Universal Robots

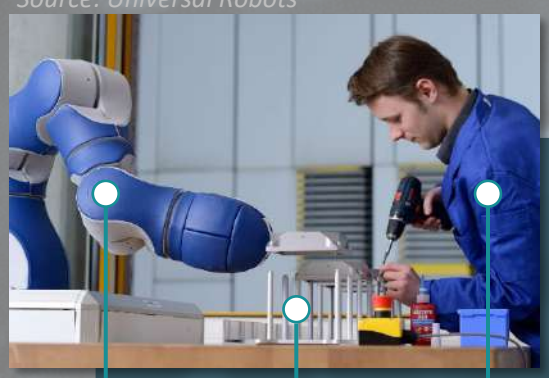

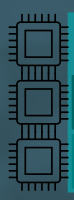

Observer → *Déplacer* → *Sécuriser*

parallèle**: les étapes sont effectuées **simultanément

Observer → *Déplacer* → *Sécuriser*

série**: les étapes sont effectuées **successivement

Les atouts de la GPU

Les **processeurs multicœurs** tels que les cartes graphiques, ou **Graphic Processing Units (GPU)** permettent d'effectuer les calculs **simultanément** en **parallèle**.

les GPUs sont présentes dans la plupart des machines modernes.

Les algorithmes sont d'autant plus rapides que le processus est parallélisable

L'architecture GPU est en constante évolution et est très convoitée pour ses performances

Contribution scientifique

L'objectif est d'optimiser le contrôle de robots sur des processeurs parallèles pour une exécution en temps réel de différentes tâches au sein d'une cellule robotisée.

Concurrence

L'objectif est d'effectuer un maximum de calculs simultanément

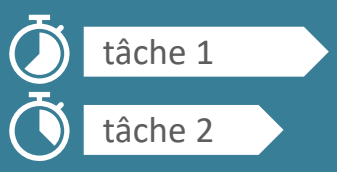

Parallélisme

Des études sont menées pour optimiser les algorithmes en calcul parallèle

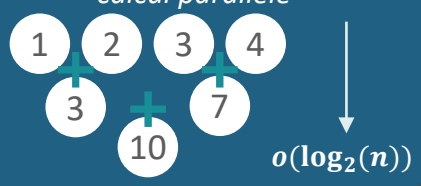

Formalisme

La reformulation de la dynamique multi-corps est considérée pour accélérer son calcul en parallèle

$$\boldsymbol{M}(q,\dot{q}).\underline{\ddot{q}} + \underline{b}(q,\dot{q}) = \underline{Q}(q,\dot{q})$$

Portabilité

L'objectif final est de concevoir un compilateur de code parallèle fonctionnant sur toute machine équipée de GPU

NVIDIA CUDA OpenCL

Simulateur de dynamique

Un premier cas d'application consiste à calculer les équations de la dynamique d'une chaîne série sur processeurs parallèles:

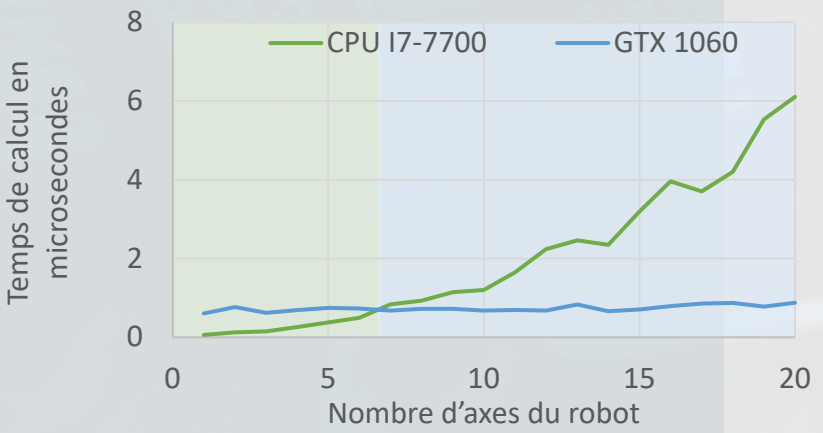

La **GPU** est performante pour les systèmes complexes avec un temps d'exécution proche du constant tant que des ressources sont disponibles mais reste plus lente que la **CPU** si peu de calculs sont à effectuer.

Premières publications

- **Dynamics of a 3R spatial robot based on a GPU approach**, ECCOMAS Multibody Dynamics 2023
- **Preliminary study on the applicability of parallel processing with Graphic Processing Units (GPU) for mechanism dynamics: The planar 4-bar case**, IFToMM World Congress 2023
- **A Case Study on Parallelization of Multibody Dynamic Equations for Graphic Processing Units (GPUs) in Real-Time Simulations - The Planar nR Serial Chain,** International Conference on Multibody System Dynamics 2024

Clustering for Trajectories Analysis

A Soubeiga*, V Antoine*, J Koko*, S Moreno**

*Université Clermont Auvergne, CNRS, LIMOS, Clermont-Ferrand, France
**Digital Health Hub, Université Simon Fraser, Vancouver, Canada

armel.soubeiga@uca.fr - armelsoubeiga.github.io

Introduction

▷ Context

Clustering for trajectory analysis has received growing interest in various research fields in recent years. Research work has multiplied around autonomous solutions applicable to diverse fields and topics. However, in social science, this task becomes more challenging when multidimensional trajectories are characterized by discrete or categorical longitudinal data or time series.

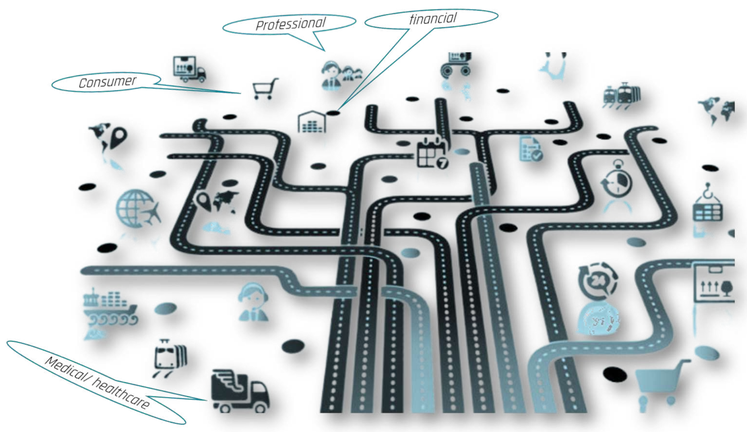

- A trajectory $\chi^{(i)}$ is a three-tensor multichannel sequence data in $\mathbb{R}^{(i)\times M\times T}$.
- Possible classification of the different types of trajectories.

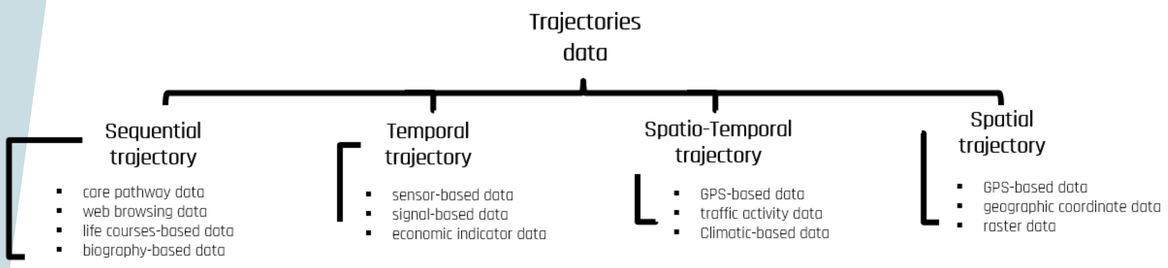

▷ Applications & Problems

- Identification and characterization of care trajectories : the case of chronic pain.
- The eDOL project and eDOL mHealth application for patient monitoring.

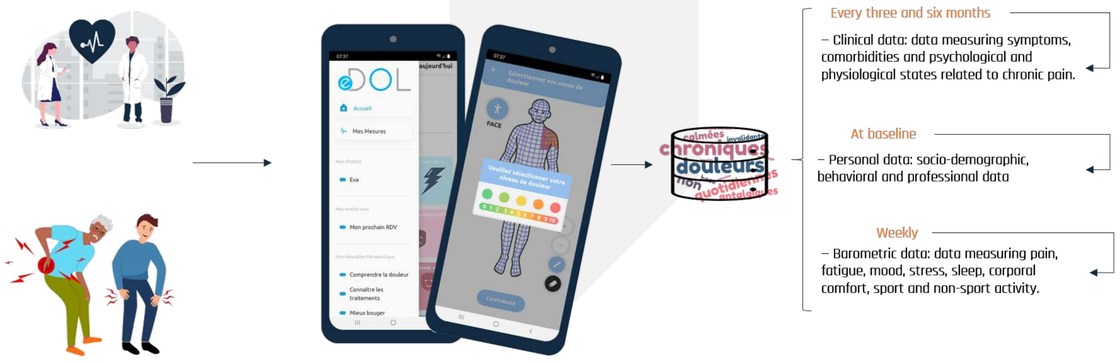

FIGURE 1 – System and circuit for eDOL data acquisition.

(1) Problem of multidimensionality : care trajectories are multichannel

(2) Healthcare challenge : the subjectivity and uncertainty of data and typology.

▷ Interesting Questions Explored

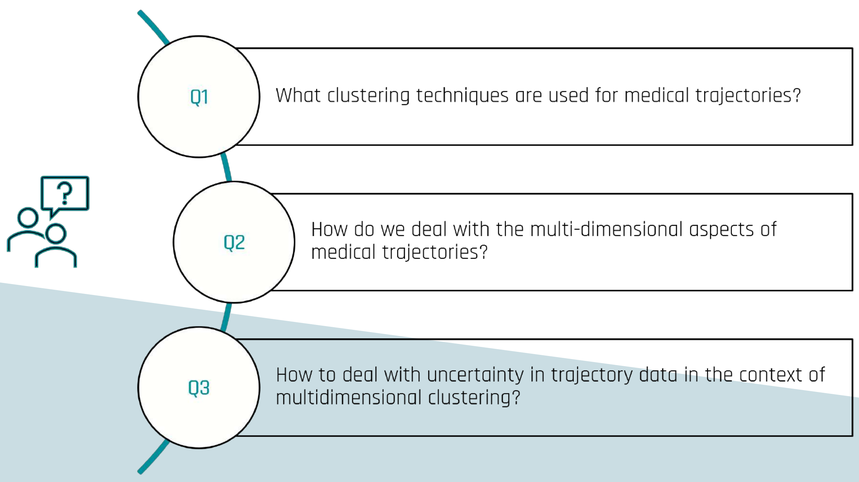

Methods

▷ Diverse formulations for trajectory Clustering

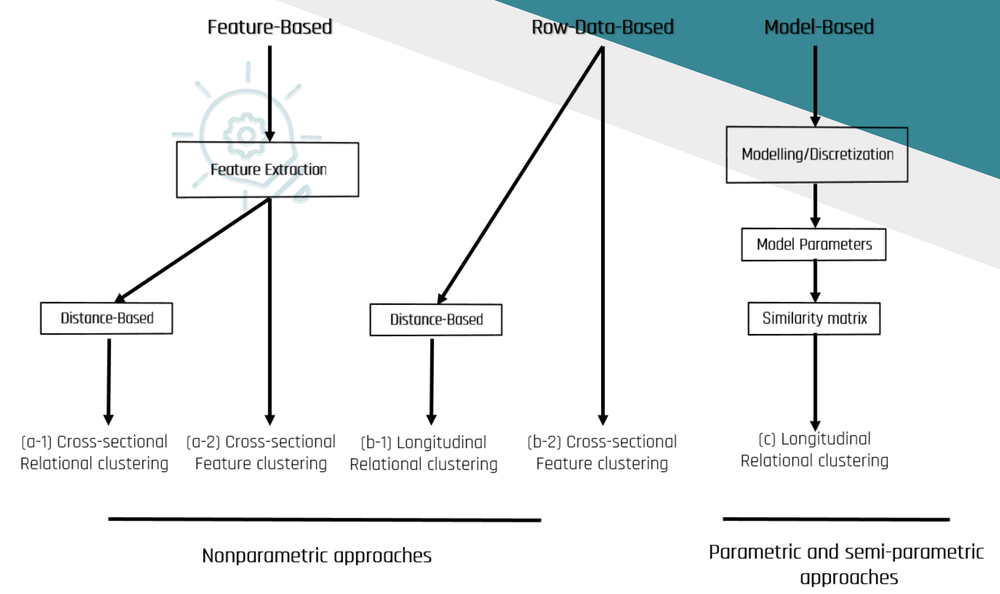

▷ Feature-Based Clustering : approches multicanales

Feature-based approaches use feature extraction and selection techniques, but are limited due to ignoring time dimensions : $\chi^{(i)} \in \mathbb{R}^{(i)\times M}$.

▷ Row-Data-Based Clustering : approches multicanales

Raw data-based approaches for clustering multichannel sequential trajectories include :

- Multichannel sequence analysis
  - Sequential processing : methods (1).
  - Sequential similarity measures : methods (2),(5).
- Relational Clustering : methods (3),(4).

Methods	Multidimensional	Parsimony	Interdependence
1 - Combination of states (Cstat)	no	yes	local
2 - Combination of costs (Ccost)	yes	yes	local
3 - Combination of distance (Cdist)	yes	yes	no
4 - Combination of clusters (Cclust)	yes	no	global
5 - Globally Interdependent Multiple Sequence Analysis (GIMSA)	yes	yes	global

▷ Soft clustering-based approach

Soft clustering based on fuzziness or belief functions, addresses ambiguity, imprecision, and uncertainty :

- (1) Fuzzy Clustering : only imprecision

$$J_{FCM}(\mathbf{U},\mathbf{V}) = \sum_{j=1}^{c}\sum_{i=1}^{n} u_{ij}^{m} d_{ij}^{2} \quad \text{subject to } \sum_{j=1}^{c} u_{ij} = 1, u_{ij} > 0 \quad \forall i = 1,...,n \tag{1}$$

- (2) Evidential Clustering : imprecision and uncertainty

$$J_{ECM}(\mathbf{M},\mathbf{V}) = \sum_{i=1}^{n}\sum_{A_j\neq\emptyset} |A_j|^{\alpha} m_{ij}^{\beta} d_{ij}^{2} + \sum_{i=1}^{n} \delta^{2} m_{i\emptyset}^{\beta} \quad \text{subject to } \sum_{A_j\subseteq\Omega, A_j\neq\emptyset} m_{ij} + m_{i\emptyset} = 1, m_{ij} > 0 \quad \forall i = 1,...,n \tag{2}$$

▷ Soft relational clustering with distance collaboration

A relational version of adapted ECM allows for the characterization of uncertainty and imprecision within a collaborative learning framework by integrating distances weight locally for each cluster (3) or globally (4). Designed as follow :

$$J_{MECMdd-RWL}(\mathbf{M},\mathbf{V},\mathbf{\Lambda}) = \sum_{i=1}^{n}\sum_{A_j\neq\emptyset} |A_j|^{\alpha} m_{ij}^{\beta} \sum_{l=1}^{p} \left(\lambda_{jl}\right)^{s} d_{ijl} + \sum_{l=1}^{p} \delta_l^{2} \sum_{i=1}^{n} m_{i\emptyset}^{\beta} \tag{3}$$

$$J_{MECMdd-RWG}(\mathbf{M},\mathbf{V},\lambda) = \sum_{i=1}^{n}\sum_{A_j\neq\emptyset} |A_j|^{\alpha} m_{ij}^{\beta} \sum_{l=1}^{p} (\lambda_l)^{s} d_{ijl} + \sum_{l=1}^{p} \delta_l^{2} \sum_{i=1}^{n} m_{i\emptyset}^{\beta}. \tag{4}$$

With p the number of distance matrices included in the collaboration. λ_{jl} the estimated relevance weight for cluster j and distance matrix l.

Conclusions

Clustering methods for sequential trajectories in social sciences are based on sequential analysis, using both additive and combinatory approaches. Collaborative methods that take uncertainty into account are particularly effective.

Fire behaviour of fusible links for fire walls in single-storey steel-framed buildings

Thi-Thuy Mai [1, 2] ; Abdelhamid Bouchair [2]; Sébastien Durif [2]; Christophe Renaud [1]; Bin Zhao [1]

[1] Fire division, CTICM

[2] Université Clermont Auvergne, Clermont Auvergne INP, CNRS, Institut Pascal, F-63000 Clermont-Ferrand, France

Introduction

- Localized collapse of the building parts exposed to fire is acceptable when the overall stability of the building is preserved.
- Fire-walls are used to limit the fire propagation and the effect of local collapse.
- To achieve the stability of fire-walls during local fire, fusible links can be used.
- The adequate **fire performance** of **fusible links** has never been really investigated.

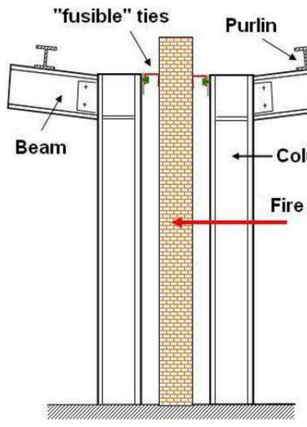

The thesis aims to **study the fire behavior** of "fusible" links for fire-walls installed in single-story steel buildings using :

- **Finite element** numerical **models** are developed (mechanical and thermal effects).
- **Experimental results** (Fishwall European project) used to validate the models.
- **Parametric studies** performed on different configurations of "fusible" systems to propose practical recommendations and calculation rules for engineering.

Modeling of fusible links

First fusible link

Second fusible link

*3D FE models for **thermal analyses** of two fusible links*

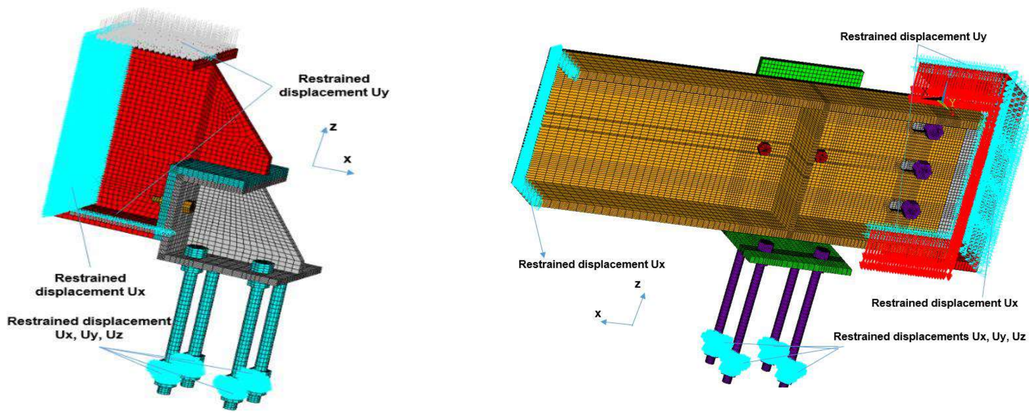

*3D FE models for the **mechanical analyses** of fusible links*

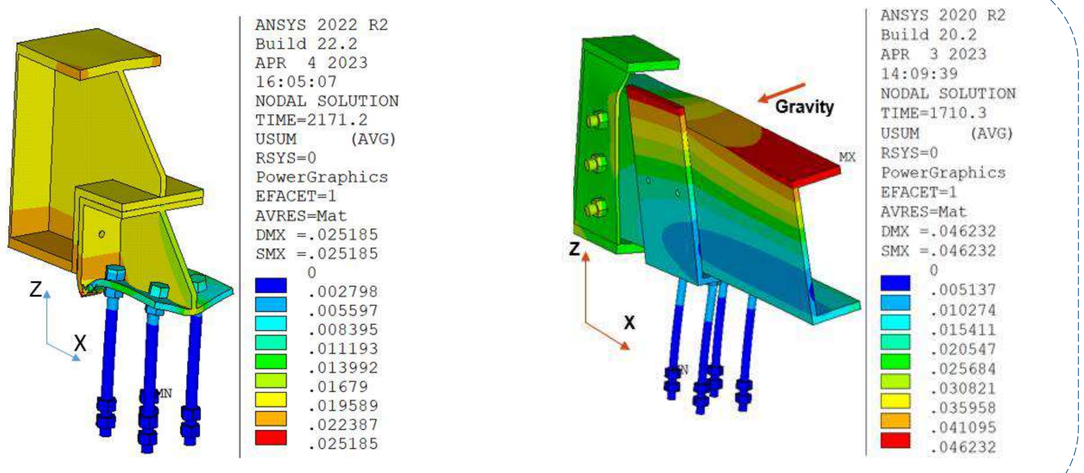

***Deformed shapes** of fusible links at failure time*

Experimental results

Fishwall project fire test on studied fusible links

Fusible links after the fire test

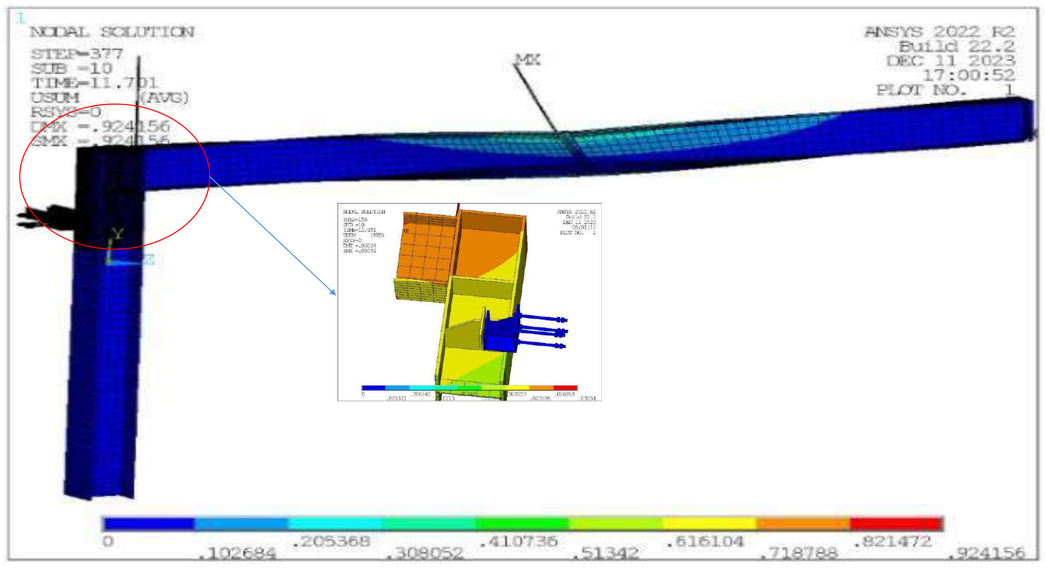

Numerical model** of **tested specimen

Conclusions

- ✓ The developed FE models can predict successfully the fire behaviour of fusible links in fire situation.
- ✓ The results of the FISHWALL project fire test have fully confirmed the relevance of the studied fusible links.
- ✓ The detailed analysis and interpretation of the test results validated the three-dimensional FE numerical models developed.
- ✓ The parametric studies on different configurations of "fusible" systems is in progress.

Bibliography

1. C. Renaud, «Guide de vérification du comportement au feu des bâtiments à simple rez-de-chaussée en charpente métallique,» 2017.
2. Mid-term report, RFSC project FISHWALL: Fire and Seismic performances of Hybrid fire WALLs in case of single-storey industrial and commercial steel buildings", 2023.
3. Deliverable D3.3: Fire test report on fire wall connected to an unprotected steel structure by means of fusible links, RFSC project FISHWALL, 2023.

Construire en métal, un art, notre métier

CLERMONT AUVERGNE INP — ÉCOLE DOCTORALE DES SCIENCES POUR L'INGÉNIEUR

UNIVERSITÉ Clermont Auvergne

clermont auvergne métropole

Modèles numériques évolutifs du système ferroviaire :
Outils d'aide à la décision dans une approche par l'analyse de risques

Alexis Chartrain[1,2] Gilles Dessagne[1] Noël Haddad[1] David R.C. Hill[2]

[1]SNCF Réseau,
Direction Générale Industrielle & Ingénierie,
F-93210 Saint-Denis, FRANCE

[2]Université Clermont – Auvergne, CNRS, Clermont – Auvergne INP,
Mines de Saint-Étienne, LIMOS UMR CNRS 6158,
F-63000 Clermont-Ferrand, FRANCE

26 juin 2024

Contexte

A ce jour, dans un contexte de transformation numérique de l'entreprise, les différents métiers de SNCF Réseau (ingénierie, exploitation et maintenance) ont la nécessité de bâtir une représentation commune et partagée du système ferroviaire afin de faciliter leurs interactions mutuelles. Par ailleurs, cette représentation permettrait aux métiers de mieux appréhender la complexité du système ferroviaire par une meilleure identification et caractérisation de l'intrication de ses constituants, due aux interdépendances entre sous-systèmes.

1. Jakob Von Uexküll, *Milieu animal et milieu humain*. Deux êtres vivants évoluant chacun dans un même monde se construisent une représentation différente de ce monde, de par leur perception sensorielle unique. De manière analogue, les différents métiers de SNCF Réseau ont chacun leur perception du système ferroviaire, construite selon leur besoin métier et leurs usages.

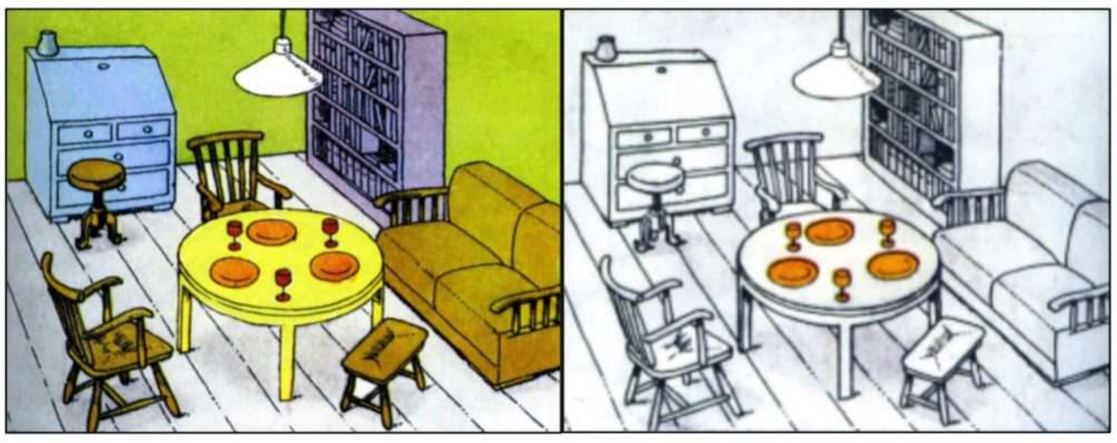

Figure – Deux représentations d'un même monde : l'une construite par l'homme (à gauche) et l'autre construite par la mouche (à droite) [1]

Problématique

L'**absence** de **représentation systémique** commune pourrait conduire à une mauvaise compréhension du système ferroviaire global, engendrant à son tour, nombres de **risques** pouvant aller jusqu'à compromettre la disponibilité du réseau, la robustesse de l'exploitation ou la sécurité des personnes. **Dès lors, comment construire cette représentation globale, évolutive et partagée du système ferroviaire ?**

Finalité de la thèse et contribution visée

La thèse vise à établir le **socle scientifique** nécessaire à l'évaluation des effets de bords induits par certains systèmes et acteurs sur le reste de l'écosystème ferroviaire et réciproquement. Notre contribution, d'ordre **méthodologique**, guidera l'entreprise dans sa transformation numérique pour lui permettre d'atteindre un **optimum global** de ses activités.

Méthodes

Notre travail de recherche s'articule autour de la gouvernance de la donnée de SNCF Réseau, référence numérique de l'entreprise. Plus précisément, notre travail s'inscrit dans le cadre de la construction du **modèle systémique ARIANE**, selon la démarche suivante :

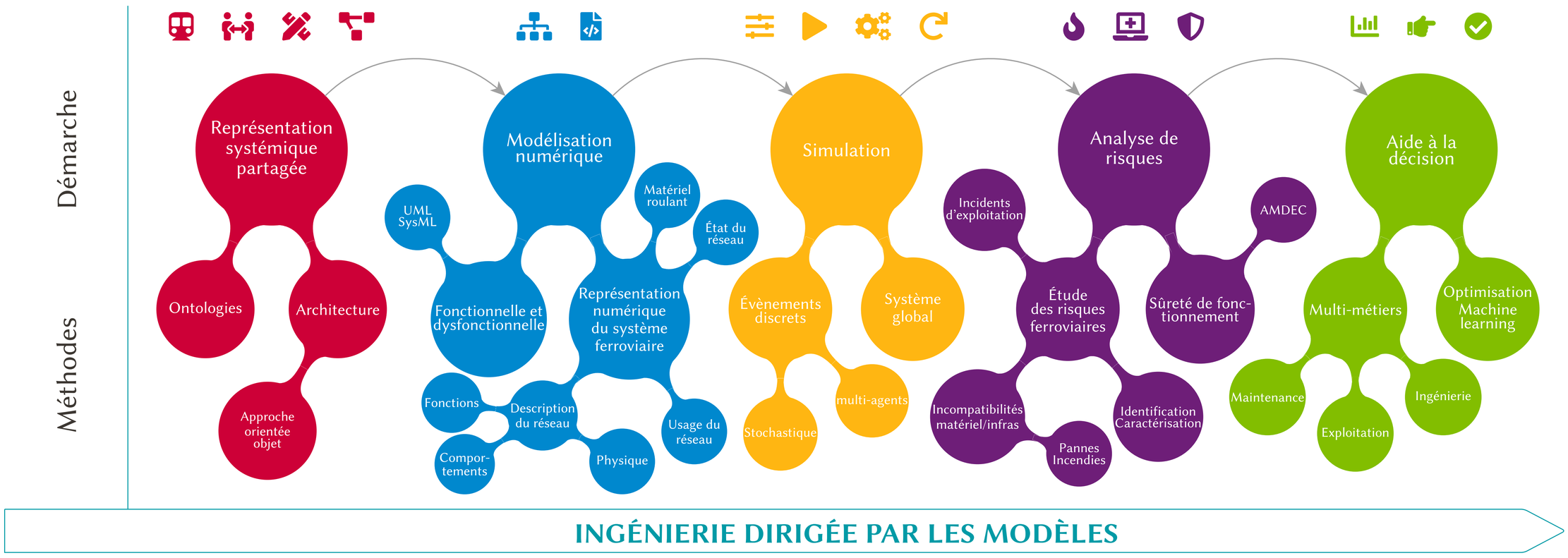

Premiers résultats

- **Glossaire** des notions clefs de la thèse
- **Ontologie** pour les modèles conceptuels de domaine
- **(Meta-)modèles** (système, processus)
- « **Framework** » pour produire un Jumeau Numérique avec une approche dirigée par les modèles
- Identification de **cas d'application** industriels ferroviaires pour la simulation et l'analyse de risques

Publications

Alexis Chartrain, Gilles Dessagne, Noël Haddad, David R.C. Hill. *Vers une simulation globale du système ferroviaire : atout pour l'aide à la décision guidée par l'analyse de risques.* ROADEF '24, 5 Mars 2024, Amiens, France.

Moussa Issa, Alexis Chartrain, Flavien Viguier, Bruno Landes, Gilles Dessagne, Noël Haddad, David R.C. Hill. *Railway system Digital Twin : a tool for extended enterprises to perform multimodal transportation in a decarbonization context.* TRA '24, 17 avril 2024, Dublin, Irlande.

Alexis Chartrain, Gilles Dessagne, Noël Haddad, David R.C. Hill. *Retrospective on the Digital Twin concept and perspectives for railways : the case of SNCF Réseau.* SAGIP '24, Mai 2024, Lyon, France

Multi-doped bioceramics for the regeneration of large bone defects

Alice Szmytko[1], Charlotte Vichery[1], Stéphane Descamps[1] and Jean-Marie Nedelec[1]

[1]Université Clermont Auvergne, Clermont Auvergne INP, CNRS, CHU Clermont-Ferrand, ICCF, F-63000 Clermont-Ferrand, France

Alice.szmytko@sigma-clermont.fr

Institut de Chimie de Clermont-Ferrand

Introduction

Background

Arthroplasty, trauma, infection, or tumor resection may lead to the formation of a critical bone defect, where the tissues will not regenerate spontaneously. One of the emerging solutions is to use synthetic bone filling materials such as calcium phosphate ceramics. Hydroxyapatite (HAp), β-tricalcium phosphate (β-TCP) and α-tricalcium phosphate (α-TCP) are already marketed and used for their osteoconduction properties[1].

Objectives

This work aims to synthesize and study biphasic calcium phosphate (BCP) doped with transition metal ions such as **copper** and **zinc** and alkaline earth metal ions such as **strontium**.

- Stoichiometric HAp ceramics are well incorporated in the body after 5 years, but 15 years may be necessary for it to be replaced by new bone tissues.[2] Additionally, to avoid soft tissue invasion, bone filling materials need an adapted degradability to keep a constant volume occupancy inside the bone cavity. A fine tuning between materials biodegradation and new bone formation kinetics is thus mandatory.
- **Copper, zinc and strontium ions** are added to the BCP composition **to control inflammation**[3], **bacterial growth**[4] and **stimulate bone cell activity.**[5]

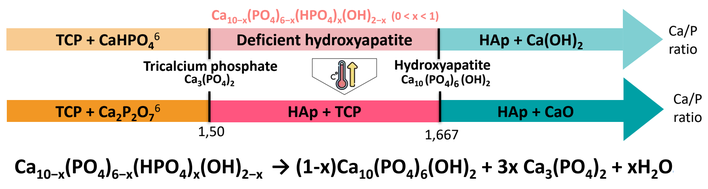

$Ca_{10-x}(PO_4)_{6-x}(HPO_4)_x(OH)_{2-x} \rightarrow (1-x)Ca_{10}(PO_4)_6(OH)_2 + 3x\ Ca_3(PO_4)_2 + xH_2O$

BCP has been synthesized through the co-precipitation of deficient HAp, followed by a thermal treatment allowing HAp and TCP formation.
In the HAp structure, strontium ions replace calcium ions, preferentially on less dense Ca(2) site (Wyckoff 6h), and zinc and copper ions are inserted and thus form an interstitial solid solution at the Wyckoff 2b sites.[6]

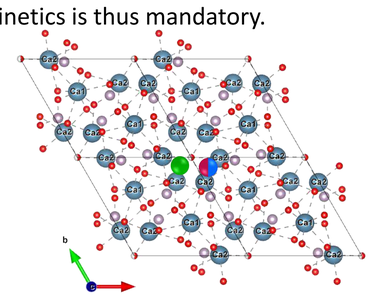

Synthesis protocol

Reactant concentrations used for the synthesis of undoped and doped samples (2.10^{-2} mol)

	$Ca(NO_3)_2{\cdot}H_2O$	$(NH_4)_2HPO_4$	dopant ions		
			$Cu(NO_3)_2{\cdot}3H_2O$	$Zn(NO_3)_2{\cdot}6H_2O$	$Sr(NO_3)_2$
HAp	0.2 M	0.12 M	0	0	0
$HApCu_1$	0.2 M	0.12 M	0.002 M	0	0
$HApZn_1$	0.2 M	0.12 M	0	0.002 M	0
$HApSr_2$	0.196 M	0.12 M	0	0	0.004 M
$HApCu_1Zn_1Sr_2$	0.196 M	0.12 M	0.002 M	0.002 M	0.004 M

➡ $Ca_{10-z}Cu_xZn_ySr_z(PO_4)_6(OH)_{2-2x-2y}(O)_{2x+2y}$

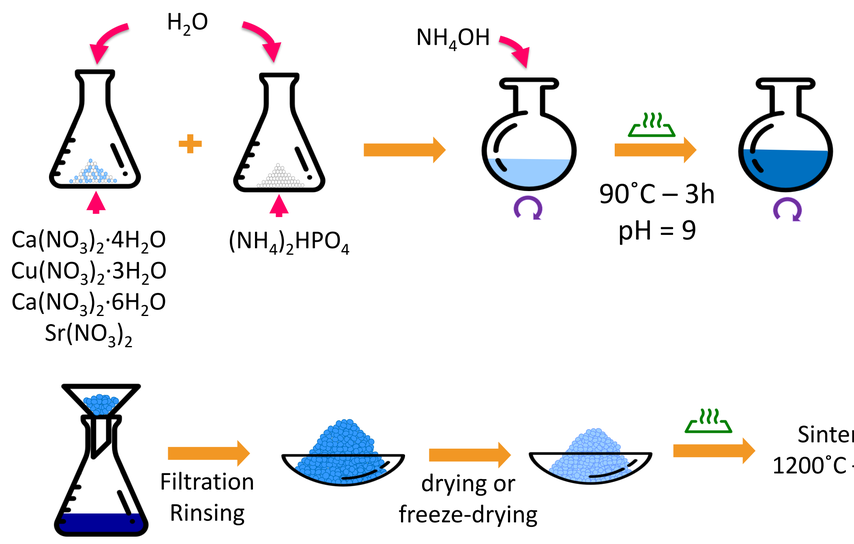

Physico-chemical analyses

SEM image of the $HApCu_1Zn_1Sr_2$ sample

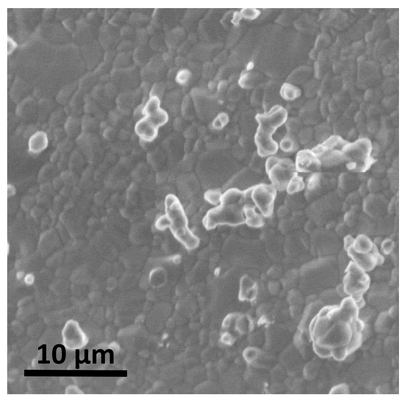

Particles size histogram of the $HApCu_1Zn_1Sr_2$ sample, fitted with a log-normal distribution function

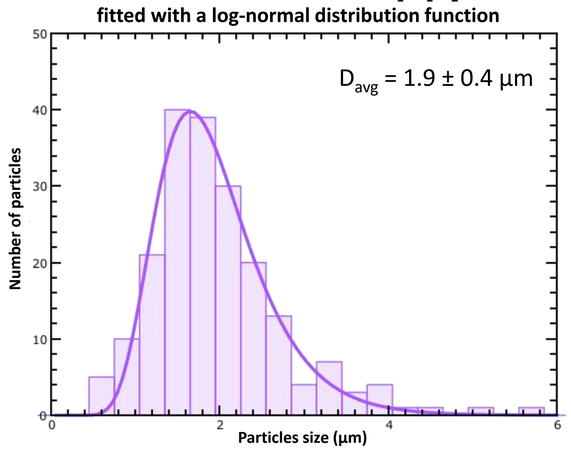

Nominal and measured (MP-AES) samples composition

	Nominal Cu/Ca ratio	Nominal Cu/Ca ratio	Nominal Cu/Ca ratio	Nominal (Ca+Sr)/P ratio	Measured Cu/Ca ratio	Measured Zn/Ca ratio	Measured Sr/Ca ratio	Measured (Ca+Sr)/P ratio
Hap	-	-	-	1.667	-	-	-	1.9 ± 0.1
$HApCu_1$	0.01	-	-	1.667	0.0028 ± 0.0005	-	-	1.8 ± 0.2
$HApZn_1$	-	0.01	-	1.667	-	0.0029 ± 0.0007	-	1.9 ± 0.2
$HApSr_2$	-	-	0.02	1.667	-	-	0.018 ± 0.001	1.99 ± 0.06
$HApCu_1Zn_1Sr_2$	0.01	0.01	0.02	1.667	0.0029 ± 0.0002	0.0029 ± 0.0002	0.017 ± 0.001	1.9 ± 0.1

X-ray diffractograms

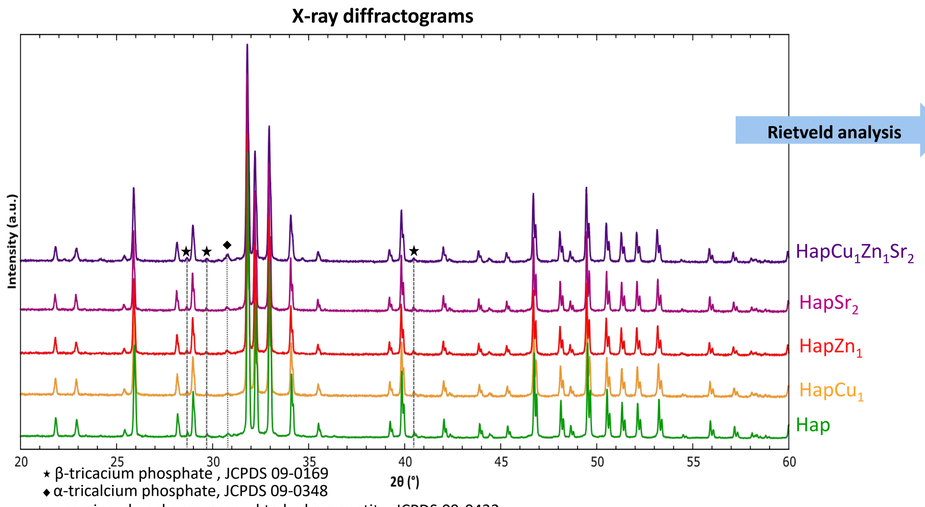

★ β-tricacium phosphate , JCPDS 09-0169
◆ α-tricalcium phosphate, JCPDS 09-0348
unassigned peaks correspond to hydroxyapatite, JCPDS 09-0432

Rietveld analysis

Phase %	$Ca_{10}(PO_4)_6(OH)_2$	α-$Ca_3(PO_4)_2$	β-$Ca_3(PO_4)_2$
HAp	98.9 ± 0.8	0	1.1 ± 0.3
$HApCu_1$	98.5 ± 0.9	0.9 ± 0.3	0.7 ± 0.3
$HApZn_1$	97.1 ± 0.9	1.8 ± 0.3	1.0 ± 0.1
$HApSr_2$	99.5 ± 0.6	0	0.5 ± 0.2
$HApCu_1Zn_1Sr_2$	94.5 ± 0.9	4.7 ± 0.3	0.8 ± 0.3

IR spectra

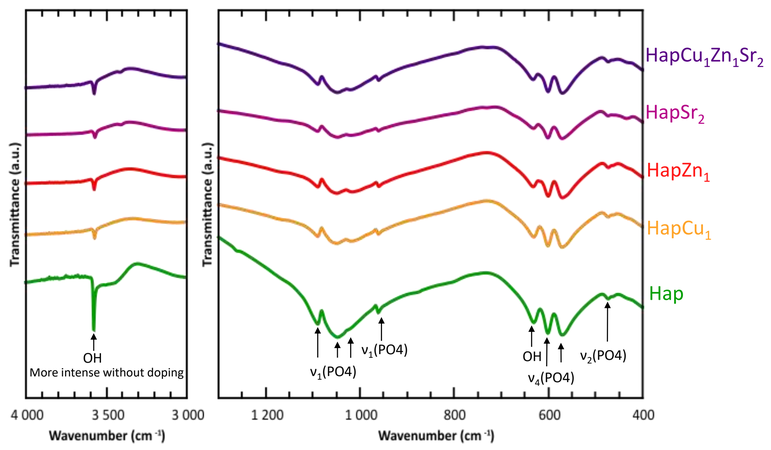

Conclusions

- **BCP powders with a high percentage of hydroxyapatite, undoped, doped with Cu^{2+}, Zn^{2+} or Sr^{2+}, or multi-doped with the 3 ions, were successfully synthesized.**
- XRD and IR spectroscopy were used as qualitative analyses and Rietveld as quantitative analysis to determine their phase composition.
- All the dopants were not inserted in the phases, as shown by the atomic emission spectroscopy analyses on the synthesized powders.

References

[1]**Marchetti** *et al. EMC - Tech Chir - Orthopédie - Traumatol*. 2010 ; 5(1):1-22; [2]**Matsumine** *et al. J Bone Jt Surg - Ser B*. 2004, 86(5):719-725; [3]**Velard** *et al Biomaterials*. 2010, 31(8):2001-2009; [4]**Colin** *et al. J Hosp Infect*. 2020, 104(3):283-292; [5]**Braux** *et al. Acta Biomater*. 2011, 7(6):2593-2603; [6]**Gomes** *et al. Chem Mater*. 2011;23(12):3072-3085

Acknowledgment

The authors acknowledge the support of the French Agence Nationale de la Recherche (ANR) for the PIMyBone project under reference ANR-21-CE19-0055.

Exact and metaheuristic approaches for short term open pit mine scheduling

AALLAOUI Soufiane[a,b], AZZAMOURI Ahlam[a], Libo Ren[c] , TCHERNEV Nikolay [a,b]
[a]EMINES, School of Industrial Management, Mohammed VI Polytechnic University 43150 Benguerir, Morocco
[b]LIMOS (UMR CNRS 6158), Clermont Auvergne University, 1 rue de la Chebarde, 63177 Aubière Cedex, France
[c]CLeRMa EA3849, Clermont Auvergne University, 11 boulevard Charles de Gaulle, 63000 Clermont-Ferrand, France

Context:

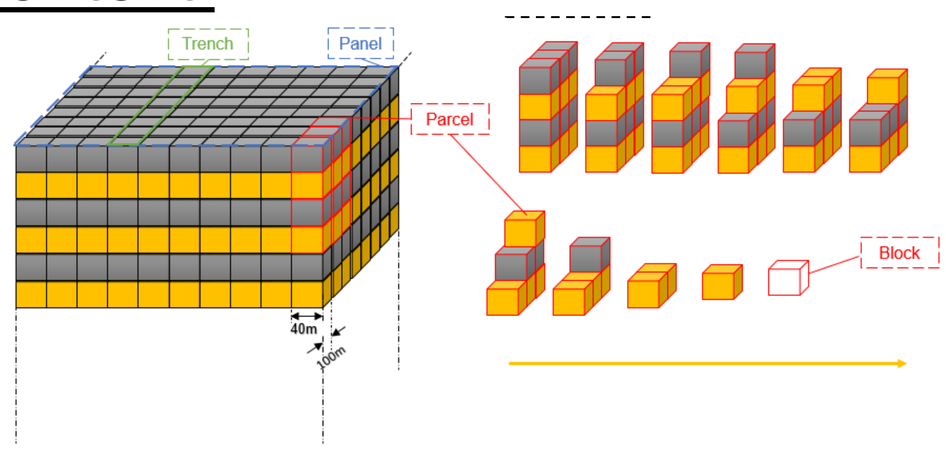

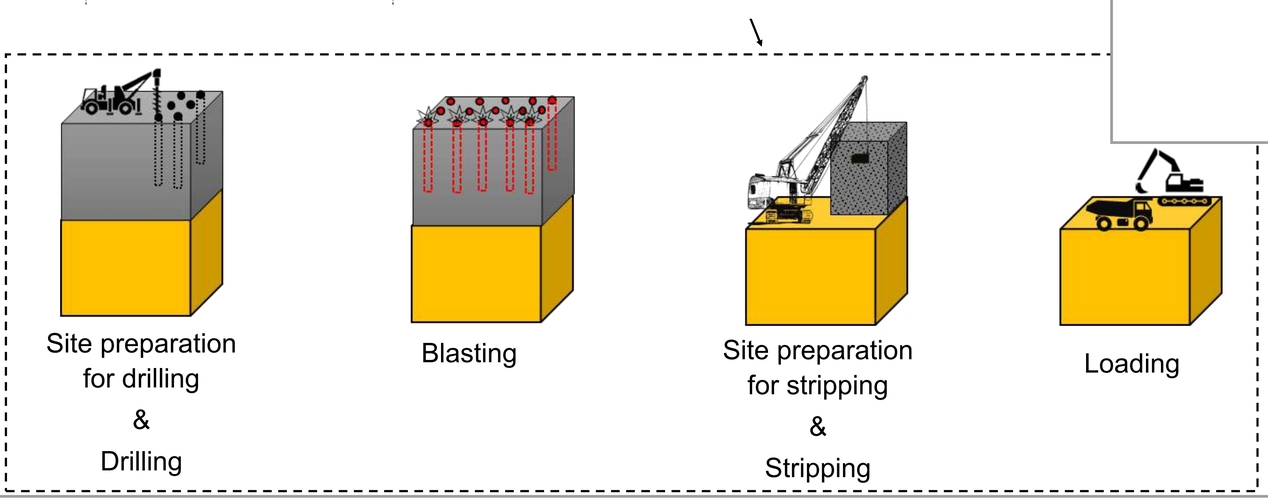

How to find the best short-term extraction process schedule?

Identification of the best spatio-temporal machinery affectation and the feeding of the extracted grades. All of this is constrained by a number of factors:

- Operations sequencing
- Machines compatibility
- Machines avaibility
- Machines motions
- Priorities of layers (urgency of obtaining certain qualities)

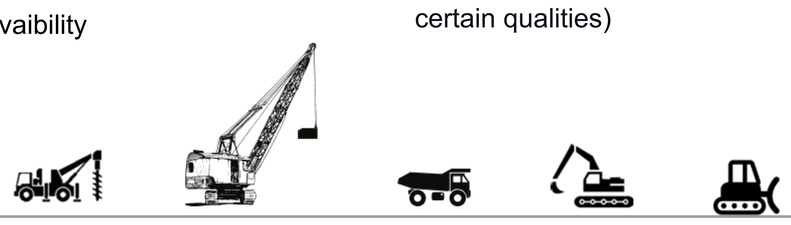

Problem formulation: Flexible Job Shop Scheduling Problem with generic minimum Time-Lags (FJSP-GTL)

FJSP represents an extension of the job shop scheduling problem which allows an operation to be processed by any processor from a given set. The problem is to affect each operation to a machine and to schedule the operations on the machines, such that makespan, the maximal completion time, of all operations is minimized. An NP-hard optimization problem (Dauzère-Pérès et al., 2023) that introduces additional complexity due to generic minimum time-lags and additional precedence constraints. The time lags are used to model the machines empty travels.

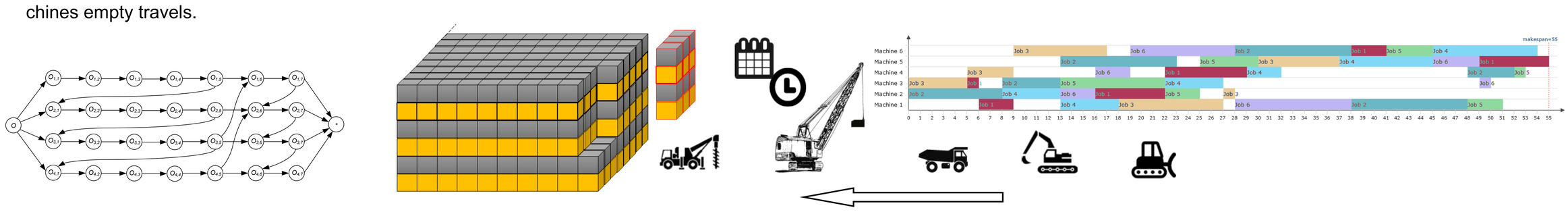

MILP formulation for FJSP-GTL

Data sets & parameters

- $J = \{1, \dots, |J|\}$ — *Set of jobs*
- $O_j = \{O_{j,1}, O_{j,2}, \dots, O_{j,|Oj|}\}$ — *Set of operations of the job j*
- $\Omega = O_1 \cup O_2 \cup \dots \cup O_{jJ|}$ — *Set of operations*
- $M_{Oj,o}$ — *Set of compatible machines with $O_{j,o}$*
- $p_{Oj,o,m}$ — *Processing time of $O_{j,o}$ processed by the machine m*
- $TL_{Oj,o,Oj',o',m}$ — *Minimum time lag between $O_{j,o}$ and $O_{j',o'}$*
- $GMT_{Oj,o,Oj',o',m}$ — *Generic time lag between $O_{j,o}$ and $O_{j',o'}$*
- $Succ_{Oj,o}$ — *The set of $O_{j,o}$'s successors*
- H — *A large positive number*

Continuous variables

- $p_{Oj,o}$ — *Processing time of the operation $O_{j,o}$*
- $St_{Oj,o}$ — *Starting time of the operation $O_{j,o}$*
- C_{max} — *Makespan, i.e. the completion time of the last operation*

Binary variables

- $y_{Oj,o,m}$ — *=1 if $O_{j,o}$ is assigned to the machine m*
- $x_{Oj,o,Oj',o',m}$ — *=1 if $O_{j,o}$ is processed before $O_{j',o'}$ on the machine m*

Objectif function

$$\text{Minimize } C_{max} \quad (1)$$

Subject to

$$St_{Oj,o} + p_{Oj,o} \le C_{max}, \ \forall O_{j,o} \in \Omega \quad (2)$$

$$\sum_m y_{Oj,o,m} = 1, \ \forall O_{j,o} \in \Omega \quad (3)$$

$$p_{Oj,o} = \sum_m y_{Oj,o,m} * p_{Oj,o,m}, \ \forall O_{j,o} \in \Omega \quad (4)$$

$$x_{Oj,o,Oj',o',m} + x_{Oj',o',Oj,o,m} - y_{Oj,o,m} - y_{Oj',o',m} \ge -1, \ \forall O_{j,o}, O_{j',o'} \in \Omega, O_{j,o} \ne O_{j',o'}, \forall m \in M_{Oj,o} \cap M_{Oj',o'} \quad (5)$$

$$2x_{Oj,o,Oj',o',m} + 2x_{Oj',o',Oj,o,m} - y_{Oj,o,m} - y_{Oj',o',m} \le 0, \ \forall O_{j,o}, O_{j',o'} \in \Omega, O_{j,o} \ne O_{j',o'}, \forall m \in M_{Oj,o} \cap M_{Oj',o'} \quad (6)$$

$$St_{Oj,o} + p_{Oj,o} + TL_{Oj,o,Oj',o',m} \le St_{Oj',o'} + H(1 - y_{Oj,o,m}), \ \forall O_{j,o} \in \Omega, \ \forall O_{j',o'} \in Succ_{Oj}, \ , \forall m \in M_{Oj,o} \quad (7)$$

$$St_{Oj,o} + p_{Oj,o} + GMT_{Oj,o,Oj',o',m} \le St_{Oj',o'} + H(1 - x_{Oj,o,Oj',o',m}), \ \forall O_{j,o}, O_{j',o'} \in \Omega, \forall m \in M_{Oj,o} \cap M_{Oj',o'} \quad (8)$$

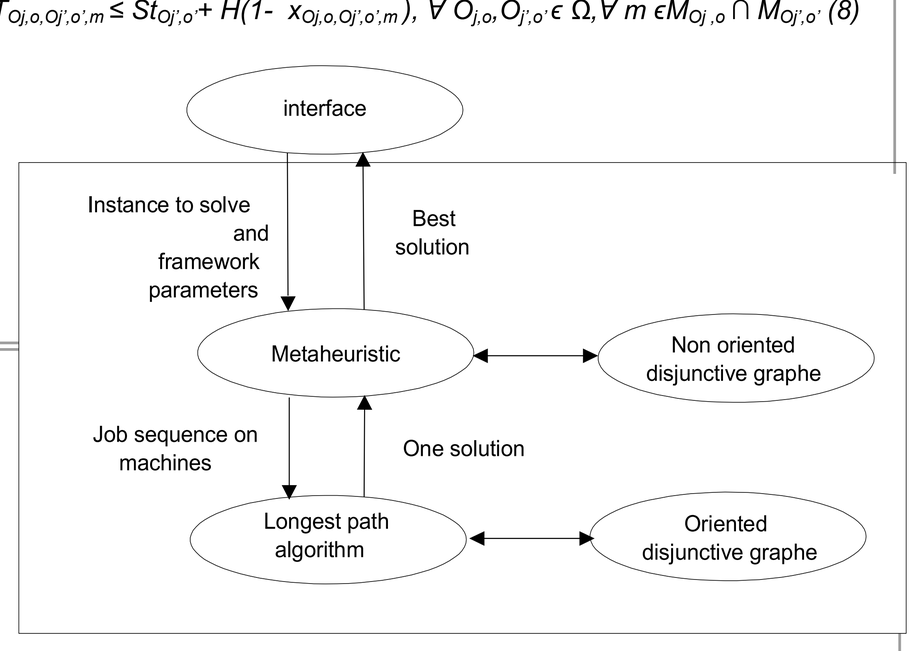

Computational experiments:

Instances	Avg. GAP (%)		Avg. CPU Time (s.)	
	MILP*	GRASPmELS	MILP*	GRASPmELS
Small instances	0	0.2	11	45
Medium instances	**0.1**	**0.1**	6972	1
Large instances	18	20	31744	81

**CPU time limited to 12h*

Contact: soufiane.aallaoui@emines.um6p.ma

Hybrid Reasoning & Dynamic Recommendations to Optimize Group Dynamics

Zineddine ZAHOUANI, Farouk TOUMANI and Marinette BOUET
Clermont Auvergne University
zineddine.zahouani@doctorant.uca.fr

1 Introduction

- Improving the group dynamics by leveraging the power of AI.
- ECCIPE serves as a collaborative platform for students.

2 Key Research Questions

- The identification of primary antecedent behaviors.
- Formal description of the group dynamics.
- Crafting a hybrid reasoning mechanism, including both inductive and deductive reasoning.
- Providing timely and contextually relevant feedback founded on group dynamics.

3 Approach

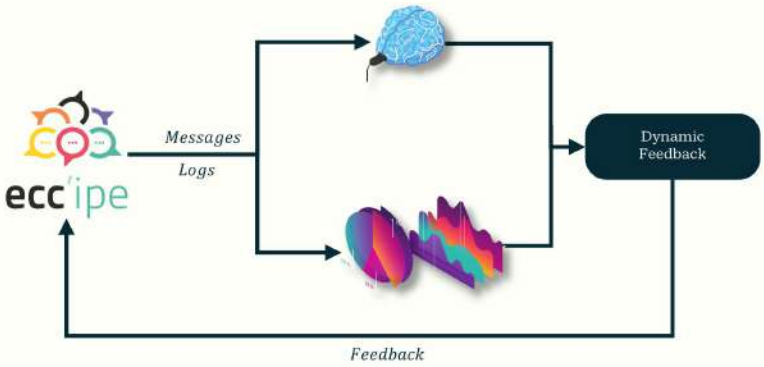

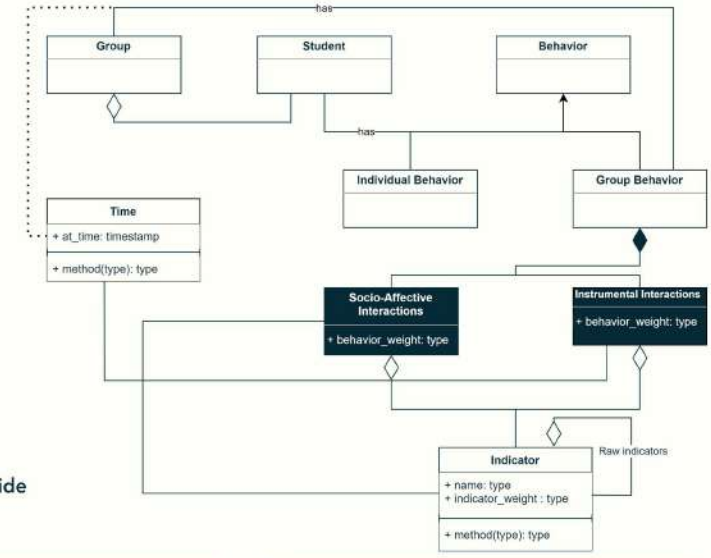

- The usage of statistics and AI-driven solutions to process real-time data and provide dynamic recommendations.

4 Preliminary Results

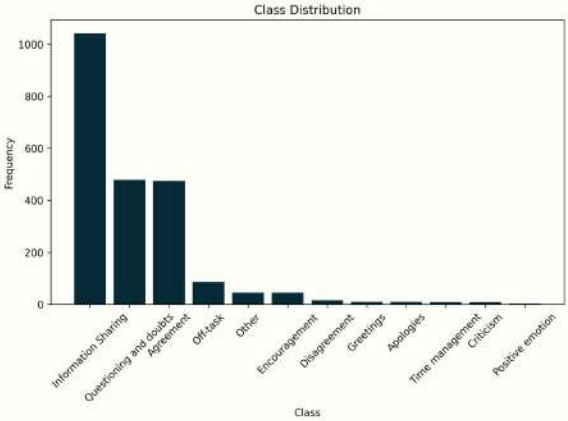

Text Generation models:

Model	Context	Accuracy	T-per request
Llama2	w=10	58%	30.73s
Hermes	w=5	63%	34.37s
GPT3.5	w=5	56%	3-5s
GPT4	w=5	**79%**	3-5s

Text Classification models (without context):

Model	Accuracy	T-per request
GT + Deberta	40%	1.44s
TL-BERT-v1	79%	0.27s
TL-BERT-v2	**81%**	0.28s

5 Future work

- Leveraging the established NLP building blocks to enhance results.
- Developing an automatic dynamic context detection block, incorporating relevant previous messages.
- Conducting several analyses on the logged data aiming to induce rules.

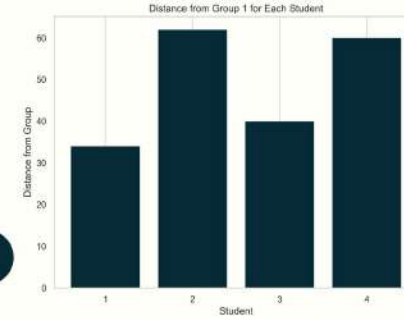

6 References

- Donelson R Forsyth. *Group dynamics*. Wadsworth Cengage Learning, 2014.
- Robert A Sottilare, et al. Designing adaptive instruction for teams: A meta-analysis.International Journal of Artificial Intelligence in Education, 28:225-264, 2018

Réglage adaptatif et générique de lois de commande pour un robot agricole

Luc Desbos[1], Christophe Debain[2], Roland Lenain[2], Caroline Acanfora[1], Jean Laneurit[2], Philippe Heritier[2]

[1]Agreenculture, 20 av Didier Daurat, 31400 Toulouse, France

[2]Université Clermont Auvergne, INRAE, UR TSCF, Aubière, F 63178, France

Introduction

Le réglage de gains est une étape cruciale de la synthèse d'un contrôleur pour robot agricole. Souvent, il est réalisé par un expert, qui fixe les paramètres de contrôle pour toute la durée de vie du véhicule autonome.

Problématique :

- Réglage fastidieux, énergivore et chronophage.
- Réglage sous optimal, ou instable, si les conditions d'utilisation évoluent dans le temps (dû au terrain, aux interactions de l'outil, etc..).

Défauts des méthodes actuelles de réglage de gains :

- Non applicables en temps réel [1]
- Non adaptées à l'utilisation sur microcontrôleur [2]
- Non génériques [2], [3]

Contexte

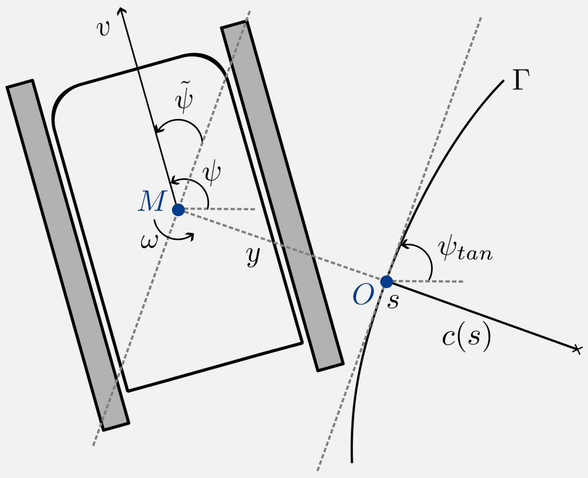

Pour le suivi d'une trajectoire Γ à une vitesse donnée v, on détermine $\omega = \omega_y + \omega_c$:

$$\begin{cases} \omega_y &= k_\psi \left(\tilde{\psi} - \arctan\left(\dfrac{k_y y}{1 - c(s) y} \right) \right) \\ \omega_c &= c(s) \dfrac{v \cos(\tilde{\psi})}{1 - c(s) y} \end{cases}$$

avec k_y et k_ψ des gains, et ω_c un terme qui peut être adapté par une approche prédictive.

Approche

Proposition d'une nouvelle approche permettant l'adaptation des paramètres de guidage d'un contrôleur backstepping avec un terme de prédiction feedforward ou MPC.

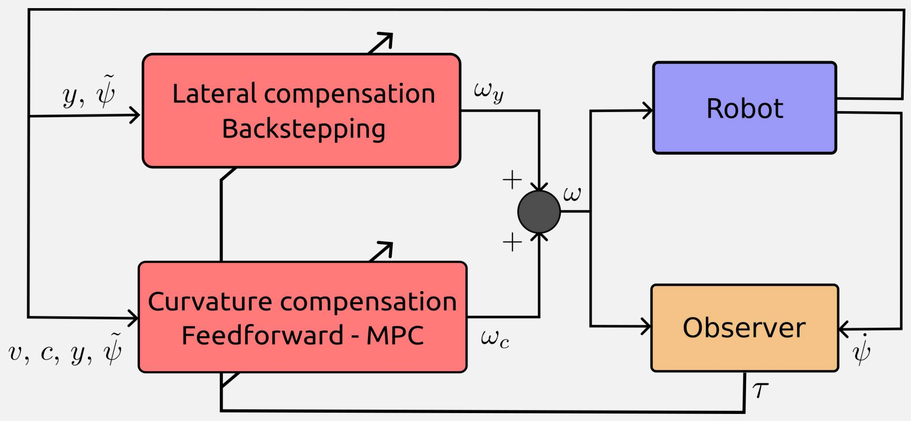

L'observateur non linéaire évalue la réactivité du système robotique via l'estimation d'une constante de temps τ associée à un modèle d'ordre 1. Les gains du backstepping, et les paramètres des approches prédictives sont ajustés. Le contrôleur est ainsi adapté aux capacités du véhicule.

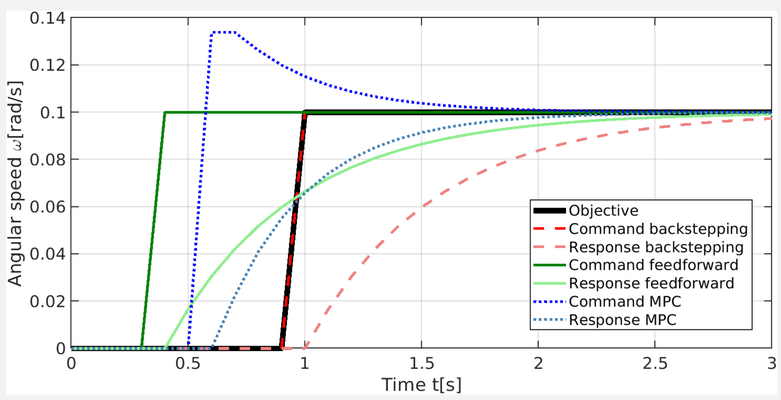

Résultats expérimentaux

Réalisation d'essais avec le robot Céol d'Agreenculture. On dégrade volontairement les performances du bas niveau pour créer différents scénarios, et ainsi évaluer la faculté d'adaptation de l'approche proposée.

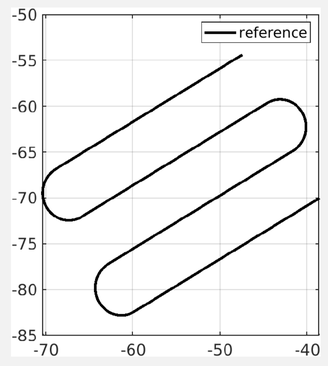

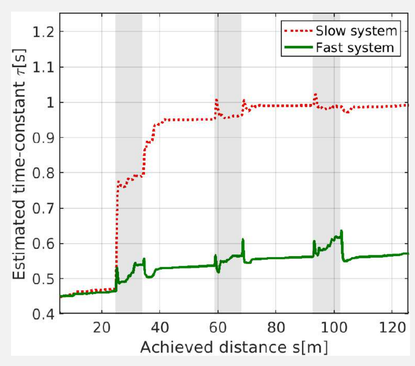

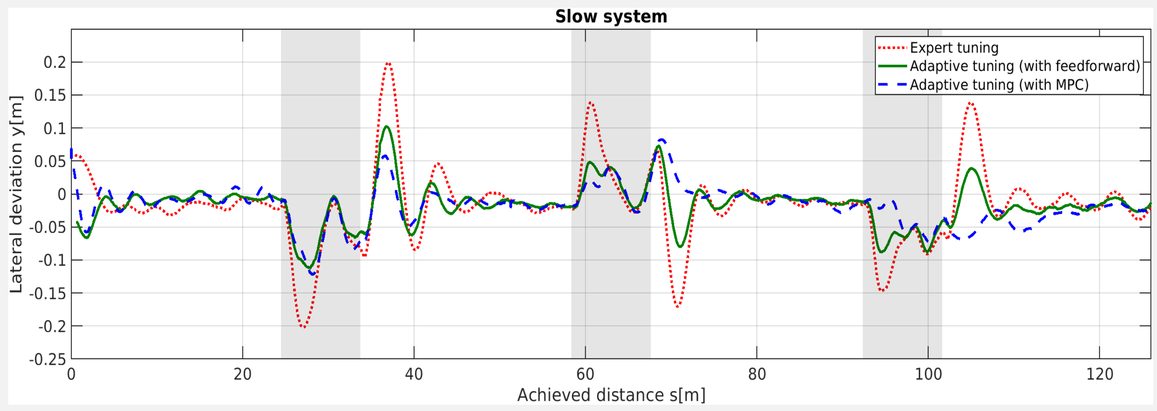

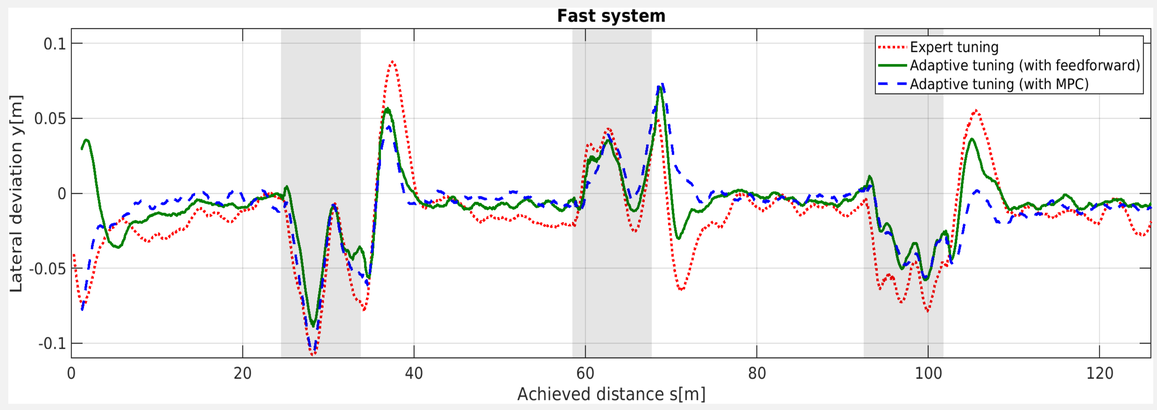

La nouvelle approche permet d'adapter les gains et paramètres de prédiction en fonction de l'estimation de τ. Ainsi, de meilleures performances de suivi de trajectoire sont obtenues quel que soient les capacités de la machine.

Conclusions

Avantages de la solution :

- Gains qui s'adaptent aux conditions d'adhérence changeantes (vitesse longitudinale, terrain, usure véhicule, etc...).
- Performances optimales en toute situation.
- Généricité, applicable aux véhicules skid-steering et ackermann.
- Adaptée pour l'utilisation temps réel sur des cibles embarquées.

Perspectives :

- Tests à grande échelle (RX20, Karl, …).
- Utilisation d'un modèle véhicule plus représentatif.
- Adaptation aux véhicules évoluant dans un espace 3D.

Bibliographie

1. **N. J. Killingsworth et M. Krstic, « PID tuning using extremum seeking: online, model-free performance optimization », IEEE control systems magazine, vol. 26, no 1, p. 70-79, 2006.**
2. **F. Berkenkamp, A. P. Schoellig, et A. Krause, « Safe Controller Optimization for Quadrotors with Gaussian Processes », août 2017.**
3. **A. Hill, J. Laneurit, R. Lenain, et E. Lucet, « Online Tuning of Control Parameters for Off-Road Mobile Robots: Novel Deterministic and Neural Network-Based Approaches », IEEE Robotics & Automation Magazine, vol. 30, nº 3, p. 44-55, sept. 2023.**

luc.desbos@agreenculture.fr

Étude des interactions contenant-contenu entre des préparations ophtalmiques et des flacons de collyres multidoses

M. Barrieu, P. Chennell, V. Sautou

Université Clermont Auvergne, CHU Clermont-Ferrand, Clermont Auvergne INP, CNRS, ICCF, Clermont-Ferrand F-63000, France

Contexte

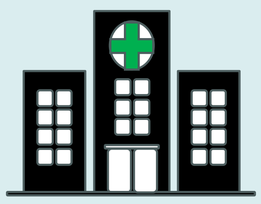

Les pharmaciens hospitaliers mettent en œuvre des préparations pharmaceutiques (PP) pour apporter une réponse thérapeutique à des pathologies pour lesquelles il n'existe pas de solution commercialisée disponible et/ou adaptée. Le pharmacien, en plus de vérifier la faisabilité clinico-technique de la préparation, doit s'assurer de sa sécurité et du maintien de son intégrité, de l'étape de préparation jusqu'à l'administration, via des études de stabilité physico-chimique et microbiologique.

Problématique

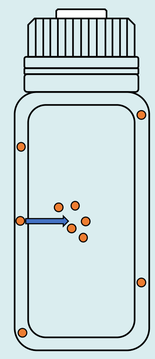

Certains additifs contenus dans les articles de conditionnement et les dispositifs médicaux d'administration sont susceptibles, dans certaines conditions, de migrer au sein de la préparation. Lors d'études de stabilité simulant un usage patient, il a été constaté que des phénomènes d'interactions contenu-contenant peuvent se produire. Par exemple, lors du développement d'un collyre de tacrolimus, des phénomènes non prévus de relargage ont été mis en évidence lors de la mise en contact de la préparation avec le dispositif de délivrance multidoses (1).

Objectifs

Ces phénomènes de relargage soulèvent plusieurs questions, comme celle de la toxicité potentielle pour l'œil des composés relargués ou encore celle de la présence de ce(s) composé(s) dans d'autres préparations que le tacrolimus, conditionnées aussi dans les flacons multidoses. Il en découle les objectifs suivants :

1. Identification et quantification des extractibles et relargables des flacons multidoses sans conservateur en contact avec des préparations hospitalières
2. Analyse des matériaux et de l'interface matériau/préparation
3. Analyse de la toxicité cellulaire des composés identifiés

Matériel et méthodes

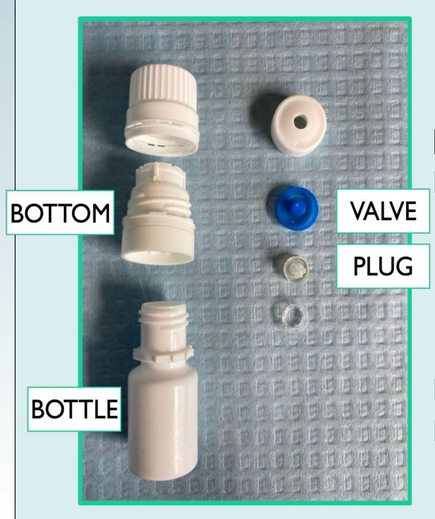

Pièces constituant le dispositif ophtalmique multidose (DOM)

PARTIE 1 : IDENTIFICATION ET QUANTIFICATION DES EXTRACTIBLES ET RELARGABLES

Recherche des extractibles et des relargables (2,3) → Quantification des extractibles et des relargables

EXTRACTIBLES

- ❑ Contact des pièces avec des solvants :
  - Polaires : Eau pH 3 et pH 9
  - Apolaires : Hexane
  - Intermédiaires: IPA*, IPA/H_20 (1:1), Acétone
- ❑ Macération pendant 3 jours
- ❑ Analyse à t0, à 24h, 48h et 72h

RELARGABLES

- ❑ Contact du DOM avec des PP :
  - Tacrolimus 0,2 mg/ml,
  - Ciclosporine 1 et 10 mg/ml,
  - Atropine 0,1 mg/ml,
  - H_20/Éthanol 1:1 (4)
- ❑ Analyse à t0, 4 et 6 mois de stockage
- ❑ Analyse de flacons couchés et debout
- ❑ Simulation d'administration (essai in-use)

IDENTIFICATION DES COMPOSÉS* :

- ❑ Composés non volatiles → LC-MS/MS
- ❑ Composés semi-volatiles → LC-MS/MS et GC-MS
- ❑ Composés volatiles → HS/GC-MS
- ❑ Composés inorganiques → ICP-MS

SEMI-QUANTIFICATION* :

$$RRF composé = \frac{AUC\ RS}{AUC\ IS} * \frac{CIS}{CRS} \qquad Ccomposé = \frac{AUC\ composé}{RRF\ composé} * \frac{CIS}{AUC\ IS}$$

PARTIE 2 : ANALYSE DES MATÉRIAUX ET DE L'INTERFACE MATÉRIAU/PRÉPARATION

FTIR* | Microscopie optique électronique + EDS* | XPS* | Potentiel zêta | Angles de contact

PARTIE 3 : ANALYSE DE LA TOXICITÉ CELLULAIRE DES COMPOSES IDENTIFIÉS

Analyse de la littérature
+
Essai de cytotoxicité in vitro au MTT* selon ISO 10993-5

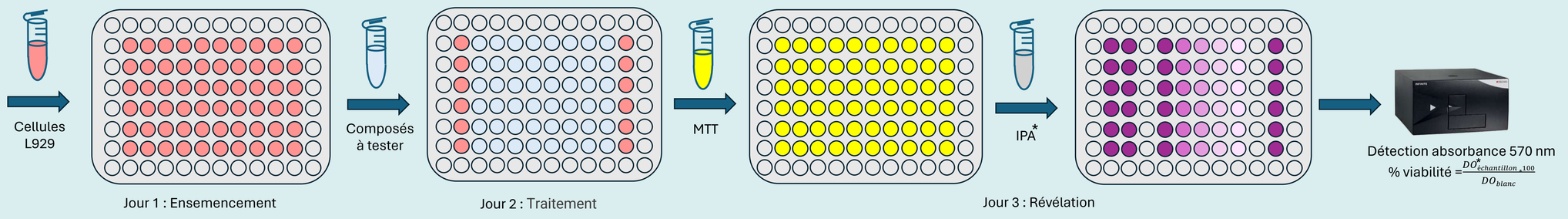

Résultats préliminaires et discussion

Exemple du 2,4 di-tert-butylphenol (DTBP)

PARTIE 1 – EXTRACTIBLE

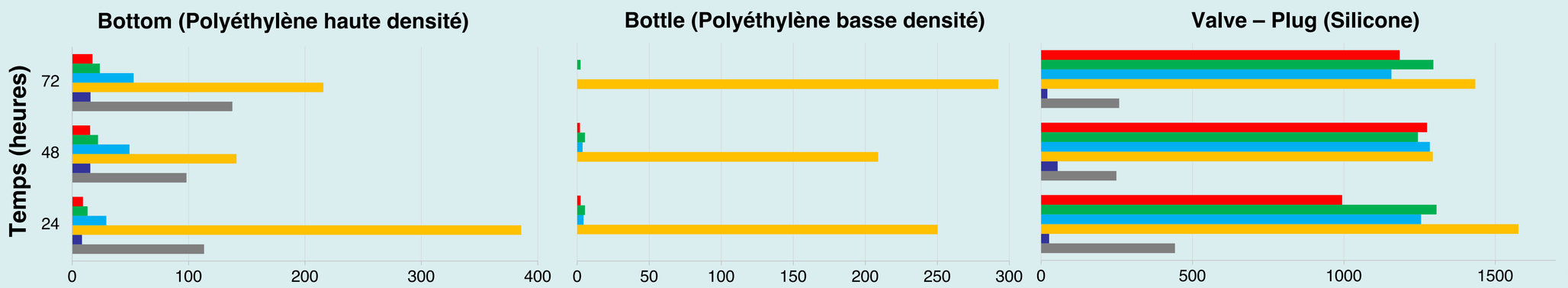

Concentration du 2,4 DTBP (ng/ml) extrait des pièces du DOM au contact des différents solvants

→ 2,4 DTBP retrouvé dans les différentes pièces analysées mais principalement au sein de la valve/plug en silicone

PARTIE 1 – RELARGABLE

Concentration du 2,4 DTBP retrouvé dans des préparations après 4 mois de stockage. Moyenne (ng/ml) ± Ecart type n=4		
Type de conditionnement	**Ethanol/H_20 (1:1)**	**Atropine 0,1 mg/ml**
Témoin (flacon en verre)	2,3 ± 0,5	3,3 ± 0,3
Stockage flacon couché (DOM)	15,5 ± 19,6	2,3 ± 0,4
Stockage flacon debout (DOM)	1,6 ± 0,8	2,2 ± 0,3

→ Impact du mode de conservation sur le relargage du 2,4 DTBP
→ Issu du contact du plug en silicone avec la préparation en stockage couché
→ Présence du 2,4 DTBP dans les témoins : Contamination par process de fabrication ?

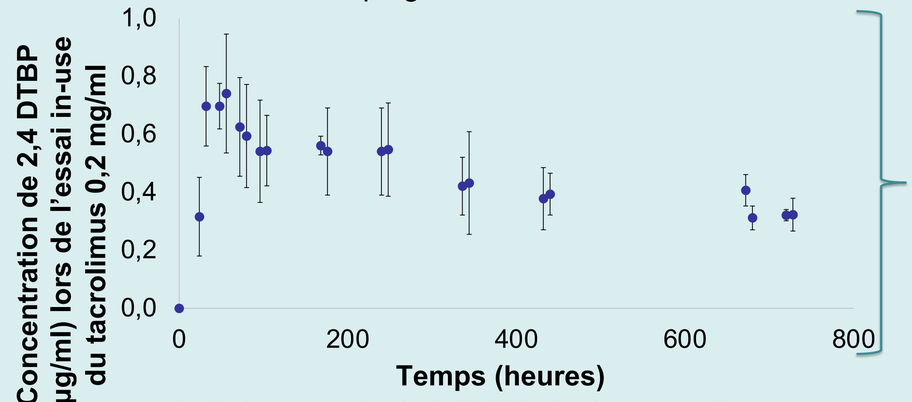

→ Relargage du 2,4 DTBP dès les premières gouttes
→ Décroissance au cours du temps

Références et abréviations*

(1) Barrieu et al. "Physicochemical Stability of a Novel Tacrolimus Ophthalmic Formulation for the Treatment of Ophthalmic Inflammatory Diseases." Pharmaceutics vol. 14,1 118. 4 Jan. 2022, doi:10.3390/pharmaceutics14010118
(2) Jenke et al. "Extractables characterization for five materials of construction representative of packaging systems used for parenteral and ophthalmic drug products." PDA journal of pharmaceutical science and technology vol. 67,5 (2013): 448-511.
(3) Jenke et al. « Simulated Leaching (Migration) Study for a Model Container-Closure System Applicable to Parenteral and Ophthalmic Drug Products » PDA J Pharm Sci and Tech 2017, 71 68-87
(4) Jenke et al « A Means of Establishing and Justifying Binary Ethanol/Water Mixtures as Simulating Solvents in Extractables Studies » PDA J Pharm Sci and Tech 2015, 69 366-382

IPA : Isopropanol – **LC** : Chromatographie liquide – **MS** : Spectrométrie de masse – **GC** : Chromatographie gazeuse – **HS** : Headspace – **ICP** : Spectrométrie à plasma à couplage inductif – **RRF** : Relative Response Factor – **AUC** : Area Under Curve – **RS** : Standard de référence – **IS** : Standard interne – **C** : Concentration – **FTIR** : Spectroscopie infrarouge à transformée de Fourier – **XPS** : Spectroscopie de Photoélectrons X – **EDS** : Spectroscopie à rayons X à dispersion d'énergie – **MTT** : 3-(4,5-diméthylthiazol-2-yl)-2,5-bromure de diphényltétrazolium – **DO** : Densité optique

OLAP cube extension

Présenté par :Alassane COULIBALY[1],
encadré par: Sandro BIMONTE[1], Stefano RIZZI[2]
[1]TSCF, INRAE Clermont-Ferrand, 9 Avenue Blaise Pascal, Aubière, 63178, France
[2]DISI, University of Bologna, Viale Risorgimento, 2, Bologna, 40136, Italy

Introduction

Managing unstructured and heterogeneous data, integrating them, and enabling their analysis are among the key challenges in data ecosystems, together with the need to accommodate a progressive growth in these systems by seamlessly supporting extensibility. This is particularly relevant for OLAP analyses on multidimensional cubes stored in data warehouses (DWs), which naturally span large portions of heterogeneous data, possibly relying on different data models (relational, document-based, graph-based).

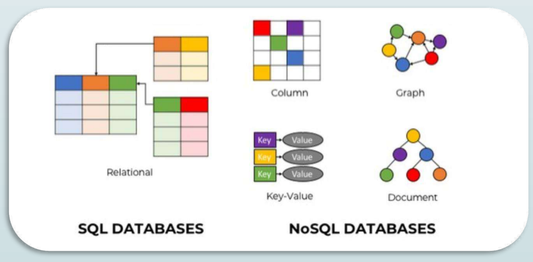

In a previous a paper we have investigated a schema-on-read scenario aimed at granting the extensibility of multidimensional cubes by proposing an architecture to support it and discussing the main open issues associated.

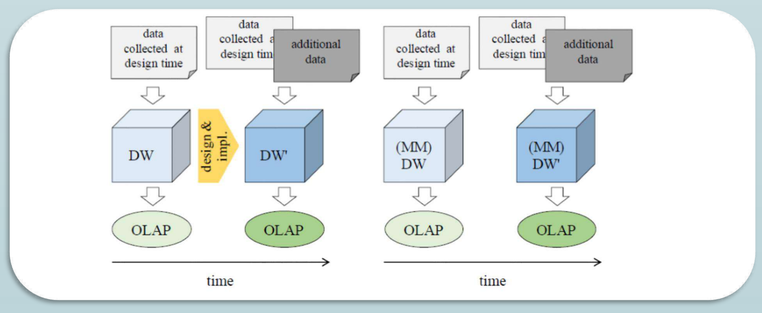

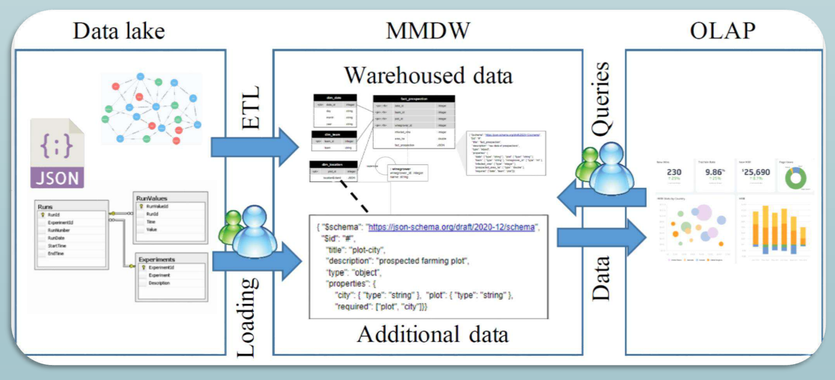

The main novel contributions with respect to the previous work are:

- ✓ A lightweight formalization of the three models we will consider in the paper is provided, and dependency trees are introduced as a tool to model multidimensional schema and support their extension
- ✓ The xCube approach is explained in detail, and the algorithms for extending dependency trees are formalized
- ✓ A proof-of-concept implementation of xCube using AgensGraph and Mondrian is described.

Methods

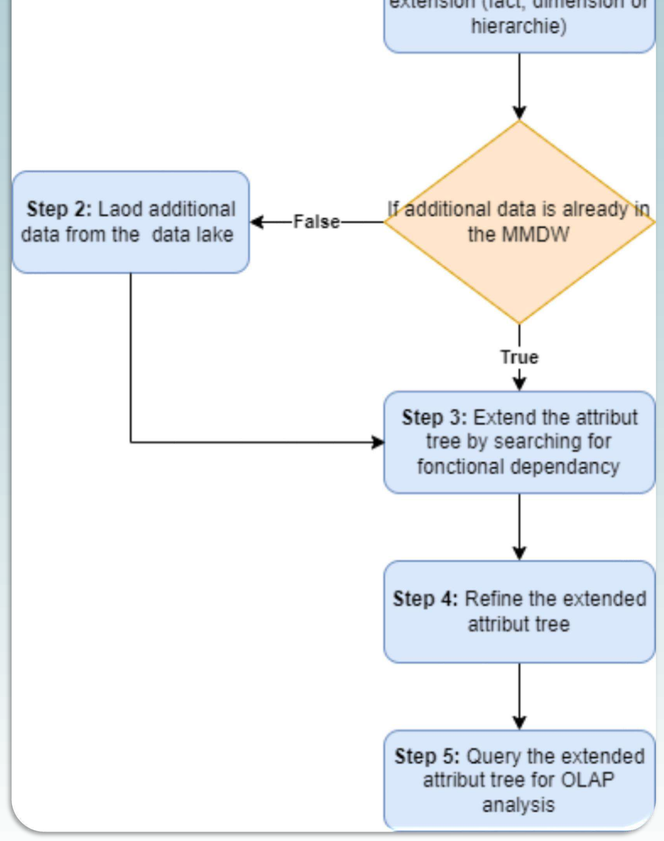

Results

Given the dependency tree of a multidimensional cube

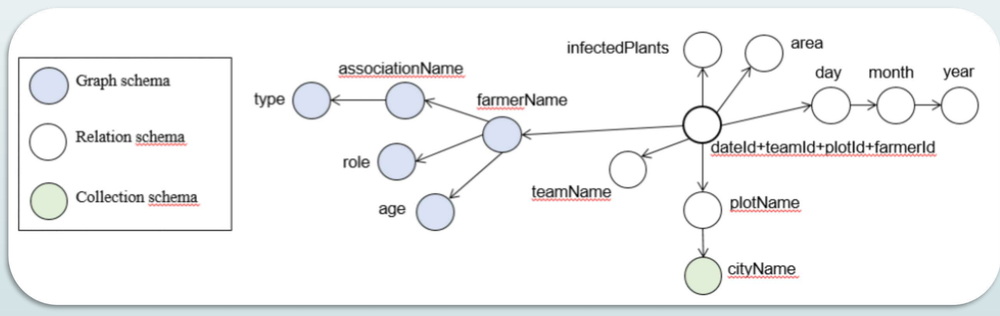

The xCube approach can extend it to add new measure (a), hierarchy (b) or level (c) and execute OLAP queries other the extended cube

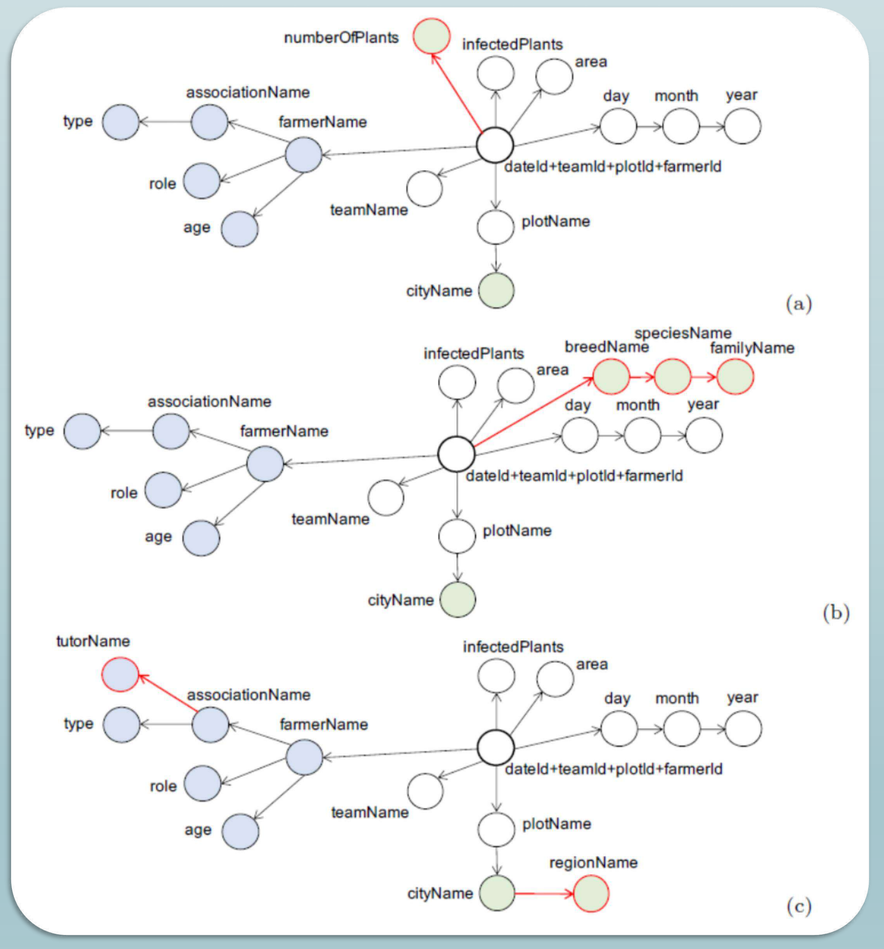


```
<Dimension name="Farmer" foreignKey="farmerId">
  <Hierarchy hasAll="all" primaryKey="farmerId">
    <View alias="farmersNetwork">
      <SQL>
        select cast(n->>'farmerId' as integer) as farmerId,
               n->>'farmerName'     as farmer,
               m->>'associatioName' as association,
               l->>'tutorName'      as tutor
        from (match (n:farmer)-[:ismember]->(m:association)-[:supportedBy]->(
             l:tutor)
               return n,m,l)  as dev
      </SQL>
    </View>
    <Level name="Tutor"       column="tutor"       uniqueMembers="true"/>
    <Level name="Association" column="association" uniqueMembers="true"/>
    <Level name="Farmer"      column="farmer"      uniqueMembers="true" />
  </Hierarchy>
</Dimension>
```

Conclusions

We have presented xCube, a schema-on-read, supply-driven approach to extend multidimensional cubes on demand using multi-model data sources. The motivation for extending cubes comes from the need to accommodate a progressive growth in data ecosystems, to let researchers add on-demand the fresh data they need to test their theories. By adopting an MMDBMS for storage, schemaless data can be seamlessly warehoused next to relational ones, so as to ensure maximum flexibility and extensibility. Users can then select how to extend the multidimensional schema of a cube with new dimensions, levels, and measures, by selecting pieces of data from a data lake and having them uploaded to the MMDW layer.

Bibliography

1. **Coulibaly, F. A., Sandro, B., & Rizzi, S. (2023). Towards a Multi-Model Approach to Support User-Driven Extensibility in Data Warehouses: Agro-ecology Case Study. In Proceedings 2nd International Workshop on Data Platform Design, Management, and Optimization (DataPlat 2023) (Vol. 3379, pp. 1-5). CEUR.**
2. **Bimonte, S., Coulibaly, F. A., & Rizzi, S. (2024). An approach to on-demand extension of multidimensional cubes in multi-model settings: Application to IoT-based agro-ecology. Data & Knowledge Engineering, 150, 102267.**

Evaluation of the artificial perception in dusty environments with experimental and numerical approaches

***Safae Nejjari*[1,*] - *Amine Ben Daoued*[1] - *Frédéric Bernardin*[1] - *Christophe Debain*[2] - *Philippe Samuel Heritier*[2]**

[1]***CEREMA*** *– 8 Rue Bernard Palissy, 63100 Clermont–Ferrand –* ***France***
[2]***INRAE*** *– 9 Av. Blaise Pascal, 63170 Aubière –* ***France***
[*]***safae.nejjari@cerema.fr***

INTERNATIONAL RESEARCH CENTRE ON INNOVATIVE TRANSPORTATION AND PRODUCTION SYSTEMS
Université Clermont Auvergne

Motivation

Digitalization and robotics are revolutionizing agriculture by providing farmers with advanced tools to enhance the productivity, sustainability, and profitability of their crops, thereby contributing to the agroecological transition. This approach relies notably on the use of optical sensors integrated into agricultural robots, allowing for detailed monitoring of plants and soil. They are also widely employed for the automated guidance of agricultural robots, whether for their localization or to ensure the safety of their operation.

Major challenge: How to assess the impact of suspended dust in the agricultural environment on the reliability of these sensors?

Study of a robotized electric tractor for agroecology. © INRAE

The presence of dust in the air, resulting from various agricultural activities involving machinery equipped with tools for soil work or harvesting, for example, compromises the performance of optical sensors. This affects the quality of collected data, compromising the results of algorithms dedicated to tasks such as crop monitoring or navigation.

This work aims to deepen our understanding of optical sensor performance in dusty conditions, with the goal of enhancing agricultural practices to make them more resilient and effective.

Main objectives

- Build a controlled dust chamber for the experiments
- Develop numerical models to simulate the impact of dust influences artificial perception in agricultural settings
- Validate the numerical model based on measurements

Status of peanut harvesting operations in Henan, China [1]

Methods

The methodology of this study combines experimental and numerical approaches to simulate the behaviour of perception sensors (e.g., camera, Lidar, ect.) in dusty media.

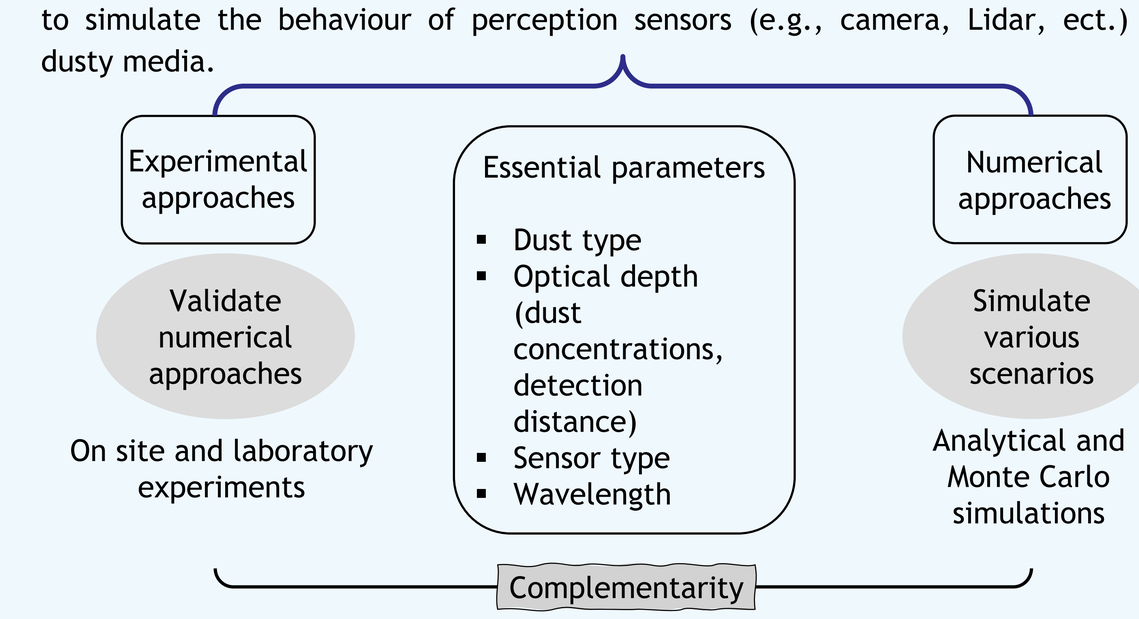

Experimental prototype

The experimental prototype ensures repeatability of realistic scenarios. This will allow to validate the numerical models to ensure their fidelity to reality.

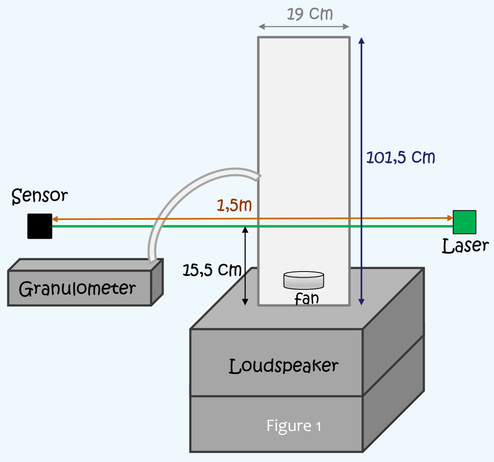

Figure 1

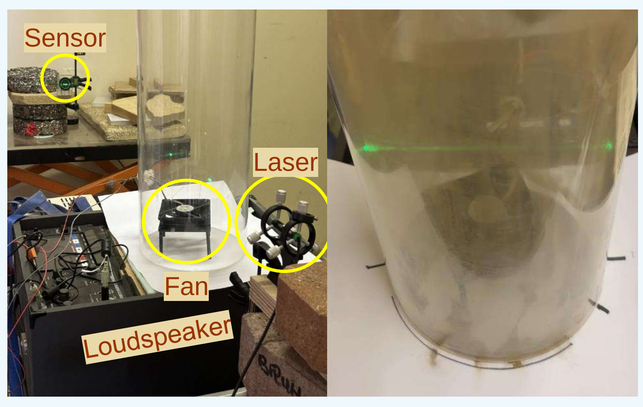

Numerical approaches

Modeling the behaviour of perception sensors in dusty media is based on the the radiative transfer theory, which allows to simulate the propagation of electromagnetic waves in a participating medium with given optical parameters.

Radiative transfer equation [2]*:*

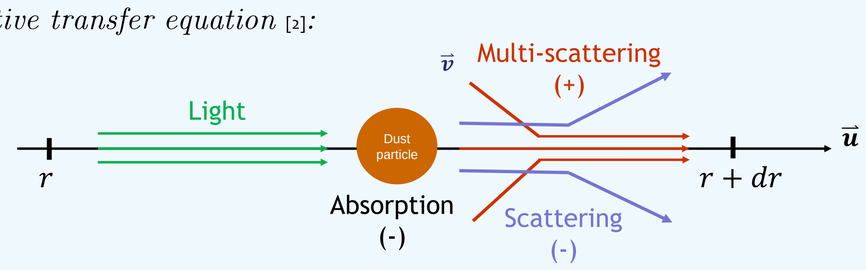

$$L_\lambda(r+dr, t+dt, \vec{u}) - L_\lambda(r, t, \vec{u}) = -Scattering - Absorption + Multi\_scattering$$

$$\frac{1}{c}\frac{\partial L_\lambda}{\partial t}(t,r,\vec{u}) + \vec{u}.\nabla_r L_\lambda(t,r,\vec{u}) = -\sigma_\lambda L_\lambda(t,r,\vec{u}) - \kappa_\lambda L_\lambda(t,r,\vec{u}) + \frac{\sigma_\lambda(r)}{4\pi}\int_{\mathbb{S}^2} L_\lambda(t,r,\vec{v})\,\phi_\lambda(r,\vec{u},\vec{v})\,dv$$

Results

Experimental measurements of particle size distribution data collected in a field in Montoldre at the AgroTechnoPôle site of INRAE. That campaign allowed to extract dust samples to be injected later in the dust experimental prototype.

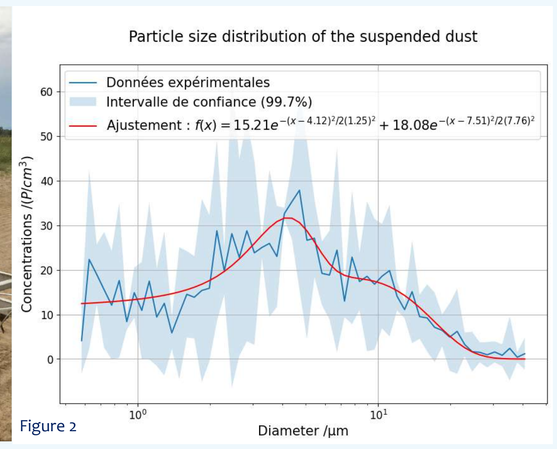

Figure 2

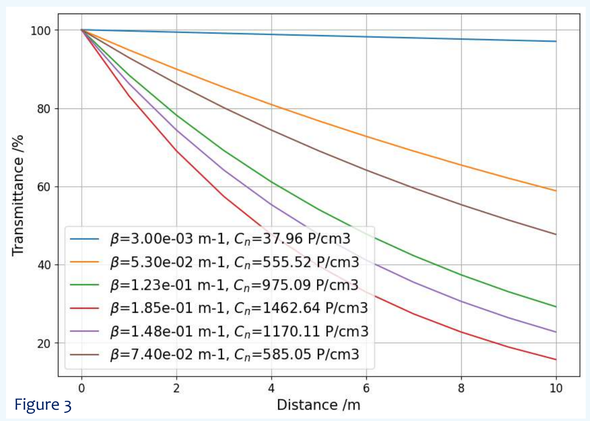

Figure 3

These initial measurements allowed us to calculate the extinction coefficients related to the dust concentration put into suspension by the tractor using Mie theory. The transmittance of a signal was then estimated as a function of its wavelength (520nm in the graph on the right) using the Beer-Lambert's law $T = e^{-\beta d}$, where β is the extinction coefficient.

Laser divergence	$0{,}17°$
Laser radius	$1\ mm$
Sensor radius	$1\ cm$
Sensor opening angle	$5°$
Extinction coeff. β	$3.10^{-3}\ m^{-1}$
Diffusion coeff. σ	$2{,}42.10^{-3}\ m^{-1}$
Absorption coeff. κ	$5{,}8.10^{-4}\ m^{-1}$
Phase asymmetry parameter g	9.10^{-1}

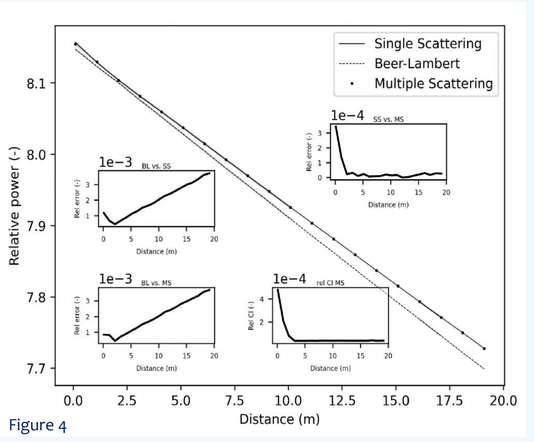

Figure 4

Flux is computed using the SWEET simulator of Cerema [2] for the cases of single scattering (SS), Beer-Lambert (BL) and multiple scattering (MS).

The simulated experiment is illustrated in Figure 1. These results show that the relative error between the BL (usually used for sensors such as transmissiometers) and SS models increases with distances. Moreover, it demonstrates that the SS model is sufficient for this particulate simulation, there's no need to employ the MS model, as the relative error between SS and SS is negligible. The parameters used in the simulation are provided in the table above.

Next steps

- Finalize the construction of the definitive dust chamber,
- Include the analytical SS and BL models in the comparisons,
- Compare experimental measurements with those from existing models to evaluate performance,
- Determine which model is best suited for each type of sensor.

References:

[1] Peng Zhang, Hongbo Xu, Zhichao Hu, Youqing Chen, Mingzhu Cao, Zhaoyang Yu and Enrong Mao. Characteristics of Agricultural Dust Emissions from Harvesting Operations: Case Study of a Whole-Feed Peanut Combine - Journal Agriculture - 2021.
[2] Amine Ben-Daoued, Pierre Duthon and Frédéric Bernardin. SWEET: A Realistic Multiwavelength 3D Simulator for Automotive Perceptive Sensors in Foggy Conditions - Journal of imaging - 2023.

This work was supported by the International Research Center "Innovation Transportation and Production Systems" of the I-SITE CAP 20-25.

A System Dynamics Stock-and-Flow Approach for Sustainable Territorial Policies

Ammar HDAIFEH, Sylvie HUET, Jean-Denis MATHIAS
Université Clermont Auvergne,
INRAE UR LISC

Objective

1. To investigate how integrating socio-technical dynamics, using a stock-and-flow approach, can influence meeting local policy objectives for Households' biowaste management.
2. To model the interplay between technical infrastructure development and social behavioural changes.

Introduction

The integration of socio-technical dynamics in biowaste management policies is essential for sustainability. This study uses a stock-and-flow model to analyze how technical and behavioral factors affect biowaste management outcomes.

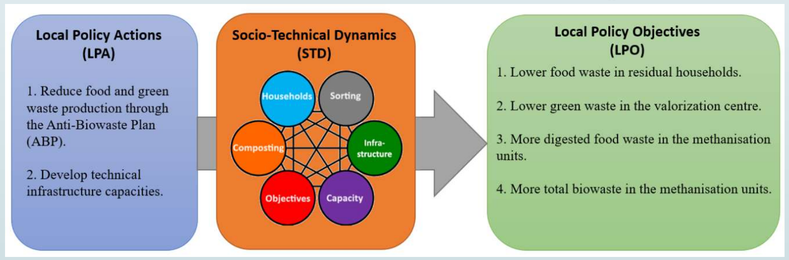

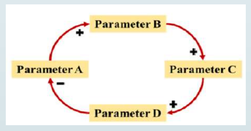

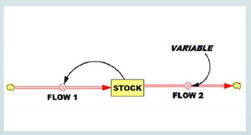

Methods

Computational Simulation

Model Development:

Stock-and-Flow Model: Integrates infrastructural developments and social behavioural dynamics.

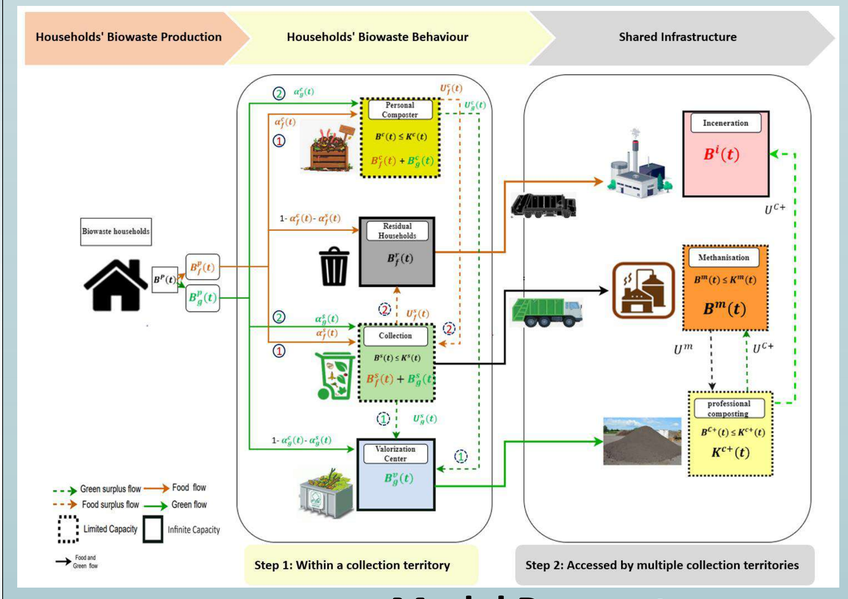

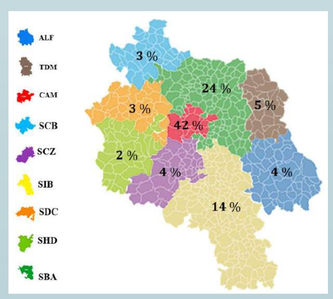

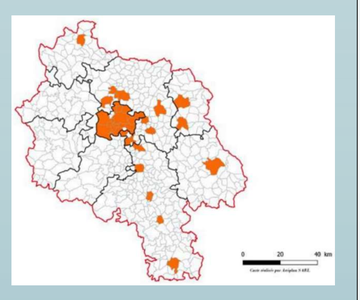

Model Parameters

Table 2. Initial state variables and parameters, shared infrastructure capacities K^m = 20000, K^{c+} and K^i are infinite, Note:"-" indicates no infrastructure.

Collection territories	Demographic parameters		Initial per capita waste production in Kg/year		The initial intention expressed in % (composting and Sorting)				Infrastructure capacities (composter and Collection)	
	P	r	b_g^p	b_f^p	α_g^c	α_f^c	α_g^s	α_f^s	K^c	K^s
SBA	165000	0.006	92	71	12.7	20.1	0	0	4255	0
CAM	284672	0.009	78	77	3.3	4	36	3	1617	8660
TDM	37559	0.004	100	75	4.1	5.5	0	0	304	-
ALF	28197	-0.001	61	89	16.2	13.5	0	0	614	-
SCZ	26516	0.004	46	75	18.5	13.4	0	0	495	-
SIB	93225	0.003	80	91	13	14.3	0	0	2152	-
SCB	17804	0.004	86	91	9.6	10.7	0	0	318	-
SDC	18216	0.001	83	89	10.5	11.2	0	0	346	-
SHD	16001	-0.002	84	107	7.8	7.5	0	0	230	-

Shared infrastructure capacities: $K^m = 20000$, K^{c+} and K^i are infinite.

Table 3. Fixed parameters used in the simulations

Collection territories	Anti-biowaste production ABP		
Anti-biowaste characteristics	the objective of food waste reduction	the objective of green waste reduction	intention diffusion half-time (green and food)
	o_f^p	o_g^p	m_f^p, m_g^p
SBA	0.3	0.106	3.5
CAM	0.5	0.049	3.5
TDM	0.5	0.080	3.5
ALF	0.3	0.155	3.5
SCZ	0.5	0.169	3.5
SIB	0.5	0.124	3.5
SCB	0.5	0.091	3.5
SDC	0.5	0.094	3.5
SHD	0.5	0.092	3.5

Simulation Scenarios:

- Scenario 0: Biowaste production with and without Anti-Biowaste Plan (ABP).
- Scenario 1: No change in behaviour, increased infrastructure.
- Scenario 2: Behavior changes, no infrastructure limitations.
- Scenario 3: Combined behavioural changes and infrastructure growth.

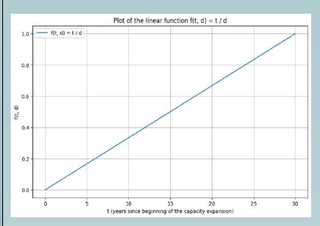

Table 4. Values of the composter, collection unit capacities reached in 2024 in the simulations for the scenario 1 on the left, the scenario 2 on the right, with methanisation unit capacity at 20,000 since 2017. Note:"-" indicates no infrastructure.

Collection territories	Scenario 1					Scenario 2				
	K^c	K^s	K^m	K^{c+}	K^i	K^c	K^s	K^m	K^{c+}	K^i
SBA	6918	2214	-	-	-	infinite	infinite	-	-	-
CAM	4228	10360	-	-	-	infinite	infinite	-	-	-
TDM	1178	-	-	-	-	infinite	-	-	-	-
ALF	1279	-	-	-	-	infinite	-	-	-	-
SCZ	836	-	-	-	-	infinite	-	-	-	-
SIB	4310	-	-	-	-	infinite	-	-	-	-
SCB	740	-	-	-	-	infinite	-	-	-	-
SDC	663	-	-	-	-	infinite	-	-	-	-
SHD	642	-	-	-	-	infinite	-	-	-	-
Shared infrastructure	-	-	20000	infinite	infinite	-	-	infinite	infinite	infinite

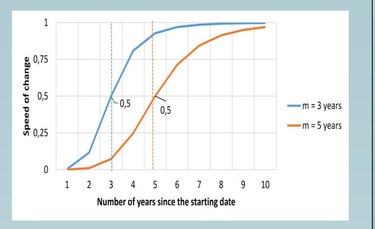

$$f(t,d) = t/d$$

$$z = \frac{t^5}{(t^5+m^5)}$$

Key Equations:

1. Households' Biowaste Production

1. Food waste production

$$B_f^p(t) = b_f^p\ P(t)\ \left(1 - o_f^p\ z\left(t, m_f^p\right)\ \right)$$

2. Green waste production

$$B_f^p(t) = b_g^p\ P(t)\ \left(1 - o_g^p\ z\left(t, m_g^p\right)\ \right)$$

2. Households' Biowaste Behaviour

1. Compostable food waste

$$\widehat{B_f^c}(t) = \alpha_f^c(t) B_f^p(t)$$

1. Compostable green waste

$$\widehat{B_g^c}(t) = \alpha_g^c(t) B_g^p(t)$$

1. Food Composting intention rate:

$$\alpha_f^c(t) = \alpha_f^c(0) + \left(1 - \alpha_f^c(0)\right) z(t, m^c)$$

2. Green Composting intention rate:

$$\alpha_g^c(t) = \alpha_g^c(0) + \left(1 - \alpha_g^c(0)\right) z(t, m^c)$$

1. Sortable food waste

$$\widehat{B_f^s}(t) = \alpha_f^s(t)\ B_f^p(t) + U_f^c(t)$$

1. Sortable green waste

$$\widehat{B_g^s}(t) = \alpha_g^s(t)\ B_g^p(t)$$

1. Food Sorting intention rate:

$$\alpha_f^s(t) = \begin{cases} 1 - \alpha_f^c(t) & if\ \alpha_f^c(t) + \alpha_f^s(t) > 1 \\ \alpha_f^s(0) + \left(o_f^s - \alpha_f^s(0)\right) Z(t, m^s) & otherwise \end{cases}$$

2. Green Sorting intention rate:

$$\alpha_g^s(t) = \begin{cases} 1 - \alpha_g^c(t) & if\ \alpha_g^c(t) + \alpha_g^s(t) > 1 \\ \alpha_g^s(0) + \left(o_g^s - \alpha_g^s(0)\right) Z(t, m^s) & otherwise \end{cases}$$

Infrastructure capacity:

1. Composter infrastructures

$$K^c(t) = K^c(0) + \left(o^c - K^c(0)\right) f(t,d)$$

2. Collection infrastructures

$$K^s(t) = K^s(0) + \left(o^s - K^s(0)\right) f(t,d)$$

3.Shared Infrastructure

1. Methanisation

$$K^m(t) = K^m(0) + \left(o^m - K^m(0)\right) f(t,d)$$

2. Professional composting

$$K^{c+}(t) = K^{c+}(0) + \left(o^{c+} - K^{c+}(0)\right) f(t,d)$$

1. Methanisation

$$\widehat{B^m}(t) = \left(\sum_{j=1}^{n} B_f^s(t)_j + B_g^s(t)_j\right) + U^{c+}(t)$$

2. Incinerator

$$B^i(t) = \left(\sum_{j=1}^{n} B_f^r(t)_j\right) + U^{c+}(t)$$

3. Professional composting

$$\widehat{B_g^{c+}}(t) = \left(\sum_{j=1}^{n} B_g^v(t)_j\right) + U^m(t)$$

Results

Simulation Outcomes:

- Population Growth vs. ABP Impact: Trends in Households' biowase production.

Table 6. Critical times (t*) occurrence and biowaste production in 2024 across Valtom Collection Territories

Collection territories characteristics	Results	SBA (Urban)	CAM (Urban)	Rural collection Territories	Total collection territories
Critical time for food waste trajectory	t*	2025	2025	2029	**2026**
Food waste production in 2024	$B_f^p(2024)$	8698	11958	11242	**31900 (-41.25%)**
Critical time for green waste trajectory	t*	2023	**2022**	2026	**2023**
Good waste production in 2024	$B_g^p(2024)$	14198	22560	16583	**53342 (-4.71%)**

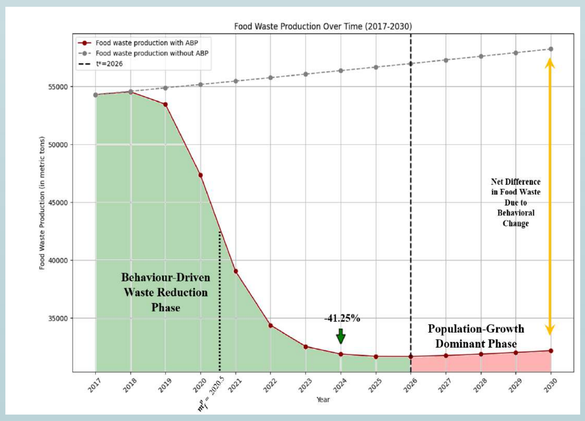

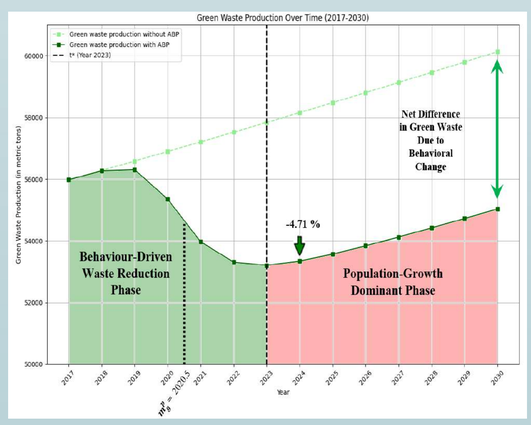

- ABP Impact and Technical Infrastructure:

Table 7. The evolution of flows and stocks in comparison of the LPOs.

Initial state in tons per year of Infrastructure setup	Local Policy Objectives	Local policy Objectives (2024)	Impact of ABP in 2024 without any infrastructure development	Impact of ABP in 2024 and any infrastructure development
Initial food waste in residual households: 47944	Reduction in Food Waste in Residual Households (%)	**-50%**	- 41.61%	- 41.61%
Initial green waste in valorization centers: 43261	Green Waste in Valorization Centers (%)	**-12%**	-5.59%	-5.59%
Initial methanized food waste: 662 t	Methanized Food Waste Production (tons)	**+5700 t**	-298 t	-298 t
Initial total methanized biowaste: 8662 t	Total Methanized Biowaste Production (tons)	**+12000 t**	-175 t	-175 t

- Social Behavior vs Technical Infrastructure: Comparison of different scenarios.

Social Dynamics

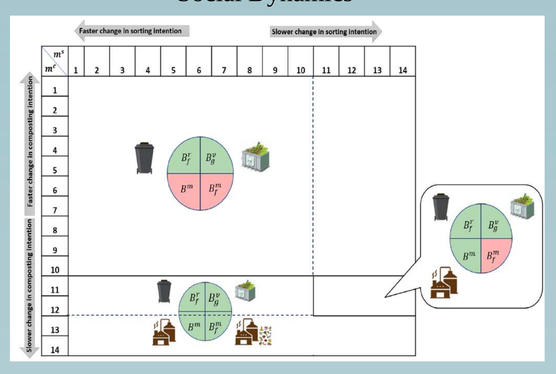

Socio-Technical Dynamics

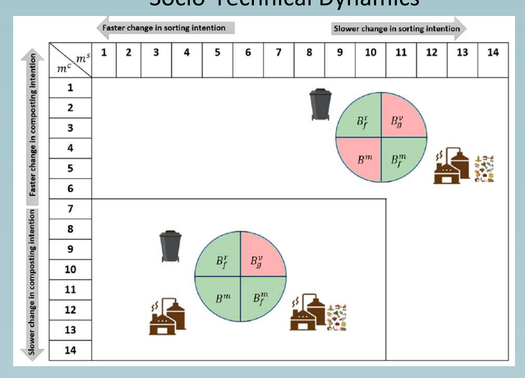

Key Findings:

- **Population Growth and Policy Impact**: Biowaste production increases with population growth, but effective policies, such as the Anti-Biowaste Plan (ABP), can mitigate this increase.
- **Infrastructure Limitations**: Improvements in technical infrastructure alone are not sufficient to achieve waste management objectives.
- **Importance of Behavioral Shifts:** Shifts in behavior are crucial for meeting all policy objectives and maximizing the effectiveness of infrastructure improvements.

Conclusions

Key Insights:

- Balanced Approach: Integrate technical infrastructure improvements with social behavior interventions to achieve desired biowaste management outcomes.
- Gradual Behavioral Shifts: Encourage gradual adoption of composting and sorting behaviours to effectively complement and enhance infrastructure capabilities.
- Future Work: I will Investigate **ABM** to capture the complexity of individual behaviours and further refine biowaste management strategies..

Bibliography

- Huet, Sylvie. 2023. "2008-Huet-Deffuant-Differential Equation Models Derived from an Individual-Based Model Can Help to Understand Emergent Effects. https://doi.org/10.25334/Z0SZ-0783
- Mathias, Jean-Denis, Susan Clark, Nuri Onat, et Thomas Seager. 2018. « An Integrated Dynamical Modeling Perspective for Infrastructure Resilience ». Infrastructures 3 (2): 11. https://doi.org/10.3390/infrastructures3020011
- Rogers, Everett M. 1995. Diffusion of Innovations. 4th ed: https://doi.org/10.2307/3104547.
- Babalola, Micky A. 2019. « A System Dynamics-Based Approach to Help Understand the Role of Food and Biodegradable Waste Management in Respect of Municipal Waste Management Systems ». *Sustainability* 11 (12): 3456. https://doi.org/10.3390/su11123456.

HYBRIDIZATION OF DESCRIPTION LOGIC AND LOGIC PROGRAMMING

Arun RAVEENDRAN NAIR SHEELA, First Year Phd Student
Supervisors - Christophe REY(LIMOS), Florence DE GRANCEY(Thales), Victor CHARPENAY(LIMOS), Farouk TOUMANI(LIMOS)

CONTEXT

Virtual Assistant built on top of a knowledge representation and reasoning system to assist pilots during flight operation. But existing system has challenges:

1. Performance Concerns
2. Expressiveness

REQUIREMENTS

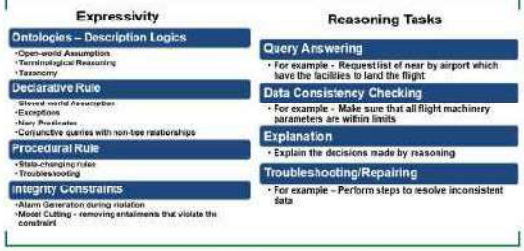

OBJECTIVES

1. Define a language that capture the above expressivity .
2. Build a efficient reasoner for the language to execute the required reasoning tasks

DESCRIPTION LOGICS

- Define knowledge in terms of classes, properties and individual.
- Express relationships and constraints between them using predefined constructors
- Web Ontology Language (OWL) is popular ontology language based on Description Logics.
- Several sublanguage of OWL was introduced with different expressive features.
  a. OWL 2 DL - SRIOQ(D)
  b. OWL lite - SHIQ(D)
  c. OWL 2 RL - DLP
  d. OWL 2 QL - DL-Lite
  e. OWL 2 EL

```
#TBox - Every student who is enrolled in atleast
one phd program is a phd student.
Student and (hasEnrolled some PhdProgram) SubClassOf PhdStudent.

#ABox - Arun is student.
Student(arun).
# computerscience is phd program
PhdProgram(computerscience).
# arun enrolled in computerscience.
hasEnrolled(arun,computerscience)
```

- An example is given above:
  a. Student is class and hasEnrolled is a property.
  b. and, some, subclass are constructors.
  c. Query - Is Arun a phd student? - Yes

RULES

- Format - If "condition" then action.
- Two kind of rule:
  a. Procedural Rules - Represent how to achieve a task.
  b. Declarative Rules/Logic Programming - What to achieve.
- Different kind declarative rules based on expressivity

```
% Background knowledge:
    isFather("John", "Dan") % John is Dan's father
    isFather("Paul", "John") % Paul is John's father
    isWife("Alice", "Paul") % Alice is Paul's wife

    isGrandmother(X,Y):-isWife(X,Z),
                        isGrandfather(Z,Y) % X is Y's grandmother
                                           % if X is Z's wife and
                                           % Z is Y's grandfather

    isGrandfather(X,Y):-isFather(X,Z),
                        isFather(Z,Y)  % X is Y's grandfather
                                       % if X is Z's father and
                                       % Z is Y's father

% Logic programming query:
    ?-isGrandmother("Alice","Dan") % Is Alice Dan's grandmother?
```

SOLUTION

Benefits:

1. Enhanced Expressivity.
2. Combine Open-world and Closed-world reasoning.
3. Combine efficient terminological reasoning feature of Description Logics and query answering feature of rule engines.

Challenges:

1. DL and rule has entirely different semantics.
2. Undecidability.

METHODS TO COMBINE DESCRIPTION LOGIC AND RULES

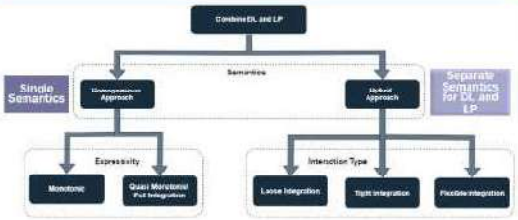

1. Homogeneous - *Single Semantics*
   a. Monotonic - Based on First-order semantics
      Examples - SWRL, DLP, DL-Rules, ELP
   a. Quasi-monotonic - Based on non-monotonic FO semantics
      Examples - Hybrid MKNF, OASP
1. Hybrid - *Separate semantics for DL and Rules(*
   a. Loose Integration - Share logical consequences Example - DL-Program
   b. Tight Integration - Model-based interaction
      Example - DL+Log, HD-Rules

GENERAL ARCHITECTURES TO BUILD REASONER FOR HYBRID KNOWLEDGE BASE

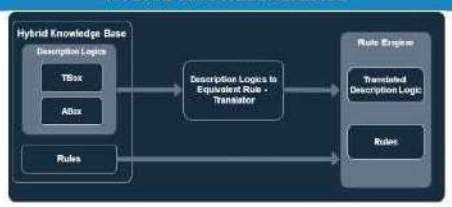

Similarly, there are several other architectures
For Instance:

1. Couple a Description Logics reasoner with a rule engine and exchange consequence using a middleware.
2. Expand Description Logic knowledge base using a reasoner and then translate the inference to a rule engine.

METHODOLOGY

Finally, evaluate the reasoner with other hybrid reasoners with respect to below parameters:

1. Expressivity
2. Reasoning Performance
3. Scalability
4. Efficiency

EXISTING HYBRID REASONERS

Reasoner Name	Language/Type	Features Available	Missing Features
Nolfr	Hybrid MKNF/Quasi-monotonic	• Query Answering Tool • Available as protege plugin • Support most of the features	• Procedural rules • Explanation generation • DL Expressivity restrictions
DLV-dlex	DL-program/loose integration	• Support most features especially procedural rules • Expressive DL and Rules	• Integrity Constraint • Scalability
Drew System	DL-Program/Loose Integration	• Better performance than DLV-dlex	• Procedural rules • Missing many features

- These are the three hybrid reasoners which may be adapt for industrial use cases.
- But these reasoners has expressivity limitations.
- Also, limitation in reasoner performance and efficiency - Evaluations need to be done

FUTURE WORK

1. Implement a concrete using each methodology and identify the limitations on each.
2. Perform evaluations on the selected hybrid reasoners with respect to existing benchmarks.
3. Identify the areas needed improvements.

REFERENCES

- Thomas Eiter et al, Combining answer set programming with description logics for the semantic web.
- Matthias Knorr et al, Local closed world reasoning with description logics under the well-founded semantics.
- Ricardo Rosati DI+log: Tight integration of description logics and disjunctive datalog
- Boris et al, Reconciling Description Logics and Rules
- NoHR: An Overview: Reasoning with Ontologies and Nonmonotonic Rules

Etude expérimentale et numérique du comportement mécanique de planchers mixtes et démontables combinant acier, bois et béton

Lara KACHOUH[1], Chaimaa JAAFARI[1], Sébastien DURIF[1], Abdelhamid BOUCHAIR[1]

1 Université Clermont Auvergne, Clermont Auvergne INP, CNRS, Institut Pascal, F-63000 Clermont-Ferrand, France

Contexte

Le secteur du BTP émet **242 millions** de tonnes de déchets (*chiffres 2020*).

La RE2020 exige une réduction importante de l'empreinte carbone des bâtiments neufs.

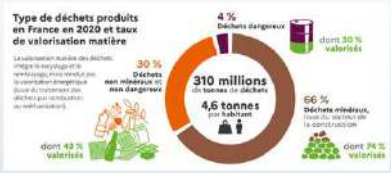

Déchets produits en France en 2020 [1]

Structures mixtes

- **Résistance** et **rigidité augmentées**
- **Déconstruction** difficile et **empreinte carbone élevée**

Objectifs

Développer des structures mixtes démontables associant **béton, bois** CLT et **acier**

- Proposer et étudier des **connexions** de cisaillement **performantes**
- Obtenir un comportement mécanique adéquat (résistance, rigidité, ductilité)
- Améliorer les caractéristiques vibratoires et acoustiques

Méthodologie

- **Modélisation numérique sur « Abaqus »** : comportement élastoplastiques, maillage [2], contact [3], interactions [4],…
- **Expérimentation** : Essais Pushout et flexion, comparaison avec les essais (validation de modèle)
- **Étude paramétrique :** espacement entre blocs de béton, nombre de blocs, propriétés des matériaux,…

❑ **Application essai pushout** : caractériser le comportement de la connexion et valider un modèle MEF

Essais Pushout expérimentaux et numériquement

❑ **Application essai flexion de plancher mixte démontable acier/panneaux en béton**

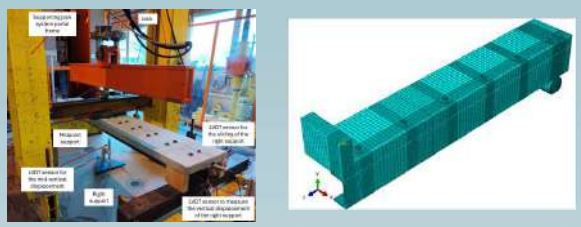

Poutre acier-béton en flexion

Résultats

❑ **Essai pushout acier/béton** : comparaison essais/MEF

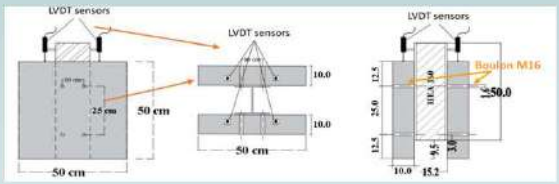

Dispositifs d'essai Pushout

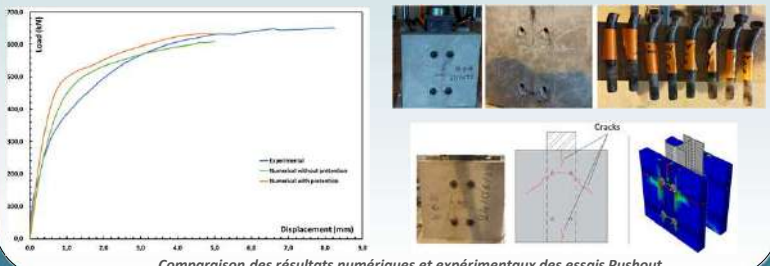

Comparaison des résultats numériques et expérimentaux des essais Pushout

Modèles numériques vérifiés.

Il est nécessaire de considérer la précontrainte des boulons, car elle assure une action mixte totale (premières phases de chargement).

❑ **Essai de flexion 3 points des poutres mixtes acier/béton :** comparaison essais/MEF

Trois configurations testées : 2, 3 ou 6 panneaux en béton

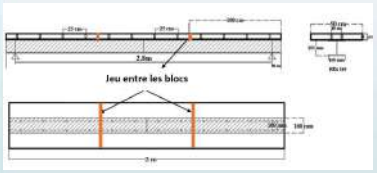

Dispositifs d'essai de flexion 3 points

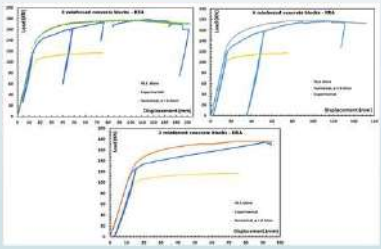

Comparaison des résultats numériques et expérimentaux

- **Courbes expérimentale et numérique proches**
- **Apport notable de la mixité au niveau de la résistance**

Comparaison numériques et expérimentaux des fissures

Configurations	Rigidité initiale (kN/mm)	Écart par rapport aux résultats expérimentales	Force maximale (kN)	Écart par rapport aux résultats expérimentales
3 Blocs	9.28	2.04%	176.54	0.62%
6 Blocs	8.09	1.37%	178.13	1.12%
2 Blocs	9.75	0.78%	175.7	0.65%

Effet de nombre de blocs de béton

- **Nombre de blocs de béton :**
  - **L'augmentation** du **nombre** de blocs diminue la **rigidité** initiale
  - Pas d'influence sur la résistance
- **Jeu entre blocs de béton :**
  - La rigidité initiale augmente avec la diminution du jeu entre blocs
  - Pas d'influence sur la résistance
  - Le jeu peut être rempli par une résine ou mortier (paramètres à analyser)

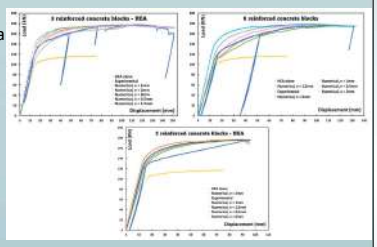

Effet de l'espacement entre les blocs de béton

Travaux en cours

❑ **Essai de flexion 3 points des poutres mixtes acier/CLT/béton :** MEF

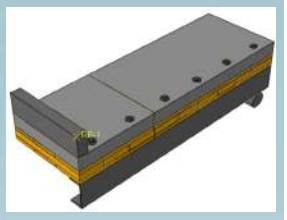

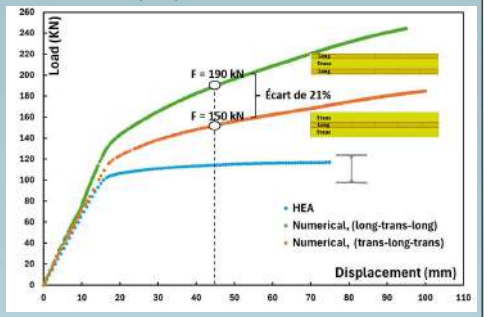

Comparaison entre deux configurations des panneaux CLT (0°, 90°, 0° et 90°, 0°, 90°) dans le cas d'une poutre mixte démontable acier/CLT/béton

D'autres configurations en cours d'études

Conclusions

- **Comportement des connecteurs démontables satisfaisant** : rigidité, résistance et ductilité.
- **Modèle MEF représentatif du comportement observé lors des essais.**
- **Nombre de blocs et jeux entre eux :** influence sur la rigidité initiale mais pas sur la résistance.
- **Connexion par boulons :** augmente de façon significative la rigidité en flexion par rapport au profilé en acier seul.
- **Jeux entre blocs et formes des connecteurs :** à évaluer pour les systèmes bois-acier-béton

Références

[1] Barbara Pompili, «Eco-construire pour le confort de tous - Réglementation environnementale RE 2020 », Février 2021.

[2] A. Béreyziat, « Étude du comportement thermomécanique de poutres mixtes acier-bois en situation d'incendie », Thèse de doctorat, Ecully, Ecole centrale de Lyon, 2022.

[3] Hibbitt, Karlsson & Sorensen, « ABAQUS/CAE User's Manual », Inc. 2000.

[4] Litewka P., « The penalty and lagrange multiplier methods in the frictional 3d beam-to-beam contact problem », 2005.

Study and design of interpretable models for detecting anomalies in spectral data stream: Application to the contamination of vacuum process chambers for microelectronics.

N. Rojas Varela, J. Ah-Pine, E. Mephu Nguifo

INTRODUCTION

A continuous transfer of data, or **data streams,** have become a vital source of big data which in various industries stands as the predominant form of business data.

Data stream anomaly detection refers to the process of identifying unusual patterns or events in a continuous flow of data.

Spectral data is a type of data measured for specific wavelengths of radiation related to a phenomenon studied.

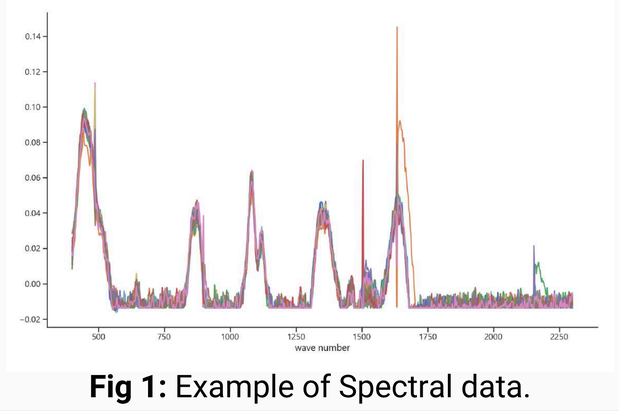

Fig 1: Example of Spectral data.

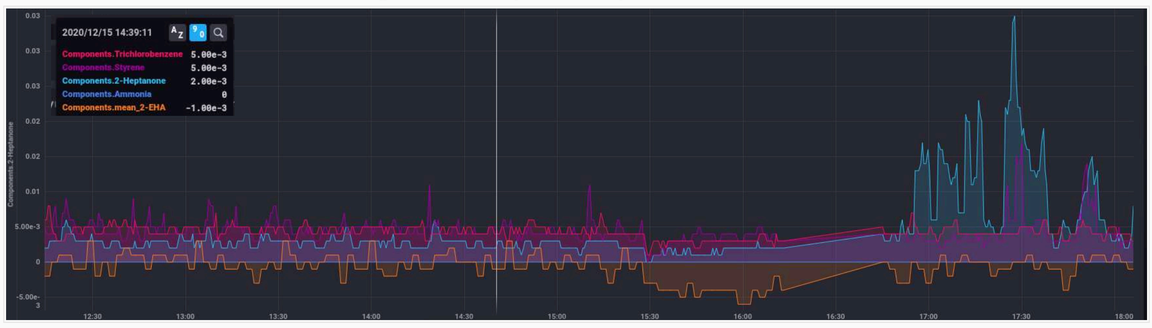

Fig 2: Example of Data Stream. [1]

CHALLENGES

Compared to static data, data stream anomaly detection faces challenges due to:

- Full dataset not available in advance.
- High velocity of streams.
- Data characteristics evolving over time.

TYPE OF METHODS

Categories for algorithms based on:

- Offline learning.
- Semi-online learning.
- Online learning.

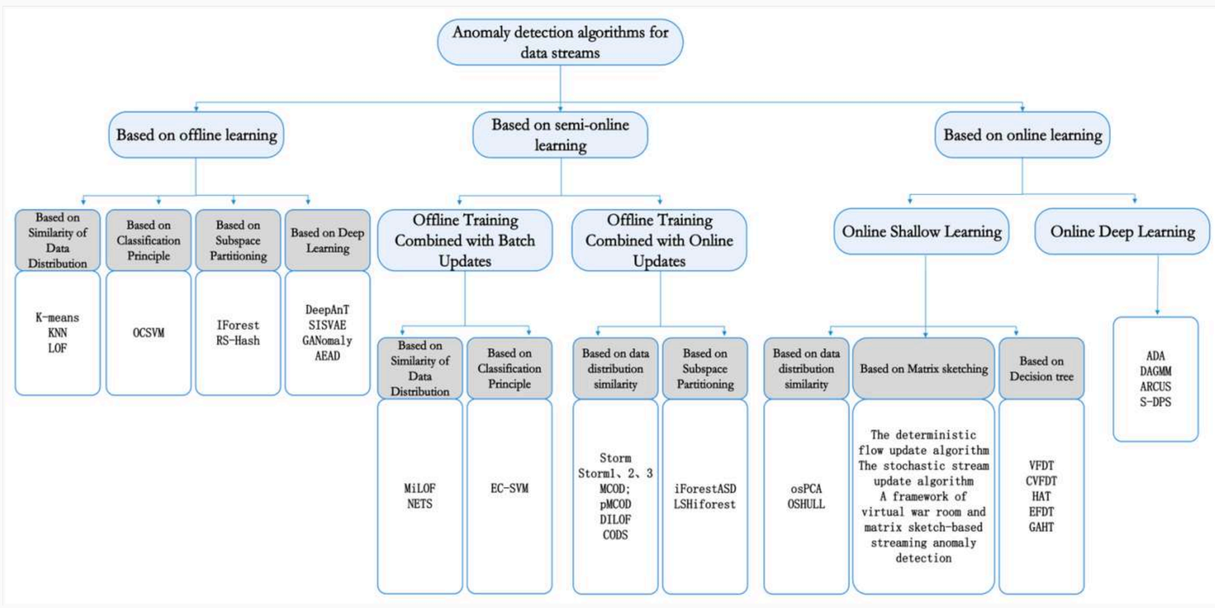

Fig 3. Categories for anomaly detection techniques. [2]

VALIDATION

1. Streaming Data

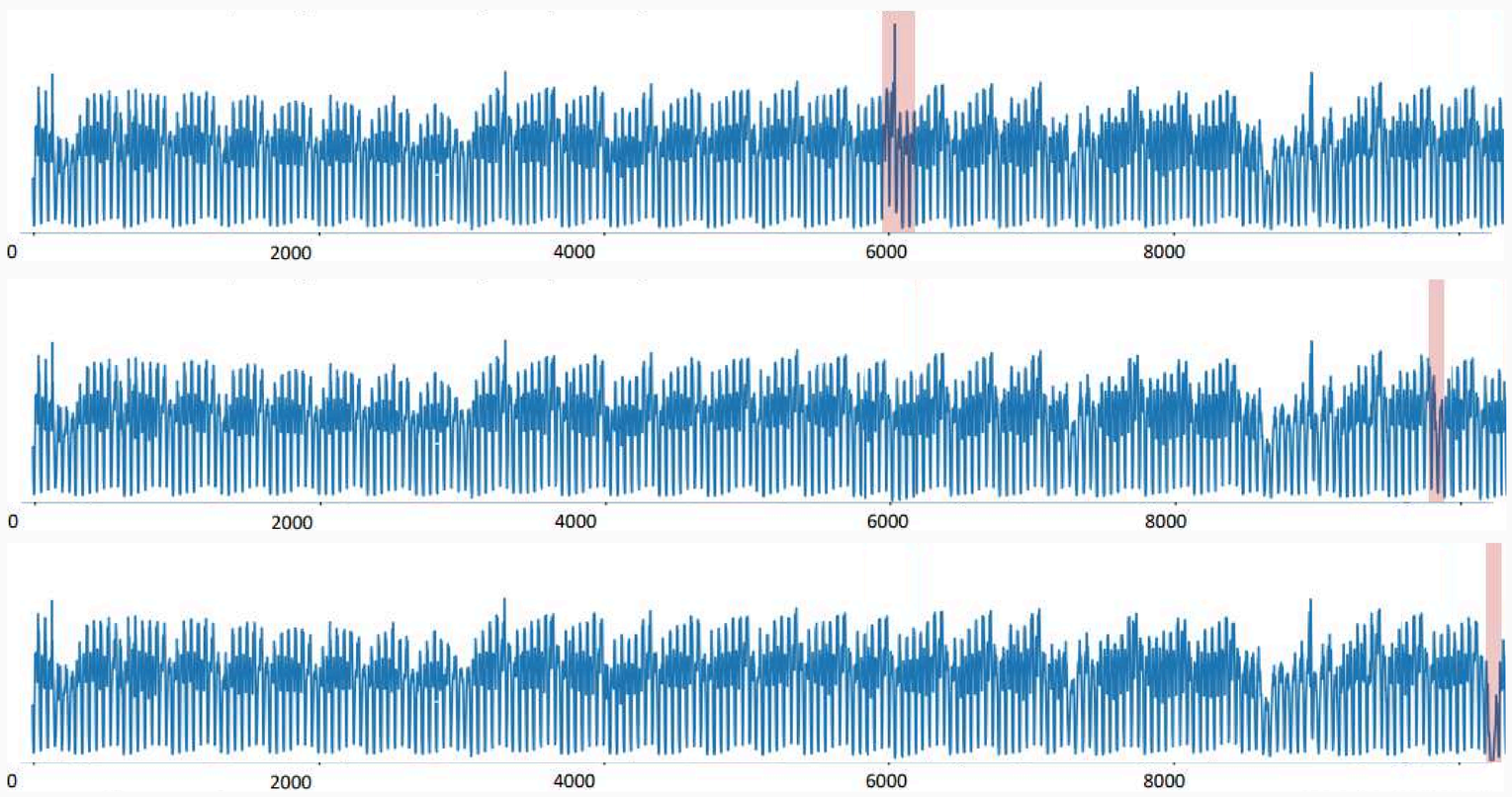

2. Model Selection

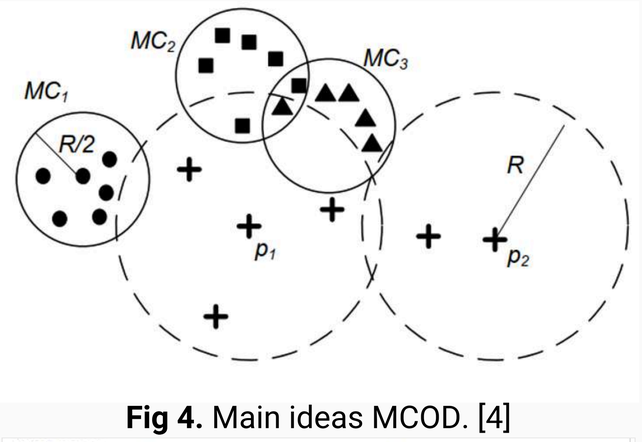

Fig 4. Main ideas MCOD. [4]

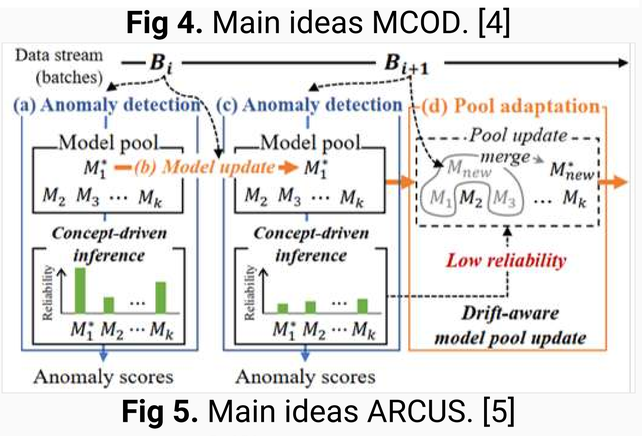

Fig 5. Main ideas ARCUS. [5]

3. Anomaly Score

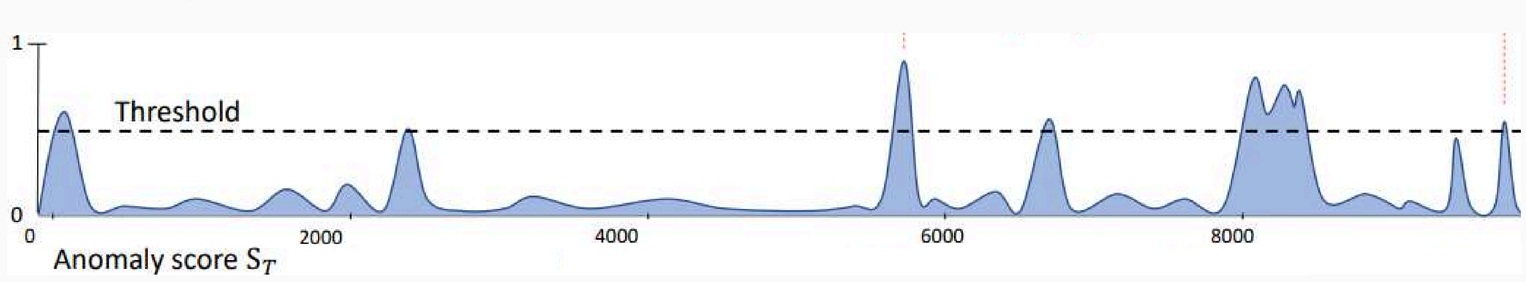

4. Interpretability

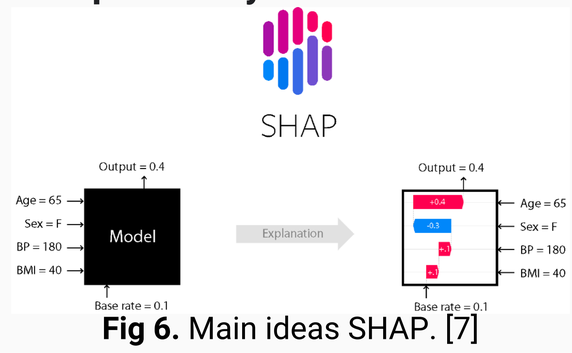

Fig 6. Main ideas SHAP. [7]

FUTURE DIRECTIONS

Improve existing algorithms in:

- **Real-time** processing and learning capabilities.
- Effective **handling** of **concept drift**.
- Dynamic selection of **adaptive thresholds** based on current data distribution or time period.
- Model **interpretability**.
- Energy **efficiency** to reduce computational resources and energy consumption.

ACKNOWLEDGEMENTS

This work is currently sponsored by National Association for Research and Technology (ANRT)

REFERENCES

1. Florentin Jiechieu et al. (2024) SEDAF : Prototype d'un Système Explicable de Détection d'Anomalies dans les Flux de Données. Revue des Nouvelles Technologies de l'Information, EGC, Dijon, France, pp. 441-448.
2. Lu, T., Wang, L., & Zhao, X. (2023). Review of anomaly detection algorithms for data streams. Applied Sciences, 13(10), 6353.
3. Liu, F.T.; Ting, K.M.; Zhou, Z.H. Isolation Forest. In Proceedings of the 2008 Eighth IEEE International Conference on Data Mining, Pisa, Italy, 15–19 December 2008; IEEE: New York, NY, USA, 2008; pp. 413–422.
4. Kontaki, M., Gounaris, A., Papadopoulos, A. N., Tsichlas, K., & Manolopoulos, Y. (2011, April). Continuous monitoring of distance-based outliers over data streams. In 2011 IEEE 27th International Conference on Data Engineering (pp. 135-146). IEEE
5. Yoon, S., Lee, Y., Lee, J. G., & Lee, B. S. (2022, August). Adaptive model pooling for online deep anomalydetection from a complexevolving data stream. In Proceedings of the 28th ACM SIGKDD Conference on Knowledge Discovery and Data Mining (pp. 2347-2357).
6. Boniol, P., Paparizzos, J., & Palpanas, T. (2023). New Trends in Time Series Anomaly Detection. International Conference on Extending Database Technology.
7. Štrumbelj, E., & Kononenko, I. (2014). Explaining prediction models and individual predictions with feature contributions. Knowledge and information systems, 41, 647-665.

Theoretical and experimental modeling of the energy and environmental behavior of bio-based building materials

BAKKOUR Amer[1], OULDBOUKHITINE Salah-Eddine[1], BIWOLE Pascal[1], AMZIANE Sofiane[1]

1 Université Clermont Auvergne, Clermont Auvergne INP, CNRS, Institut Pascal, F-63000 Clermont–Ferrand, France

Introduction

❑ **Context:**

- Modeling of hygrothermal transfer in bio-based envelopes in various environmental conditions is important to accurately describe their behavior at the building scale.

❑ **Problematic:**

- Lack of knowledge of the intrinsic characteristics of bio-based materials,
- High variability of the thermo-hydric parameters that depend on several factors such as water content, density, and temperature.

❑ **Objective:**

- Fully understand the hygrothermal behavior of bio-based materials at the material, wall, and building scales.

State of Arts

❖ ***Material scale: Characteristics of bio-based composites [1]***

- High porous micro-structure
- Low density
- Good thermal performance ($\lambda \searrow$)
- Moisture regulation capacity (MBV$\nearrow$)

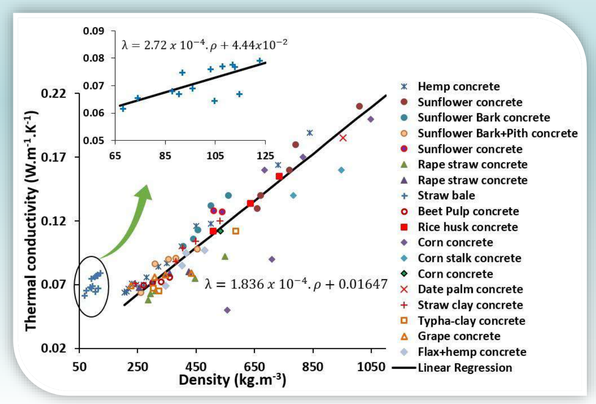

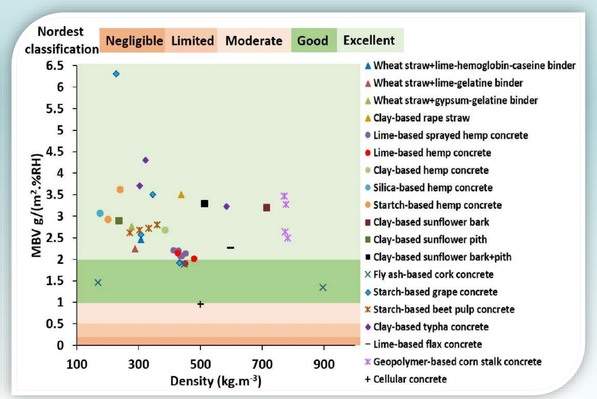

Methodology

❖ ***Modeling at the wall scale: Wood-cement concrete (WCC) [2]***

1 WCC characterization

Wood aggregate

80% wood volume additive in concrete

Cement + Water

2 Monitored building

Wood-cement building

Monitoring

From 20/04/2023, to 20/10/2023

In situ measurements of:
- Indoor **T** and **RH**,
- Wall **T** and **RH**,
- Outdoor **T** and **RH.**

Laboratory testing

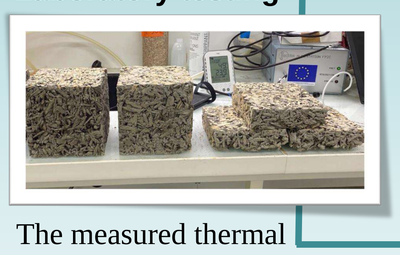

The measured thermal properties are used as input parameters.

3 Model implementation

Wood-cement wall

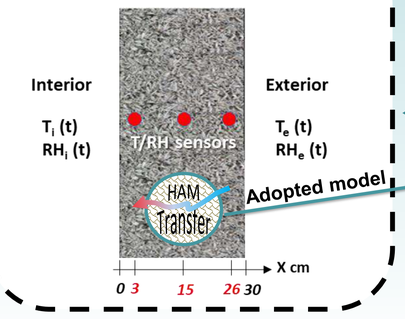

The Reduced Heat, Air, and Mass (R-HAM) transfer model [3]:

$$\begin{cases} C_p \rho_s \frac{\partial T}{\partial t} = div[\lambda \nabla T] + L_v\, \rho_s\, C_m \frac{\partial P_v}{\partial t} \\ C_m \rho_s \frac{\partial P_v}{\partial t} = div[K_m \nabla P_v] \end{cases}$$

❖ ***Modeling at the building scale: Straw house***

1 Monitored building

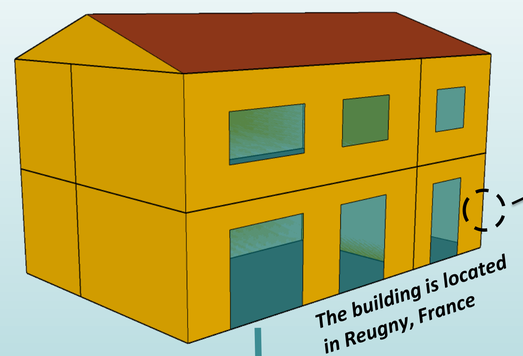

The building is located in Reugny, France

Wall configuration

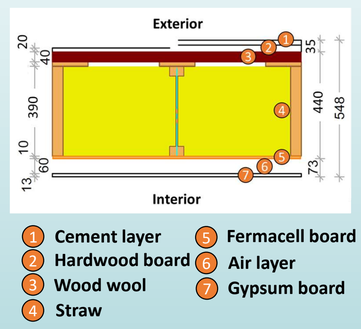

1. Cement layer
2. Hardwood board
3. Wood wool
4. Straw
5. Fermacell board
6. Air layer
7. Gypsum board

Monitoring

From 01/01/2023, to 31/05/2023

In situ measurements of:
- Indoor and outdoor **T** and **RH**,
- Wall **T** and **RH**.

2 Co-simulation HAM-BES

Wall model (HAM) — MATLAB

Building Energy Simulation (BES) model — TRNSYS

Data Exchange

Results

➢ ***Modeling at the wall scale***

Evaluation of **T** and **RH** at the center of the wood wall: measured vs. simulation

- The R-HAM model validation: The model generates results closely matching the in-situ measurements taken on the Northern wall.
- Calculated error:

Average Error	T (°C)	RH (%)
Relative Error (RE)	3.21 %	8.06 %
Root Mean Square Error (RMSE)	0.84 °C	6.54 %

➢ ***Modeling at the building scale***

Evaluation of **T** inside the straw building: measured vs. simulation

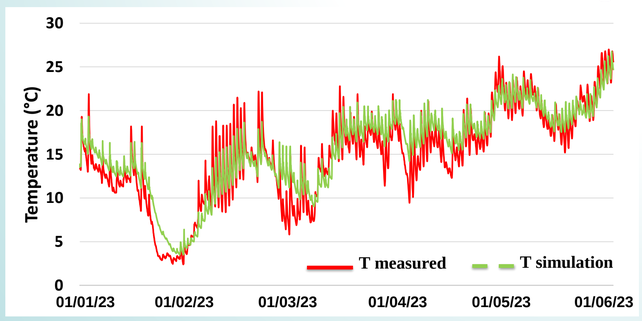

- The **T** is well predicted inside the straw building.
- The predicted **T** trend follows that of the measured **T**.
- Calculated error:

Average Error	T (°C)
Root Mean Square Error (RMSE)	1.9 °C
Coefficient of Variation of RMSE	12.6 %

Perspective

➢ Integration of green roofs into bio-based buildings

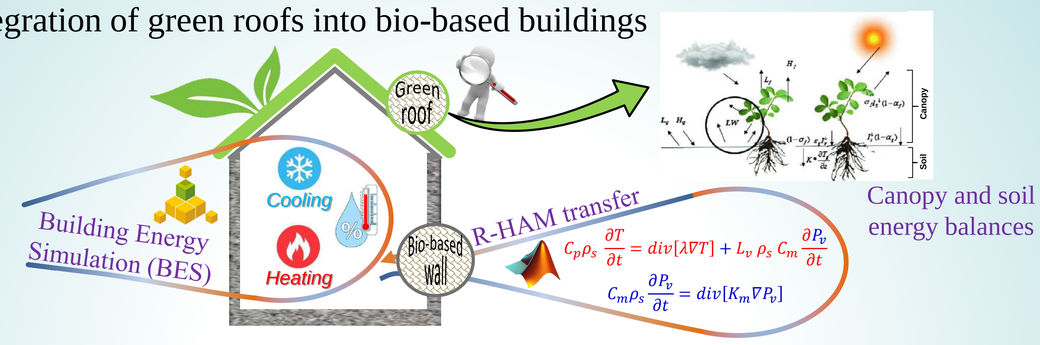

- To assess the evolution of T and RH inside a green bio-based building.
- To predict energy demand and energy savings.

Bibliography

1. **Bakkour, A., Ouldboukhitine, S. E., Biwole, P., & Amziane, S. (2024). A review of multi-scale hygrothermal characteristics of plant-based building materials. *Construction and Building Materials*, 412, 134850.**
2. **Bakkour, A., Ouldboukhitine, S. E., Biwole, P., Godi, G., & Amziane, S. (2023). Experimental and Numerical Investigation of Hygrothermal Transfer through Bio-Based Materials: An Application to Wood–Cement Walls. *Buildings*, 13(12), 2986.**
3. **Benkhaled, M., Ouldboukhitine, S. E., Bakkour, A., & Amziane, S. (2022). Sensitivity analysis of the parameters for assessing a hygrothermal transfer model HAM in bio-based hemp concrete material. *International Communications in Heat and Mass Transfer*, 132, 105884.**

amer.bakkour.95@gmail.com

Conductometric Gas Sensors for Hydrogen Leakage Detection Based on Copper Phthalocyanine Decorated by Palladium Nanoparticles

S. Rajab-Pacha [1], J. Brunet [1], A. Ndiaye [1], A. Pauly [1], C. Varenne [1]

[1] Université Clermont Auvergne, Clermont Auvergne INP, CNRS, Institut Pascal, F-63000 Clermont-Ferrand, France

Motivations and Context

In the context of global warming, research on alternative energy sources distinct from fossil fuels is becoming essential. To this end, the use of hydrogen as an energy source has emerged as a major priority in the current quest for clean and sustainable energy sources. However, despite its many potential advantages, the deployment of hydrogen as an energy vector presents considerable challenges to overcome. Hydrogen is a colorless and odorless gas that exhibits explosive limits between 4% and 75% in air. These properties demand rigorous safety protocols from production to use via transport and storage.

Scientific objectives

- ✓ Development of advanced microsensor technology with high metrological performances
- ✓ Optimization of the sensing materials to benefit from high response to hydrogen
- ✓ Measurements of low hydrogen concentrations to monitor hydrogen leaks
- ✓ Development of microsensors with higher sensitivity, high resolution and fast responses

Methods and Materials

Original Conductometric microsensors implementing Copper Phthalocyanine ($Cu\{C_8H_4N_2\}_4$) decorated by Nanoparticles of Palladium (Pd NPs) have been realized:

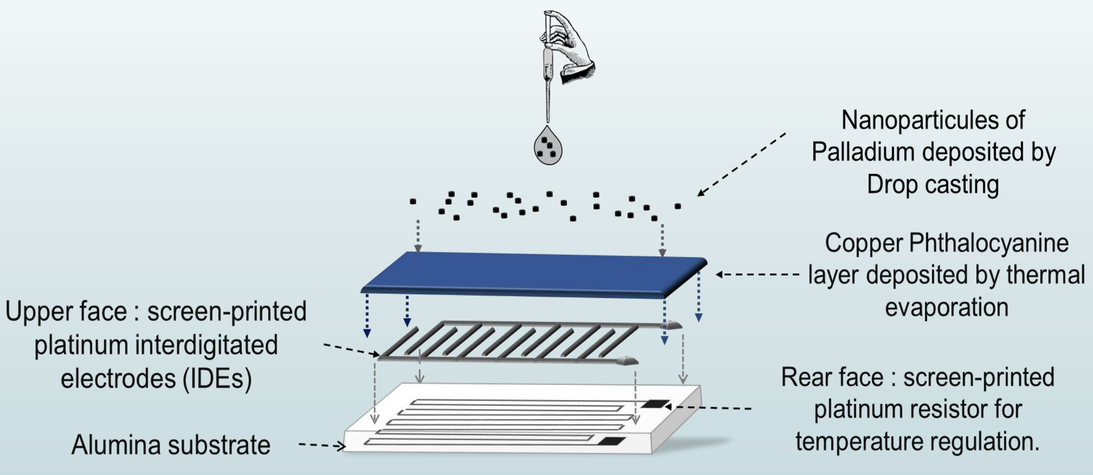

Deposition process

- Step 1: Deposition of copper phthalocyanine (thickness = 100nm) onto the interdigitated electrodes (IDEs) through thermal evaporation under vacuum.
- Step 2: Elaboration of Palladium nanoparticles by wet chemistry from palladium ions reduced by sodium borohydride. We simplify the equation of this reaction as follow :

$$Pd^{2+} + 2e^{-} = Pd^{0}$$

- Step 3: Dispersion of Palladium nanoparticles onto the copper phthalocyanine film through drop casting process.

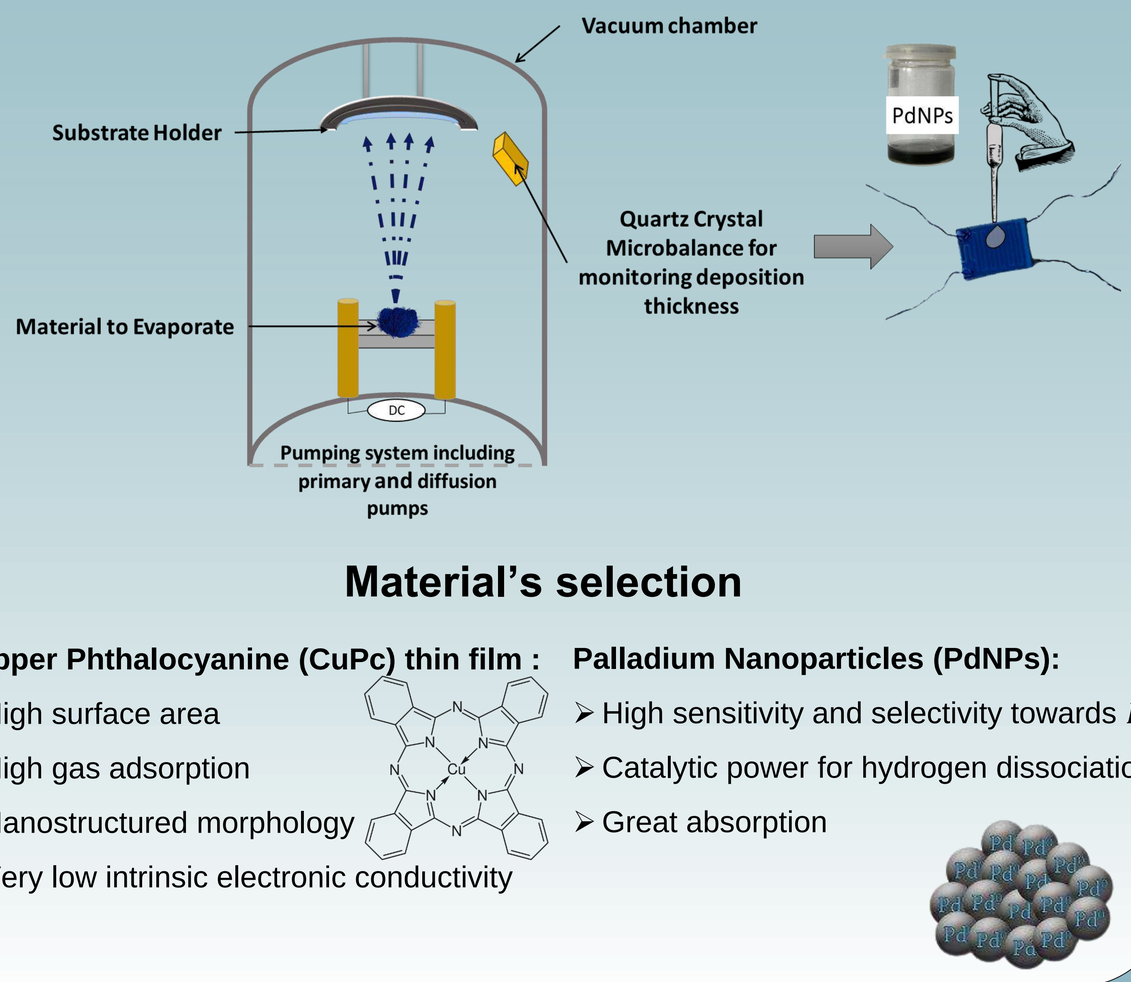

Material's selection

Copper Phthalocyanine (CuPc) thin film :

- ➢ High surface area
- ➢ High gas adsorption
- ➢ Nanostructured morphology
- ➢ Very low intrinsic electronic conductivity

Palladium Nanoparticles (PdNPs):

- ➢ High sensitivity and selectivity towards H_2
- ➢ Catalytic power for hydrogen dissociation
- ➢ Great absorption

Experimental setup and results

Experimental setup

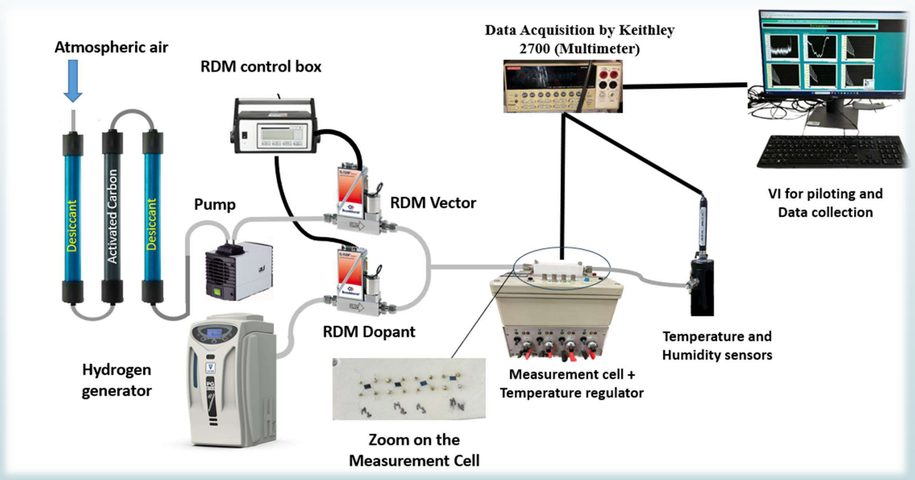

- ➢ Atmospheric air extracted by a pump passes through two silica gel columns to remove humidity and an activated charcoal cartridge for gaseous pollutant removal.
- ➢ An ad-hoc VI (LabVIEW program) was developed to perform gas dilutions, to modulate hydrogen concentrations and to maintain a constant flow rate during experiments.
- ➢ Humidity and temperature sensors are inserted into the fluidic line to measure all variations during the experiments.
- ➢ All variations of temperature, humidity, flow rates, microsensor signals. are synchronously acquired by a Keithley multimeter driven by the VI controller.

Results

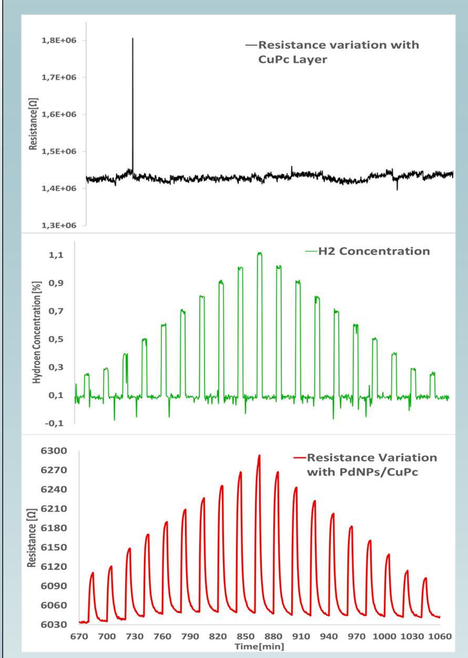

- ➢ Tests with only a CuPc layer do not provide reliable responses to H2 exposure

Tests with CuPc Layer plus PdNPs show :

- ➢ Resistance increases upon H_2 exposure,
- ➢ High sensitivity of microsensors to H_2 in the [0.2%-1%] concentration range,
- ➢ Variation of Resistance is correlated to $[H_2]$ concentration,
- ➢ Good level of repeatability,
- ➢ Response and Recovery times at room temperature are estimated to 2.5 minutes and 7 minutes, respectively.

Linear calibration curve highlights :

- ➢ a sensitivity close to 200Ω/% ,
- ➢ a low hysteresis,
- ➢ a limit of detection (LOD) estimated to 0.07% (700ppm) at ambient temperature.

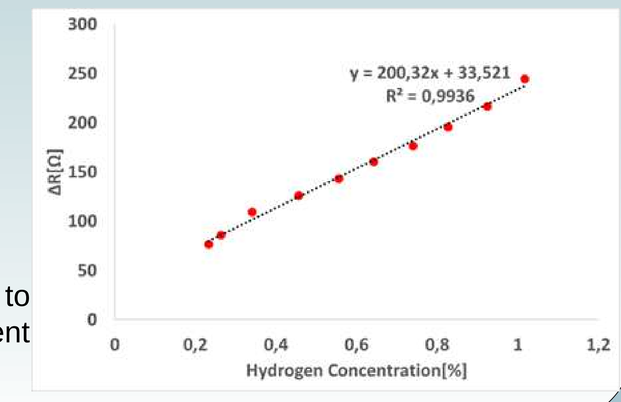

Conclusions and outlooks

- ➢ Promising results are obtained by combining CuPc layer and Pd nanoparticles.
- ➢ More investigation is needed to determine:
  - The effect of nanoparticle density on sensing performances,
  - The effect of temperature on sensing mechanisms,
  - The cross-sensitivity of devices to water vapor and other interfering gases.

Potential applications of Hydrogen sensors